Using Photolabile Protecting Groups for the Rapid Triggering of Fast Biological Events

Thesis by

Kirk C. Hansen

In Partial Fulfillment of the Requirements
for the Degree of
Doctor of Philosophy

California Institute of Technology
Pasadena, California

2002

(Submitted October 3, 2001)

Acknowledgements

I have had the privilege of spending the last five years working and living in a unique environment which has been both intellectually stimulating and personally supportive. I feel fortunate to have been a student in this prestigious community. My research grew out of productive interactions with numerous members of the Caltech community. First, I would like to thank my thesis advisor, Sunney Chan, for his guidance and support, his patience and understanding. I have benefited from his meticulous way of reasoning, his insistence on excellence, and his emphasis of putting a problem within its broader context.

The Chan group, with its wide variety of interests, has been a stimulating place to work. Most of all, I owe Brian Schultz for his intellectual guidance. I am indebted to Mike Stowell for getting me started on the bc_1 project. His direction was instrumental in my start at Caltech. Ron Rock was responsible for getting me started on the GCN4-p1 folding project and for that matter in peptide chemistry. I am grateful to Sean Elliott for invaluable advice, being an excellent roommate and friend. Derek Debe for insight into the protein folding problem, constant encouragement, and keeping me laughing late into the night. Shao-Ching Hung, Tim Chang, Hung Kay Lee, Reggie Waldeck, Guangyang Wang and the rest of the Chan group.

I also benefited from the advice (and equipment) of several people in the Rees, Imperiali and Mayo groups, including Carlos Bosques, Sarah O'Connor, Jennifer Ottesen, Kevin McDonnell, Tina Iverson, Rob Spencer, Dan Bolon and Pavel Strop.

Randy Larsen at the University of Hawaii helped perform the photoacoustic calorimetry experiments. Susanna Horvath was responsible for some of the peptides in

this work. Gary Hathaway, Zoe and Felicia performed mass measurements. Priscilla Boon and Dian Buchness with their smiles and helpfulness have made my time here a little easier. I would like to thank all colleagues and coworkers who have aided me during my graduate work.

Living in California I have had the pleasure of spending my free time in some of the worlds most spectacular settings. Making my way up the gritty domes of Joshua Tree to the Dizzying smooth granite walls in Yosemite, I have had a unique opportunity to learn about life, friends, and myself. Thanks to Pavel Strop for endless good times and camaraderie, Kai Zinn for teaching me to work hard and play hard, Ken Brameld for his selflessness, Char Backes, a close friend I will never forget, also to friends Eric Connor, Heather Maynard, Dave McCusker, Mike Abrams, John Burke, Todd Younkin, JP Morgan, Bob Grubbs, and Stephanie Peacock. To those that I have trusted my life to, thanks for being there.

I would like to thank my family for their constant love and support. Throughout my life they have encouraged and supported me in all of my various endeavors. I owe more than I can ever hope to repay. Finally, I thank my girlfriend Amy who continues to inspire me more everyday. To all of the people mentioned above and some that I am sure I have failed to mention, you have made my life rich. Thank you, everyone!

Abstract

To circumvent problems associated with rapid mixing we have used photolabile protecting groups for rapid initiation of biochemical processes. Specifically we have utilized laser triggering to initiate electron transfer in quinol-oxidizing enzymes and to study conformational changes in proteins.

In order to probe the reaction chemistry of respiratory quinol-oxidizing enzymes on a rapid time scale, a photoreleasable quinol substrate was synthesized by coupling decylubiquinol with the water-soluble protecting group 3',5'-bis(carboxymethoxy)benzoin (BCMB). Photolysis of DQ-BCMB led to the release of the BCMB group in less than 10^{-6} s. The electron transfer from decylubiquinol to the respiratory enzymes *Escherichia coli* cytochrome bo_3 and mitochondrial cytochrome bc_1 was studied using "caged" decylubiquinol. Cytochrome bc_1 reacted with photoreleased decylubiquinol with distinct kinetic phases corresponding to rapid *b*-heme reduction and slower *c*-heme reduction. The discrimination of kinetic phases in the reaction of cytochrome bc_1 with ubiquinol substrates has provided a means of exploring the bifurcation of electron transfer that is central to the operation of the Q-cycle in this enzyme.

A general, rapid method for triggering protein unfolding and folding has been developed using the photolabile protecting group 3',5'-dimethoxybenzoin (DMB) and the photolabile linker 3'-(carboxymethoxy)benzoin (CMB) respectively. To study unfolding the DMB group was introduced in a site-specific manner to block a mutation known to destabilize the GCN4-p1 coiled-coil. Upon photolysis, the unfavorable interaction is unmasked and the peptide unfolds allowing for kinetic characterization.

The 35 amino-acid headpiece subdomain of the actin bundling protein Villin was constrained in a non-native state by cyclization of the N-terminus to a cysteine residue introduced in the middle of the protein. Since destabilization of the native state is accomplished by the conformational constraint of a head-to-side chain cyclization, the folding of the Villin headpiece can be initiated by rapid photolysis of the photolabile linker. The ensuing folding process was studied in real time, in the absence of added denaturants. This work demonstrates a general methodology for studying early events in protein folding, a process that is crucial for the understanding of how a protein reaches its native state.

Table of Contents

Abbreviations and Nomenclature

Aaa	a generic amino acid
BCMB	3′,5′-Bis(carboxymethoxy)benzoin
Boc	t-Butyloxycarbonyl-
BOP	Benzotriazole-1-yl-oxy-tris-(dimethylamino)-phophoniumhexafluorophosphate
BrAc-	Bromoacetyl
BrAc-CMB	*O*-Bromoacetyl-3′-carboxymethoxybenzoin
CD	Circular dichroism
CMB	3′-carboxymethoxybenzoin
CMBD	(±)-1-Hydroxy-1-[3-(carboxymethoxy)phenyl]-2-phenyl-2-(1,3-dithian-2-yl)ethane
CO	Carbon monoxide
Dab	L-α,γ-diaminobutyric acid
DBU	1,8-Diazabicyclo[5.4.0]undec-7-ene
DCC	N,N-Dicyclohexylcarbodiimide
DDM	*n*-dodecyl-β-D-maltoside
DCM	Dichloromethane
DIEA	N,N-Diisopropylethylamine
DIPCDI	Diisopropylcarbodiimide
DMAP	N,N-Dimethylaminopyridine
DMB	3′,5′-Dimethoxybenzoin
DMBoc	3′,5′-Dimethoxybenzoinyl-oxycarbonyl-
DMF	N,N-Dimethylformamide
DQ	decylubiquinone
DQ-BCMB	carbonate ester of decylubiquinol and 3',5'-bis(carboxymethoxy)benzoin
DQ-CO_2	carbonate monoester of decylubiquinol
DQH_2	decylubiquinol
EDT	1,2-Ethanedithiol
FAB-MS	Fast atom bombardment mass spectrometry
Fmoc	Fluorenylmethyl-oxycarbonyl
Gdm·Cl	Guanidinium chloride
HBTU	2-(1H-Benzotriazole-1-yl)-1,1,3,3-tetramethyluronium hexafluorophosphate
HMB	2-Hydroxy-4-methoxybenzyl
HOBt	N-Hydroxybenzotriazole
IR	Infrared
MALDI-TOF	Matrix assisted laser desorption / ionization - time of flight
Mmt	p-Methoxytrityl-
MS	Mass Spectrometry

MTBE	Methyl t-butyl ether
Na-PO_4	sodium phosphate buffer
NMP	N-Methylpyrrolidone
PAC	Photoacoustic calorimetry
Pbf	2,2,4,6,7-Pentamethyldihydrobenzofuran-5-sulfonyl-
PTOC	pyridine-2-thioneoxycarbonyl
Q	ubiquinone
$Q^{\bullet}$	ubisemiquinone
QH_2	ubiquinol
Reagent K	82.5% TFA / 2.5% EDT / 5% phenol / 5% thioanisole / 5% water
RP-HPLC	Reversed-phase high pressure liquid chromatography
S-Bz	Benzyl mercaptam
TBAF	Tetrabutylammonium fluoride
TBTU	2-(1H-Benzotriazole-1-yl)-1,1,3,3-tetramethyluronium tetrafluoroborate
TFA	Trifluoroacetic acid
TGR©	Tentagel rink resin
THF	Tetrahydrofuran
TIS	Triisopropylsilane
TMS	tetramethylsilane
T-jump	Temperature jump
Trt	Trityl
VHP	Villin headpiece subdomain

Standard three letter amino acid abbreviations are used throughout the text, with the first letter capitalized, i.e., Aaa. Standard designations for amino acid protecting groups are used. One-letter amino acid abbreviations, with capital letters, are used for sequences. Any unnatural amino acids or linkers are set off from the sequence with hyphens, to distinguish them from the sequence information. Side chain protecting groups at specific positions in the sequence are set off with parentheses, as above. When a mutation is specified in abbreviated sequence names, it is specified by the one-letter code for the original residue, followed by the sequence position number, followed by the new residue, i.e., VHP-34 (M12C).

Chapter 1:

Using Photochemically Sensitive Compounds to Cage Biomolecules

Introduction

Chemical kinetics includes two distinct parts: One is the measurement of the rate of a reaction and its dependence on experimental conditions; the second step is to explain the effects in terms of a molecular mechanism. Dynamic processes such as energy conversion and consumption, molecule biosynthesis, and even evolution permeate all of biology. Some of these such as our visual response or the folding of a synthesized protein are exceedingly fast even though they represent the consequences of a complicated chain of events. The goal of kinetic experiments in general is to measure individual rates of these events so that a detailed description of the molecular processes can be obtained.

The most widely used approach for initiating biochemical reactions that occur on the sub-minute time scale relies on turbulent mixing to achieve a rapid change in solvent conditions or introduction of substrate. Rapid mixing methods allow the use of a wide range of solution conditions and detection methods, which is a main reason for its popularity. However, the study of many biological events such as muscle contraction and neuron excitation are not amenable to this technique due to the specific sample preparations necessary. Rapid mixing requires sample species that are freely soluble in buffer; this excludes the study of insoluble macromolecular species and whole cells. Until recently, experimental studies of this type have been limited to a time resolution of approximately 2 to 5 milliseconds. A remarkable feature of many biochemical reactions observed by stopped-flow methods is the presence of a submillisecond burst phase. Within this short time scale much of the reaction is over. In fact, some enzymes such as Superoxide Dismutase catalyze reactions with a rate that is close to the diffusion-

controlled association rate (10^9 s^{-1} M^{-1}).[1] The upper limit on the rate constant of unimolecular or intramolecular reaction is the frequency of a molecular vibration, about 10^{12} to 10^{13} s^{-1}. However, the majority of biochemical reactions take place on the 10^1 to 10^6 s^{-1} time scale. The development of new techniques for initiating and following reactions on the submillisecond time scale has been developed to probe the fast biochemical events.

To allow for the real-time analysis of fast chemical reactions, chemists have developed the technique of flash photolysis. In 1959, Gibson and coworkers used this method for the first time to study the dissociation of CO from carboxy-hemoglobin and myoglobin, and the subsequent recombination with CO and other ligands.[2] Unlike rapid mixing and sampling methods, this type of flash photolysis cannot be generally applied to reactions because a suitable photo-trigger for the reaction is rarely available. In 1978, this was changed by the introduction of using the general procedure of photolabile-caged compounds to trigger flash photolysis reactions.[3] In this work Hoffman and coworkers used a photoprotecting group to "cage" ATP and GTP (Figure 1). This technique involves exposing the sample to a brief flash of light and then monitoring the contents of the reaction. Originally discharge lamps were used for flashes with pulses of about 10^5 s^{-1}. Today most work is done with lasers that achieve coherent pulses of about 10^9 s^{-1}, with 10^{15} s^{-1} possible using mode-locking techniques so that, ultimately, the time resolution is dictated by the chemical photolysis event. The applicability of this method depends on an appropriate chromophore to absorb a photon and keep the system of interest away from equilibrium. Any number of physical methods may then be used to follow the resulting kinetic events.

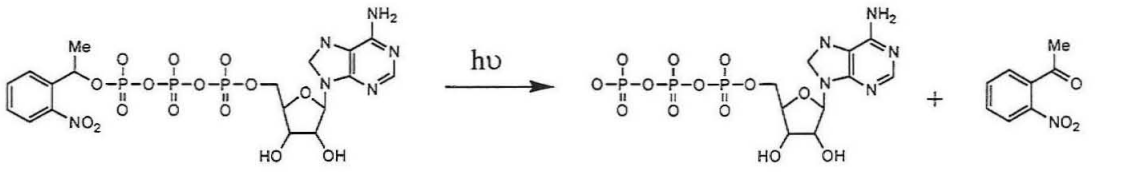

Caged ATP (inactive) ATP (active) Photoproduct

Figure 1. Nitrobenzyl caged ATP photolysis.

The advantages of this technique over conventional methods for initiating chemical kinetics are substrate release can be controlled both spatial distribution and concentration; the photoprotected substrate can be dispersed throughout a biological sample for uniform initiation before the molecule elicits its normal molecular action; and the temporal release can be varied over a range of second to picosecond time domains by first order rates, making it possible to use caged compound to pursue kinetic analysis of almost any biochemical process. Disadvantages of this method include the need to purchase or synthesize the photoprotected compound, which can be difficult or expensive; specialized equipment for fast initiation and observation of the subsequent kinetics; and the possibility of interference from resulting photochemistry and side-products. Despite these disadvantages the method of flash photolysis remains to be one of the all around most powerful methods for studying kinetics in biochemical systems.

Caging Groups

The usefulness of a photolabile protecting group is determined by several criteria: (1) the ease of modification of the functional group; (2) its reactivity towards

biomaterials; (3) the efficiency of photoremoval in terms of both the quantum yield and rate of photolysis; (4) stability to hydrolysis; (5) excitation above 300nm to avoid absorbance competition with the biological molecules; (6) and solubility under the conditions of the experiment. These criteria are seldom met in their entirety. Depending on the requirements of the application, a suitable compromise can be obtained. The first four compound classes listed in Table 1 will be described in this section: 2-nitrobenzyl substituents due to their prominence in the field of flash photolysis; benzoin; and N-hydroxypyridine-2-thione ester groups as they are the caging groups that were used in this work.

Photolysis mechanism	Ref #
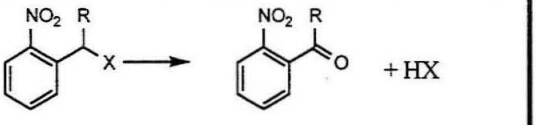	4, 5
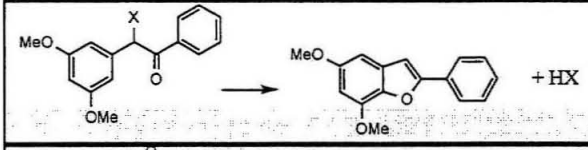	8
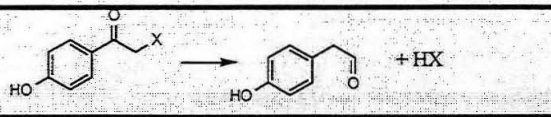	17, 18
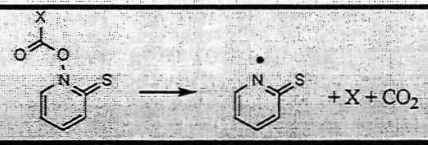	16
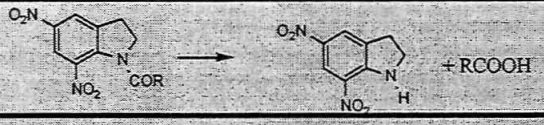	32
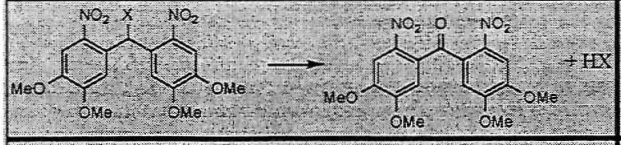	33
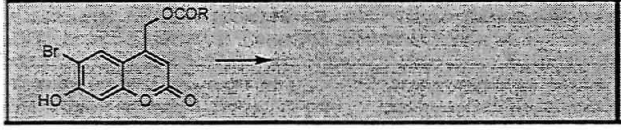	34

Table 1. Photolabile protecting groups that have been used in flash photolysis studies.

2-Nitrobenzyl Groups

By far, the most frequently used caging compounds are substituted 2-nitrobenzyl derivatives (Table 1A). 2-Nitrobenzyl is a general protecting group for chemical funtionalities, such as carboxylic acids, amines, phosphates, aldehydes and alcohols (through a carbonate linkage).[4] The kinetics and quantum yields for photolysis of 2-nitrobenzyl esters depend on the compound being caged; typical vales are around $\phi = 0.1$ and $\tau_{1/2} = 10$ μs to 100 ms.[5]

The substituted derivatives are normally used as caged compounds over the non-substituted because the photolyses proceed more smoothly with substituted compounds and by-products are nitrosoketones rather than the highly reactive 2-nitrobenzaldehyde.[3] α-carboxy-2-nitrobenzyl (CNB) and 1-(2-nitrophenyl)ethyl (NPE) are two commonly used versions. In fact over 30 compounds that use these cages are commercially available. One of the reasons for the popularity of this caging group is its ease of synthesis. This is facilitated by the availability of the starting material 1-(2-nitrophenyl)diazoethane and related compounds. These diazo compounds react with weak acids in mixed solvents to form in high yields compounds that are readily isolated. Regardless of their wide availability, ease of manipulation, and general inertness to biomaterials, these cages are generally too slow to be used for studying rapid biomolecular reaction chemistry (<ms). Another drawback is that this group can reduce metal centers in proteins instead of undergoing photolysis[6] and intermediates involved in NPE release have been shown to alter proteins.[7]

Benzoin Based

Sheehan and coworkers showed that *O*-acetyl-3',5'-dimethoxybenzoin (DMB) photolyzes with a concomitant release of acetate, with a rate constant estimated at $>10^{10}$ s^{-1}.[8] Subsequent to this work these cages have been reported to photolyze with rates exceeding 10^{10} s^{-1} and quantum yields of 0.67 to give the inert photoproduct 5,7-dimethoxy-2-phenyl-benzofuran and the caged substrate (Table #1c). Under purely aqueous conditions, however, the benzofuran is also produced, but only in about 30% overall yield. The remainder of the cage compound is undergoing photosolvolysis to produce the free cage molecule. This group has proposed a mechanism that takes this new finding into account. The key element of this mechanism is that the first intermediate is a biradical that can undergo acetoxy migration, which can then re-aromatize to give the benzofuran or undergo nucleophilic attack by water to produce the free benzoin. When studies are carried out in increasingly aqueous solutions, the free base benzoin shows up as a photoproduct. These results show that the benzylic carbon must be accessible to nucleophilic attack by water at some point along the photolysis pathway. At first, this would seem to disfavor an oxetane **1** intermediate, postulated by Sheehan, in preference to intermediates such as the cation **2**, proposed by Givens[9,10] and others[11,12] for the photolysis of benzoinyl phosphates. However, an argument against the direct formation of cation **2** is that such heterolytic cleavage is usually seen for π,π^* excited states of benzyl esters, not for the benzoyl n,π^* excited state that is responsible for this particular cyclization.[8] A modified version of Sheehan's original mechanism that can account for the product photochemistry from the carbonyl n,π^* state is proposed as follows; instead of the direct formation of the oxetane, the first intermediate is a

biradical.[13] This biradical can undergo an acetoxy migration, which can then re-aromatize to give the benzofuran photoproduct, or can undergo nucleophilic attack by water to produce the free base.

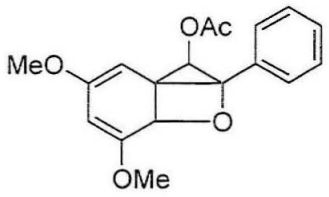

1

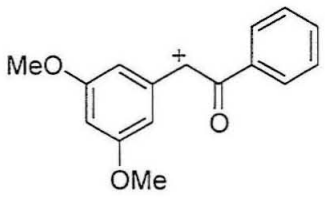

2

Figure 2. Possible intermediates in the benzoin photolysis pathway.

The advantages of DMB esters have led to their use as protecting groups for carboxylates, phosphates, and amines. Pirrung and coworkers extended the methodology to derivatize alcohols using a carbonate linkage.[11] However, biological applications have been limited due to insolubility of the benzoin cages. To make these compounds soluble, two negative charges have been introduced to produce 3',5'-bis(carboxymethoxy)benzoin (BCMB) by this group.[14]

N-hydroxypyridine-2-thione esters

N-hydroxypyridine-2-thione esters, also called thiohydroxamic esters, have been used extensively as a mild source of carbon-centered radicals that have been trapped in a variety of ways for synthetic purposes. The N-hydroxy-2-pyridone group was developed by Taylor, used for kinetic studies by Redmond *et al.*,[15] and further developed for biochemical kinetic studies by Redmond and Stubbe.[16]

The reaction mechanism most likely involves homolytic cleavage of the N-O bond, leading to the formation of a 2-pyridylthiyl radical (PyS$^{\bullet}$) and RCOO$^{\bullet}$ an acyloxy radical. When R is an aliphatic molecule, decarboxylation is expected to occur rapidly to

give a carbon-centered radical. Initial N-O bond cleavage occurs with a quantum yield of approximately 0.5 and delayed consumption of the ground-state ester occurs with a rate constant of 3-4 x 10^9 M^{-1} s^{-1}. While this caging strategy allows for the rapid decarboxylation of alcohols, a general feature that is unsatisfied by other cages, its use has been limited in biological studies due to the highly reactive 2-pyridylthiyl radical.

4-Hydroxyphenacyl Based Cages

This caging group stems from methoxyphenacyl work presented by Sheehan and Umezawa.[17] This carboxyl-photosensitive protecting group is reported to photolyze by irradiation of greater than 330 nm. Givens and coworkers reported the use of the p-hydroxyphenacyl (pHP) group as a phototrigger used to release a variety of biological compounds such as ATP, GABA and amino acids. They found that the pHP group was transformed via an overall solvolytic rearrangement to give p-hydroxyphenylacetic acid. The proposed mechanism for this reaction involves the triplet excited state of the p-HP chromophore yielding the free carboxylate and p-hydroxyphenylacetic acid. The rearrangement is preceded by an excited state deprotection of the phenolic proton to give the triplet phenolate ion; this apparently provides the driving force for the rearrangement. An important feature of this mechanism is that the leaving group is lost before rearrangement to the cyclo-dienone intermediate. Stern-Volmer analysis suggests rates for the release of substrate is in excess of 10^8 s^{-1}. Quantum yields are fairly low with values ranging from ϕ = 0.05 to 0.3.[18] These photoprotecting groups should see increased use due to their ease of synthesis and general stability.

Other cages

The bis(2-niro-4,5-dimethoxyphenyl)methyl group (Table 1e.), which essentially incorporates two 2-nitrobenzyl substituents, was found to be the most reactive nitrobenzyl based compound for protecting carboxylates. This caging group merits new attention when compared with the alternative NB based cages. 5,7-dinitroindolinylamide undergoes photosolvolysis for the release of carboxylates. It has been reported that this reaction can be initiated beyond 400 nm and is more photosensitive when compared to the dimethoxy nitrobenzyl group.

The goal of producing photoprotecting groups that photolyze in the visible has been on the minds of many chemists. These wavelengths are more convenient optically, better able to penetrate biological tissues, less damaging to biological samples, and would interfere less with observation of the sample. There are a number of potential applications that would become possible if such cages where readily available such as site specific drug release in treating human disease. Unfortunately molecules that are sensitive to visible light tend to have more complex, extended chromophores and are experimentally more difficult to work with and synthesize.

Synthesis and Characterization of Caged Compounds

One difficulty in the synthesis of caged compounds is premature photolysis. Often it is necessary to work with these compounds under subdued light. Hydrolysis is another difficulty often making purification of the end product challenging, as many of the biomolecules to be caged are charged and require aqueous solutions for solubilization. Many of the caging compounds described in this chapter are sensitive to

strong acids and bases, and oxidizing condition. This results in a narrow set of reaction conditions that the compounds must be manipulated under, often requiring non-standard mild synthetic conditions. Traditionally benzoin condensation has been carried out by the treatment of an aromatic aldehyde with potassium cyanide or sodium cyanide, usually in aqueous ethanolic solution. The condensation is greatly affected by the nature of the substituents in the aromatic nucleus and many of the substituted benzaldehydes either do not react or yield products other than benzoins. In addition, to form a unsymmetrical benzoin one aldehyde must contain a relatively unsaturated carbonyl group and the other must have a mobile hydrogen.

In this lab, the synthesis of the benzoin group has been accomplished with dithiane protection of the benzoyl carbonyl to circumvent photoylsis during manipulation.[19] Photolysis of the linker is therefore prevented, until this "safety-catch" is removed. In theory, these dithianes may be removed under a variety of mild reaction conditions, and many compounds may be caged and manipulated without photolysis, until the dithiane is removed. However, it has been found that the dithiane reduces the cage-substrate coupling efficiency in most cases and upon oxidation results in high yields of side products.

Interest in photochemical switching systems originates not only from the basic goal of elucidating complex biological mechanisms but also from the practical applications of such caged molecules. The use of protecting groups as a means of conducting selective reactions on multifunctional organic compounds has been reviewed from a chemical standpoint.[4,20] Photosensitive protecting groups provide a general route to generate unprotected compound by photochemical liberation.

Rates of Photolysis

Historically photolabile-protecting groups have been used as protecting groups in organic synthesis that are removed by light in otherwise mild conditions. Illumination was continuous and little insight was gained about the rate of photolysis. Application of caged compounds to study biological mechanisms has required knowledge about the kinetics of their photolysis. Kinetic rates and mechanisms of photorelease can be investigated by flash photolysis experiments. In general reactions that follow the initial photochemical excitation are likely to be the rate-limiting step in release of the caged compound. A major difficulty of the kinetic experiments aimed at elucidating the photolysis mechanism is that often the product of biological interest does not have a visible chromophore. Rapid spectroscopic investigations can often be used to observe an early charge transfer intermediate; this step is often facilitated by intermediates that contain a radical species. The majority of kinetic studies on caged compounds are carried out in mixed organic/aqueous solvent systems. Caution needs to be taken when extrapolating the values obtained in these studies to aqueous solutions, as the photolysis mechanism are often different, as in the case of DMB.

Extent of Photolysis

A critical parameter for a caged compound is its quantum yield, Q_p, defined as the fraction of molecules of product formed per photon absorbed. This value must be measured experimentally for each photochemical reaction. Measurements of Q_p can be

made by actinometry; often the value is obtained by comparison with compounds of known Q_p.

More often the experimentalist needs to know the concentration of compound released by a single light pulse. The fraction of caged compound photolysed is an empirical parameter that is directly related to Q_p, but may be different. The reasons can be due to inner-filter effects, and when excitation times are longer than the excited state lifetime of the compound such that several excitation events are initiated.[21] A critical factor relating Q_p to the amount of photolysis of a compound is its extinction coefficient at the irradiation wavelength. Some have suggested that an absorption of 0.7 by the caged compound is optimal as higher would lead to nonuniform photolysis.[22] In principal, one way to enhance these values, especially compounds that photolyze via the triplet state, is by energy transfer through the action of sensitizers.[23] A quencher of photochemical reactions, dissolved oxygen will bring this value down.

Caged Substrates

Attachment of a caging group requires the presence of an appropriate chemical functionality in the compound of interest. Phosphates, carboxylates, amines, amides, thiols, and phenols have all been shown to be suitable sites, to a lesser or greater extent, for attachment of a photoprotecting group.[24,25] Carboxylates and phenols will be discussed as the work herein deals primarily with the caging of these two functionalities.

Carboxylates

Although caged carboxylates have been known in the literature for a long time[26] it was only until 1990 that their utility has been used to study rapid biological kinetics.[27] Carboxylates are relatively easy to synthesis when compared to most other chemical functionalities that have been caged. A common method is through the use of the corresponding acid halide. The resulting esters are in most case stable for several days but often undergo hydrolysis in aqueous solutions to varying extents.

Phenols

Photochemical protection of phenols and alcohols has not been widely investigated. Researchers in the carbohydrate field have carried out the photolabile protection of alcohols, principally where 2-nitrobenzyl glycosides have been used for synthetic applications. 2-Nitrobenzyl carbonates have been used to protect alcohols but are readily hydrolyzed in aqueous solutions. In these systems the initial release of the carbamic acid is unlikely to be rate limiting. Instead, the slow step is the final decarboxylation of the carbamic acid to generate the alcohol, which takes a few milliseconds at pH 7.2 and faster at more acidic pH.

Caged Peptides and Enzymes

Photocleavable ligands have become an important tool used in enzymology and more generally biochemistry. The caging of amino acid side chains within a polypeptide backbone has enabled researchers to determine the affinity and selectivity of protein-

ligand interactions and protein-protein interactions, identify binding sites, and even identify the targets of therapeutics. Three different approaches have been utilized: (1) photoactivation and release of caged ligands; (2) photoactivation and release of caged proteins; and (3) photoimmobilization of ligands onto surfaces. Introduction of the photoreactive group is usually through condensation with a carboxylate to form an ester linkage. Difficulty usually arises from the presence of several nucliophilic groups present in the molecule to be caged. One strategy for obtaining selectively caged proteins or ligands is to cage an introduced cysteine (so that only one is present); the other is the 'shotgun' approach where the protection reaction is carried out nonspecifically and the resulting products are separated to give homogeneous sample (often wishful thinking).

Developing Photolabile Protecting Groups as Linkers

The photolabile groups described above have one functional group for attachment of the cage to a molecule of interest, rendering them unsuitable for bifunctional linkage. The concept of using photolysis to effect cleavage of a compound from another molecule is by no means new; the use of a photoprotecting group on a solid support was reported over twenty-five years ago.[28] Since this time various groups have used photolabile groups to selectively release protected peptide fragments from solid supports.[29] These resins can now be purchased from commercial sources. Additionally, the nitrobenzyl group has been used to develop a photocleavable biotin labeling compound for general biotin isolation and release of labeled compounds.[30] The synthesis of a photolabile linker based on the BCMB group was accomplished by this group.[31] This linker can be used to rapidly release two tethered chemical functionalities. The photolysis maximum

occurs around 300 nm but extends out to 360 nm, which allows photolysis to proceed without competing absorption by biological sample that absorb further to the blue. The benzylic hydroxyl of the parent linker was protected with Fmoc so that the carboxymethoxy group could be coupled to the N-terminus of a growing peptide chain by standard solid phase peptide synthesis (SPPS). It was found that this amide bond formation and the following Fmoc removal was facile. However, the following coupling of the benzylic hydroxyl group to the carboxyl group of the incoming amino acid was difficult at best, resulting in extremely poor coupling efficiencies even with non-branched amino acids. This work provides the starting point for using the benzoin cage as a photolabile linker.

Conclusions and Thesis Focus

Photolabile "caged compounds" are inert precursors of active molecules that are modified chemically by the attachment of a photolabile protecting group. These compounds can be equilibrated with biological samples. The active parent molecule can then be released from its cage by irradiation with a pulse of light in the near ultraviolet. The use of short pulses of light produces spatial and temporal quantity-specific jumps in concentration. The associated biochemical responses resulting from the release of the active molecule can thus be studied in a time frame that is roughly an order of magnitude slower than the photolysis event. In the case of benzoin cages, this is in the nanoseconds time frame. The general strategy of using photosensitive protecting groups to release the active form of biological molecules from an inert precursor is a powerful method for

studying biochemical kinetics. This technique eliminates many of the difficulties and limitations associated with rapid mixing and other relaxation experiments.

To understand the mechanism in which ubiquinol oxidation chemistry is linked to proton translocation and gating in cytochrome bc1, it is essential to know the details of the intermolecular electron transfer. Section I starts with an Introduction of the cytochrome bc1 complex, its proposed mechanism and structure in Chapter 2. Chapters 3 and 4 will describe the synthesis and characterization of two caged ubiquinols that have been designed to initiate rapid two-electron transfer into quinol oxidizing enzymes. Chapter 5 describes the use of the previously described caged substrates to measure specific electron transfer events in the respiratory enzymes cytochrome bc_1 and cytochrome bo_3.

Section II of this work will focus on the development of methods for the rapid triggering of protein folding using photolabile-protecting groups. Chapter 6 will introduce the protein folding problem and relevant current experimental techniques. Chapter 7 will describe the use of a photolabile protecting group used to initiate protein unfolding in the GCN4-p1 coiled-coil polypeptide system. Characterization of the rapid unfolding kinetics in this system will also be given. Finally, Chapter 8 will describe the incorporation of a photolabile linker into the backbone of a small α-helical protein and time resolved studies on the folding of this protein.

References

1)Bertini, I.; Mangani, S.; Viezzoli, M. S. *Adv Inorg Chem* **1998**, *45*, 127.

2)Gibson, Q. H. *Progr. Biophys. Biophys. Chem.* **1959**, *2*, 1.

3)Kaplan, J. H.; Forbush, B., 3rd; Hoffman, J. F. *Biochemistry* **1978**, *17*, 1929-35.

4)Binkley, R. W.; Flechtner, T. W. *Synthetic Organic Photochemistry*; Horspool, W. M., Ed.; Plenum Press: New York, **1984**, pp 375-423.

5)Zhu, Q. Q.; Schnabel, W.; Schupp, H. *J. Photochem.* **1987**, *39*, 317-332.

6)DiMagno, T. J.; Stowell, M. H. B.; Chan, S. I. *J. Phys. Chem.* **1995**, *99*, 13038-13047.

7)Du, X.; Frei, H.; Kim, S. H. *Biopolymers* **2001**, *62*, 147-9.

8)Sheehan, J. C.; Wilson, R. M.; Oxford, A. W. *J. Am. Chem. Soc.* **1971**, *93*, 7222-7228.

9)Givens, R. S.; Athey, P. S.; Kueper, L. W.; Matuszewski, B.; Xue, J. *J. Am. Chem. Soc.* **1992**, *114*, 8708-8710.

10)Givens, R. S.; Athey, P. S.; Matuszewski, B.; Kueper, L. W.; Xue, J.; Fister, T. *J. Am. Chem. Soc.* **1993**, *115*, 6001-6012.

11)Pirrung, M. C.; Shuey, S. W. *J. Org. Chem.* **1994**, *59*, 3890-3897.

12)Cameron, J. F.; Wilson, C. G.; Fréchet, J. M. J. *J. Chem. Soc. Chem. Commun.* **1995**, 923-924.

13)Turro, N. J. *Modern molecular photochemistry*; Benjamin/Cummings Pub. Co., Inc.: Menlo Park, **1978**.

14)Rock, R. S.; Chan, S. I. *J. Am. Chem. Soc.* **1998**, *120*, 10766.

15)Aveline, B. M.; Kochevar, I. E.; Redmond, R. W. *J. Am. Chem. Soc.* **1995**, *117*, 9699-9708.

16)Burdi, D.; Aveline, B. M.; Wood, P. D.; Stubbe, J.; Redmond, R. W. *J. Am. Chem. Soc.* **1997**, *119*, 6457.

17)Sheehan, J. C.; Umezawa, K. *J Org Chem* **1973**, *38*, 3771-74.

18)Givens, R. S.; Weber, J. F. W.; Conrad, P. G.; Orosz, G.; Donahue, S. L.; Thayer, S. A. *J. Am. Chem. Soc.* **2000**, *122*, 2687-2697.

19)Stowell, M. H. B.; Rock, R. S.; Rees, D. C.; Chan, S. I. *Tet. Lett.* **1996**, *37*, 307-310.

20)Greene, T. W. *Protective Groups in Organic Synthesis*; Wiley: New York, **1980**.

21)Corrie, J. E. T.; Trentham, D. R. *J. Chem. Soc. Perkin Trans. 1* **1992**, 2409-2417.

22)Scheidig, A. J.; Pai, E. F.; Schlichting, I.; Corrie, J.; Reid, G. P.; Wittinghofer, A.; Goody, R. S. *Philosophical Transactions of the Royal Society of London Series a-Mathematical Physical and Engineering Sciences* **1992**, *340*, 263

23)Turro, N. J. *Photochem Photobiol* **1969**, *9*, 555-63.

24)Adams, S. R.; Tsien, R. Y. *Ann. Rev. Of Physiol.* **1993**, *55*, 755-784.

25)Corrie, J. E. T.; Trentham, D. R. *Caged Nucleotides and Neurotransmitters*; Morrison, H. J., Ed.; Wiley: New York, **1993**; Vol. 2, pp 243.

26)Barltrop, J. A.; Plant, P. J.; Shofield, P. *Chem. Commun.* **1966**, 822.

27)Wilcox, M.; Viola, R. W.; Johson, K. W. *J. Org. Chem.* **1990**, *55*, 1585.

28)Rich, D. H. *J. Am. Chem. Soc.* **1975**, *97*, 778.

29)Holmes, C. P.; Jones, D. G. *J Org. Chem.* **1995**, *60*, 2318.

30)Olejnik, J.; Sonar, S.; Krzymanska-Olejnik, E.; Rothschild, K. J. *Proc Natl Acad Sci U S A* **1995**, *92*, 7590-4.

31)Rock, R. S.; Chan, S.I. *J. Org. Chem.* **1996**, *61*, 1526-1529.

32)Adams, S. R.; Kao, J. P.; Tsien R. Y. *J. Am. Chem. Soc.* **1989**, 111, 3212-20.

33)Amit, B.; Ben-Efraim, D. A.; Patchornik, A. *J. Am. Chem. Soc.* **1976**, 98, 843-44.

Section I

Chapter 2:
Ubihydroquinone/Cytochrome C Oxidoreductase: Mechanism of a Respiratory Enzyme

Abstract

In this work, the mechanism by which complex III accomplishes its role in respiration and the structural bases for its action are discussed. The mechanism and efficiency of proton translocation are also analyzed in terms of thermodynamics of the substrate transformations catalyzed by this enzyme. The first section describes the structural details of the complex. The next section addresses our current understanding of the energy transducing capabilities of cytochrome bc_1, and emphasizes the proposed mechanisms in terms of the current structural and biochemical knowledge.

Introduction

Adenosine triphosphate (ATP) is the central energy currency for life. The principal source of cellular ATP is formed in the process of oxidative phoshorylation (respiratory electron transport) carried out in mitochondria. Mitochondria are present in all organisms that have differentiated cells (eukareotes). They are small (1μm) membrane-surrounded structures in which oxidative metabolism occurs. The enzymes of this respiratory chain serve as proton pumps, using the energy made available from metabolic processes to transport protons across the inner mitochondrial membrane creating an electrochemical gradient used for the production of ATP. This process of cellular respiration is remarkably efficient providing roughly 20 molecules of ATP for every molecule of glucose and 84 ATP molecules for every molecule of the fatty acid palmitate.[1,2]

Figure 1 summarizes the state of our structural understanding of the components of the oxidative phoshorylation chain. This respiratory chain of enzymes consists of NADH:ubiquinone oxidoreductase (complex I), succinate:ubiquinone oxidoreductase (Complex II, SQR), ubiquinone:cytochrome c oxidoreductase (complex III, cytochrome bc1), cytochrome c

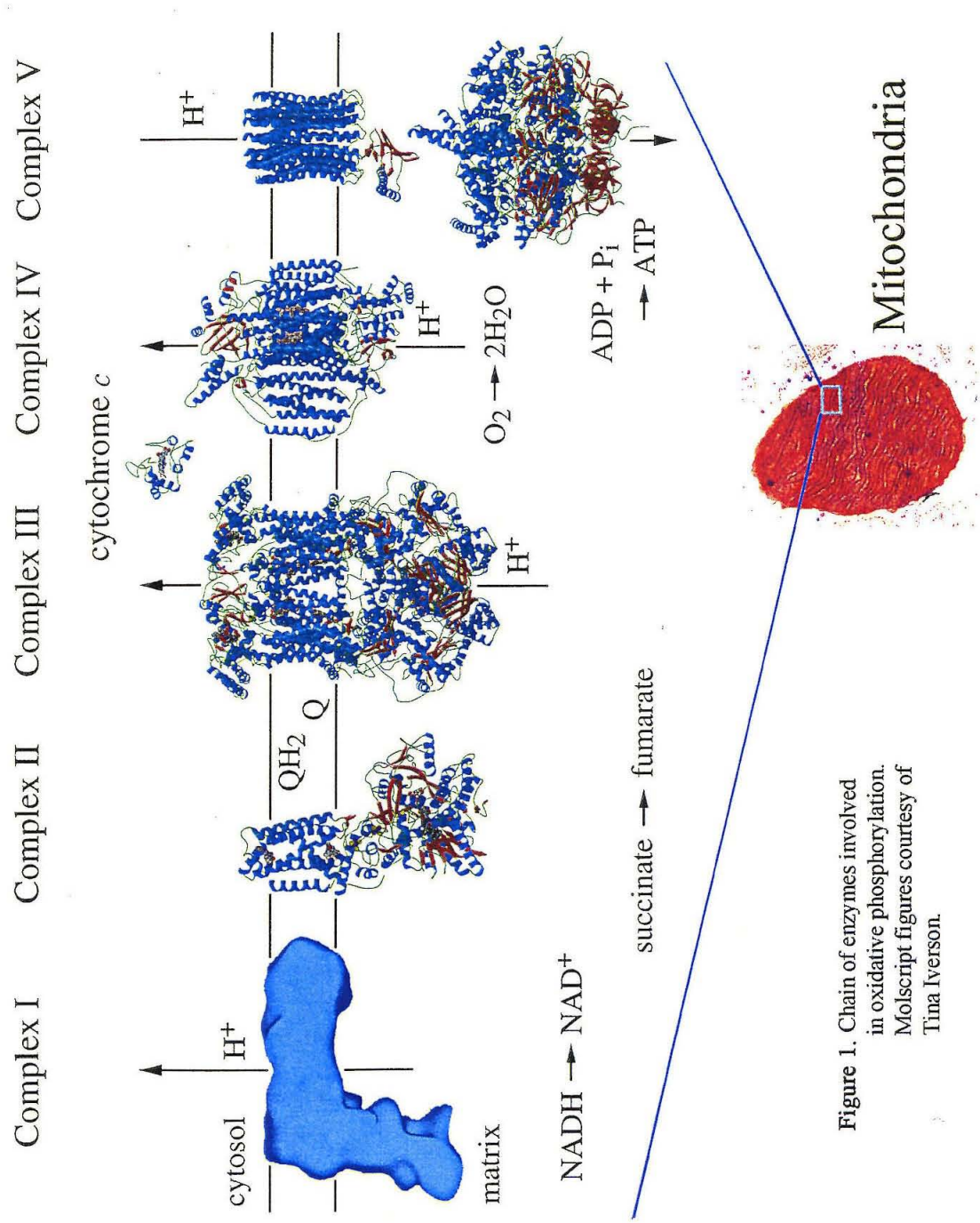

Figure 1. Chain of enzymes involved in oxidative phosphorylation. Molscript figures courtesy of Tina Iverson.

oxidase (complex IV, cytochrome oxidase), and ATP synthase (Complex V, F1F0-ATPase). Recently, X-ray crystal structures have been reported for part or all of the complexes II-V.[3-6] The complex I structure from bovine mitochondria has been solved to 22 Å resolution by electron microscopy.[7]

Complexes I, III, and IV serve as proton pumps, using the energy of electron transfers to perform the mechanical work of translocating protons from the matrix to the cytosol of the mitochondria to produce and sustain an electrochemical gradient across the inner membrane. Complex V (ATP synthase) uses the free energy released from the flow of protons back to the matrix in order to perform the chemical work of producing ATP from ADP and inorganic phosphate. This system captures the free energy available from substrate oxidation so that it may later be applied to the synthesis of ATP.

Ubiquinone –also referred to as coenzyme Q is a lipid-soluble substrate for complex III. It is a benzoquinone with four substituents, one is a long hydrophobic side chain made up of 10 repeating isoprenoid units. Ubiquinone has three oxidation states: oxidized Q, a partially reduced semiquinone free radical, and fully reduced QH_2, called ubiquinol (Figure 2). Ubiquinol is the natural substrate for complex III, supplying all electrons, and protons that are released to the cytosol.

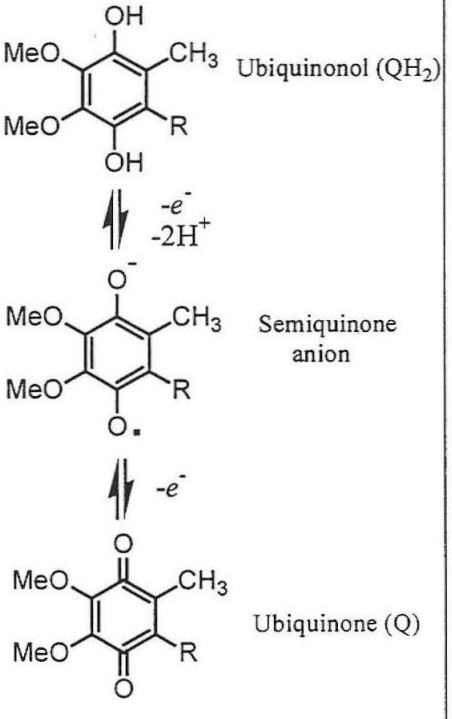

Figure 2. Oxidation of ubiquinol to ubiquinnone by two successive one-electron transfers.

Complex III (formally known as Ubihydroquinone:cytochrome c oxidoreductase) is

an integral membrane protein that forms the middle part of the respiratory chain in eukaryotes and many prokaryotes. Cytochrome bc_1 was discovered and first purified from bovine heart mitochondria in 1961.[8] Although considerable progress has been made into understanding its function, the exact mechanism of proton pumping has eluded researchers. The enzyme transfers electrons form ubiquinol (QH_2) to cytochrome c and links this electron transfer (ET) to the establishment of a proton gradient across the inner mitochondrial or bacterial plasma membrane. Cytochrome bc_1 thus contributes to the electrochemical proton gradient that drives adenosine triphosphate (ATP) synthesis.[9,10] The reaction catalyzed by the bc_1 complex is described by the equation 1, in which the subscripts "i" and "o" designate the inner (negative) and outer (positive) sides of the membrane, respectively.

$$QH_2 + 2\ \text{cyt}\ c_{ox} + 2\ H^+_i \rightarrow Q + 2\ \text{cyt}\ c_{red} + 4\ H^+_o \quad (1)$$

The bc_1 complex is a member of the bc-type complex family, that includes the b*f* cytochromes that are found in chloroplasts and in bacteria. All bc_1 complexes contain four redox prosthetic groups: a cytochrome b_{562} and b_{566}, cytochrome c_1, and a high potential iron-sulfur cluster. The mammalian enzyme is an integral membrane protein that is composed of eleven protein subunits, three of which are associated with the four-redox centers.[11] The other eight subunits are not essential for catalysis in bacteria where only the three-

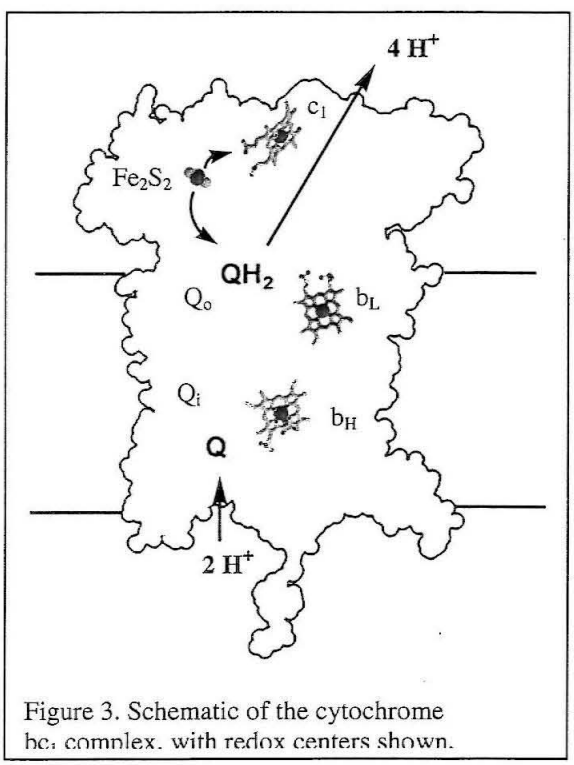

Figure 3. Schematic of the cytochrome bc_1 complex, with redox centers shown.

redox subunits are present.[9] The subunits are listed in Table 1 along with their amino acid count and molecular weight.

Table 1. The Proteins of Complex III (bovine).

Subunit	A. A. Residues	M.W.
1 Core 1	446	49132
2 Core 2	439	46471
3 Cytochrome b	379	42592
4 Cytochrome c_1	241	27288
5 Rieske Fe-S	196	21611
6 13.4 kDa	110	13347
7 "Q-Binding"	81	9590
8 c1 hinge	78	9170
9 Fe-S presequence	78	7956
10 c1 assoc.	62	7198
11 6.4 kDa	56	6363
Apo-bc1 complex	2166	240718
Fe2S2		76
Heme c_1		616
heme b_H		616
heme b_L		616
Prosthetic groups		2024
Holo-bc1 complex	2166	242,742

Structural Insights

A detailed understanding of the catalytic mechanism of this enzyme requires a structural context. Recently several X-ray crystallographic studies have been published of the bc_1 structure. The four main structures are summarized in Table 2. Analysis of enzymes from different species, with the use of inhibitors, has revealed a set of conformational states. The structural information concerning the enzyme has been consistent between the different structures with the exception of iron-sulfur protein

Table 2. Crystallographic information.

PDB Entry	1QCR	1BCC	1BE3	1BGY
Reference	*Science* 287, 60 (1997)	*Nature* 392, 677 (1998)	*Science* 281, 64 (1998)	
Protein Source	Beef heart	Chicken heart	Beef heart	
Resolution	2.7	3.16	3.0	3.0
Model Contains:	C for all 11 chains, (C-term for Cyt c1) Fe_2S2, 1 heme	Full model for 9 unit	Full model for all 11 Fe2S2, 3 hemes	
R-free	0.37	0.31	0.32	0.36
Space Group	$I4_122$	P212121	P6522	P65

location and the inhibitor binding sites, and thus the consensus structure will be described except when necessary.

The crystal structure shows that the complex resides as a symmetric homo-dimmer, in which the closely interacting monomers form two clefts through which the quinol binding pockets can be accessed. The long axis of the protein is approximately 150 Å, with 35 Å extended in the cytoplasmic space, 75 Å in the matrix space, and 40 Å inner in the mitochondrial membrane. The region in the matrix side consists primarily of core subunit 1 and 2, subunits 6 and 9, and part of subunit 7. Cytochrome b, c_1, the iron-sulfur protein, and subunits 7, 10, 11 are localized in the membrane. Subunit 8 lies solely on the cytoplasmic side along with the functional regions of Cytochrome c1, and the iron-sulfur protein.

The positions of the redox centers within the bc_1 complex and the binding sites of several respiratory inhibitors have been identified. Cytochrome b is a transmembrane protein in which the two b heme groups form an electrical circuit between the two-

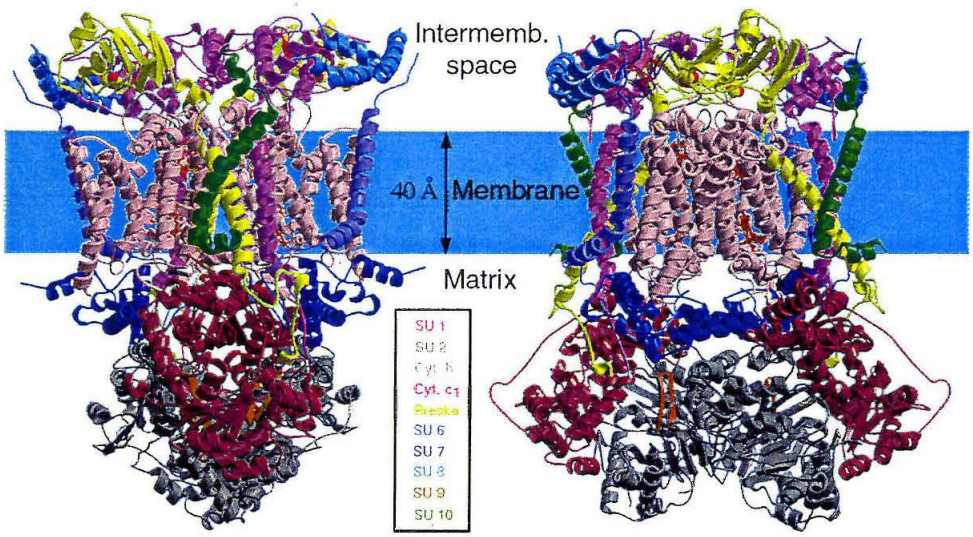

Figure 4. Structural model of the dimeric cytochrome bc1 complex with polypeptide chains drawn as ribbons. The structure to the right has been rotated by 90 degrees. The top of the structure is in the mitochondrial intermembrane space (positive or outer side), the middle is spanning the membrane bilayer, and the bottom is in the matrix (negative or inner side). Figure

ubiquinol/ubiquinone binding sites that are on each side of the membrane. The low potential b heme (b_L, or b_{566}) lies near the positive side of the membrane, and the high potential heme (b_H, or b_{562}) lies near the center of the membrane. The iron-sulfur protein (ISP) is anchored to the complex by a membrane spanning hydrophobic helix at the amino terminus of the protein.[12] Cytochrome c_1 is anchored to the membrane by a hydrophobic helix at its C-terminus, and the domain of the protein that contains the heme is accessible, where it reacts with cytochrome c.

An implication of dimer association in the bc_1 complex is the formation of two cavities (figure 5). The membrane-spanning region of each monomer in bovine structure consists of 13 transmembrane helices. Of the 13, 8 belong to cyt b; of the other 5, 1 is the C-terminal membrane anchor of cyt c_1, one is the N-terminal membrane anchor of the ISP, 1 is the C-terminal helix of subunit 7, and the other is from subunit 10. The

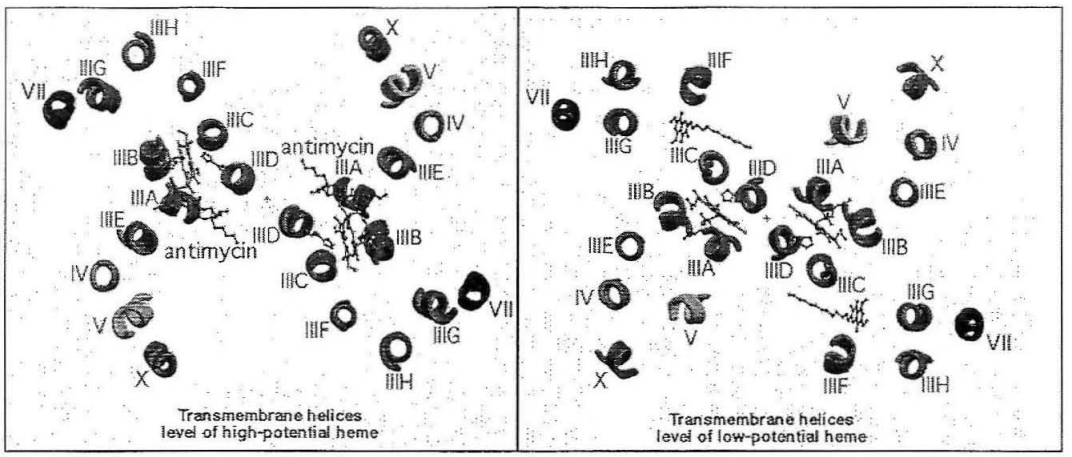

Figure 5. Ribbon diagram of the bovine structure; the ISP has been removed for the sake of clarity. The arrangement of the transmembrane helixes of the bc_1 dimer. A) Helixes on the outer (positive side of the membrane B) Helixes on the inner (negative) side of the membrane. Figure from ref. 3.

cavities are made by helices D, C, F from one cyt b monomer and D', E', A', cyt c_1, ISP, and subunit 10 from the other monomer. The Q_i pocket of one monomer and the Q_o pocket of the other monomer are accessible through the same cavity. Thus it has been proposed that quinone formed at the Q_i site can proceed to the Q_o site of the other monomer without leaving the bc_1 complex. The cavities appear tightly sealed toward the intermembrane space, but are solvent-accessible from the matrix side. This arrangement would allow proton uptake at the Q_i site from the matrix and prevent leakage of protons through the bc_1 complex. Unlike the Q_i site in this model, the Q_o site is not in direct contact with either the b_L heme or the Fe-S cluster; instead aromatic residues that surround it most likely mediate the electron transfer.

Eight transmembrane helicies (A-H), connected by loop regions, compose subunit 3 and contain the two b hemes. Both b-hemes are attached to a four helix bundle made up of helicies A-D. The close proximity of heme edges (8.2 Å) allows for efficient electron transfer between the two hemes. The Q_i binding pocket has been identified by structures in the presence and absence of the N-center inhibitor antimycin. Residues from helicies A,

D, E, and a short helix near the N-terminus of the peptide chain form this binding pocket. Electron density for the inhibitor antimycin suggests that the Q_i site is 4 Å away from the b_H heme. The Q_o binding site was identified with myxothiazol inhibitor and is 8 Å away from the b_L heme. Myxothiazol binds to the Q_o site of the bc1 complex and blocks electron transfer to both the ISP and b hemes. The binding site is surrounded by helices C, F, and ef, and the head group of myxothiazol resides in a hydrophobic pocket. A Tyrosine is between these two groups and may mediate the electron transfer from the semiquinone to the heme. Next to this binding site there is a hydrophobic channel that reaches the surface of the intermembrane space. This proposed pocket is a possible site for direct hydrogen bonding between the ubiquinol and iron-sulfur protein.

The locations of the redox centers in these structures are in good agreement with predicted distances based on EPR studie, and crystallographic data. However, the distance of 31 Å between the Fe-S cluster and the c_1 heme iron in the original structure (1QCR) is longer than expected by the observed electron transfer rate. Deisenhofer and coworkers propose a protein bridge between the two centers or a major conformational change to facilitate this electron transfer. As the following structures were solved, it was revealed that the extramembranous domain of the iron-sulfur protein could adopt a range of conformations, supporting that domain movement is an integral part of the reaction mechanism. The Fe_2S_2 center appears to undergo a rotational displacement of 57° (65° in the hexagonal crystals), resulting in a range of motion of approximately 16 Å (21 Å in

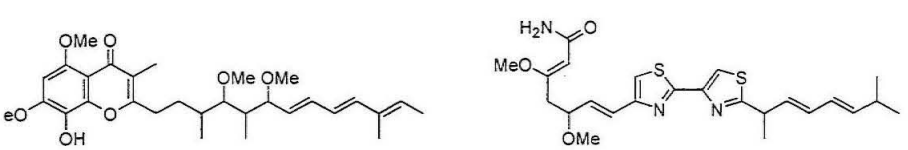

Figure 6. Q_o site inhibitors myxohtiazol (left) and stigmatellin (right).

the hexagonal crystals). The movement is from a position close to cyt c_1 in the myxohtiazol structure to a hypothetical docking interface on cyt b in the structure that contains stigmatellin. The rotational motion connecting the observed forms is made possible by a flexible linker consisting of residues 67-73 in the ISP. In the absence of inhibitors, the iron-sulfur center is adjacent to the c_1 heme, which is hydrogen bonded to His161 by propionate on the c_1 heme. The distance between the iron-sufur cluster and the b_L heme is 34 Å, and the distance to the c heme from the iron-sulfur cluster is 21 Å. Thus it is believed that this domain movement gates electron transfer by making the potentially favorable second electron transfer to the ISP impossible due to its inaccessibility (34 Å is too long of a distance for efficient electronic coupling). This possible mechanism for gating the electron-transfer events is in contrast to the more solid-state picture that is seen in most redox proteins.[13] In addition to the two positions seen in the described crystal structures for the ISP, there is a structure that shows its position intermediate between the c_1 and heme b subunits. In crystals with the Q_o site inhibitor UHDBT, there is occupation of this inhibitor intermediate between that of stigmatellin and myxothiazole, with a weak interaction with the ISP.[3] Iwata and coworkers have proposed that this is a relevant state in the gating mechanism. The dimeric structure appears to make this feature of the mechanism possible as the ISP from one monomer interacts with the cytochrome c_1 of the other monomer and is anchored by the cytochrome b proteins of each dimmer.

The Q_o site appears to have two binding modes, one distal and one proximal to the heme b_L. From these pockets there is a channel that extends to the lipid phase making ubiquinol/ubiquinone exchange possible. In the structures with the ISP located near the cytochrome b protein, the distal site opens to the ISP interface making ubiquinol/ISP contact possible.[14,15] The interface between these two proteins is conserved and tight

packing results upon association. Sequence analysis and mutagenesis studies support these findings.[16]

Cytochrome c_1 is an extramembranous domain on the cytoplasmic side of the membrane with a single transmembrane helix that anchors the subunit to the membrane. It is an all-helical protein that resembles other members of the cytochrome family. One methyl group on the porphyrin ring is solvent-exposed, likely near the binding site for cytochrome c, while one of the propionate groups of the heme extends toward the iron-sulfur protein. The most likely binding site for cytochrome c is composed of 10 acidic residues that point into the intermembrane space and surround the heme c1.[17]

The Q-cycle Mechanism

Electron transfer through cytochrome bc1 is coupled to transmembrane proton translocation with a stoichiometry of $H^+/e^- = 2$ and to the translocation of a single positive charge (*ie*, q+/e- = 1).[18] The mechanisms of electron transfer and proton translocation by cytochrome bc_1 are currently under debate. The most widely accepted and longest standing mechanism is known as the Q-cycle, which was originally proposed by Mitchell.[19] The cycle diagrammed in Figure 7, takes advantage of the fact that ubiquinol is a two-electron reductant, but is oxidized in one-electron steps. In general, cytochrome bc_1 can be thought of as a system of one high potential and one low-potential redox pathway.[20] The high potential pathway is composed of the Fe-S protein ($E_{m,7}$ = 300 mV) and cytochrome c_1 ($E_{m,7}$ = 250 mV), and the low potential pathway of cytochrome b_{566} ($E_{m,7}$ = -50 mV) and cytochrome b_{562} ($E_{m,7}$ = 50 mV). Ubiquinol donates one electron to the Fe_2S_2 protein that is then passed onto cytochrome c1. The next electron takes the low potential path to a quinone that is bound on the positive side of the membrane, creating a stabilized

semiquinone. According to the Q-cycle (figure 1.2), the withdrawal of one electron from QH_2 from the Q_o site is accompanied by vectorial release of two protons and the formation of a ubisemiquinone anion, a powerful reductant for the low-potential centers. The cycle is completed when the above steps are repeated. This time, as the second electron is passed down the low potential path, the semiquinone becomes reduced to a quinol, concomitantly taking two protons up from the matrix side of the membrane.

During one complete Q-cycle, two molecules of ubiquinol are oxidized to ubiquinones, but one molecule of ubiquinone is reduced in two steps to ubiquinol. The iron-sulfur protein, cytochrome c_1, and the two b hemes are reduced and reoxidized twice. The reduction of quinol at the Q_o site is identical, as far as we know, in the first and second half of the Q-cycle. However, at the Q_i site heme b_H reduces ubiquinone to ubisemiquinone during the first half of the Q cycle and reduces this semiquinone to ubiquinol during the second half of the cycle. The branched electron transfer of the Q-cycle doubles the efficiency of proton translocation mediated by this enzyme. This efficiency of proton pumping is made possible by bifurcation of the electron transfer with the second electron going to the high potential b heme pathway.

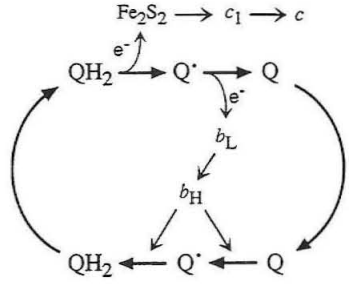

Figure 7. The Q-cycle model; the quinol at the Qi sit becomes a seiquinone in the first half of the Q-cycle and then becomes a quinone durning the second half.

One experiment that led to the formulation of the Q-cycle model observed mitochondria slowly respiring in the presence of limited oxygen, that exhibited a transiently reduced cytochrome b when pulsed with oxygen. Furthermore, this reduction of

cytochrome b was magnified if antimycin (which is known to block the Q_i site) was present. These somewhat paradoxical observations can be explained by the Q-cycle as follows: Providing a pulse of oxygen to oxygen-deprived mitochondria will oxidize the c cytochromes and the Fe-S protein, but as QH_2 becomes oxidized, it is converted to the semiquinone ($Q^{\cdot-}$) and donates electrons to cyt b, at least transiently. Thus, the pulse of oxygen must ultimately lead to a reduction of the b-hemes. In the presence of antimycin the electrons can go no further than the hemes of b cytochrome.

Over the past several years there has been experimental evidence that could not be explained by the Q-cycle mechanism, and as a result several groups have proposed modified Q-cycle mechanisms. In particular, the Q-cycle does not explain why the second electron from semiquinone at the Q_o site does not reduce the ISP even under conditions that block the b-heme pathway. The delivery of the two electrons to separate pathways occurs despite a strong thermodynamic potential favoring the delivery of both electrons to the high potential pathway. This long-standing paradox has become to be known as the mandatory bifurcation of electron transfer at the Q_o site.

Based on EPR spectral changes upon ambient redox potential and extent of quinone extraction, Ding *et al.* have proposed a double occupancy model in which the Q_o site is simultaneously occupied by two quinols.[21] The first binds strongly and the second weakly, and it is this weakly bound ubiquinol that is exchanged during catalytic turnover. This model has been used to explain the apparent observation that electrons do not "leak" rapidly from the semiquinone to the ISP, when the low potential pathway is blocked. However, there are a few problems with this model, principally being that numerous binding studies have shown that occupation of the Q_o site by inhibitors and substrate is mutually exclusive.[22] Since 1961 there has been several other "alternative" models that

have been successfully refuted by the bc_1 community, including a B-cycle mechanism, a semiquinone flip-flop mechanism and several others.[8,23,24]

It was also found that in structures with the inhibitors bound, stigmatellin and myxothiazol occupy different domains within the Q_o binding pocket. This observation could be interpreted in one of three ways: (i) these inhibitors are sufficiently different from the physiological substrate that one or both of them do not bind to the exact Q_o site. (ii) There is double occupancy of the Q_o site as proposed by Ding. (iii) There are two sites, one for the initial binding of quinol and then the second that would have a higher affinity for the semiquinone. Using the third of these explanations, the apparent observation of ISP subunit movement, and mutagenesis information,[25,26] Berry and coworkers proposed a new modified Q cycle mechanism.[14] The novel features are (a) movement of the ISP between two separate reaction interfaces; (b) movement of the occupant of the Q_o-binding pocket between a domain distal from the cyt b_L heme, but close to the ISP, and a domain proximal to heme b_L; (c) and Tyrosine residue that acts as a "trap-door " that flips to a

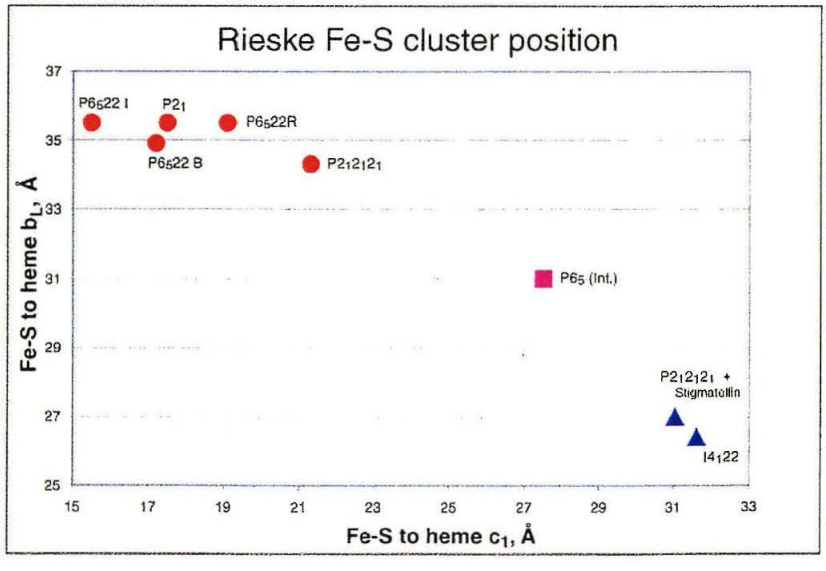

Figure 8. Distances of the Fe-S center to the heme b_L and heme c_1 in the various crystal structures.

"closed" position after the semiquinone has moved from its initial binding site within the Q_o pocket.

Although the variation in binding sites of the two respiratory inhibitors does not give strong evidence for semiquinone movement, this interpretation is not unprecedented. Rees and coworkers have shown that Ubiquinol-1 moves ~4.5 Å within the quinol binding pocket upon reduction to semiquinone in the bacterial reaction center (Q_B site).[27] There is also strong evidence for complex reorientation of charge transfer complexes in other respiratory enzymes. Ullman and Kostic have shown that protein dynamics is most likely responsible for gating the electron transfer between plastocyanin and cytochrome f in the b_6-*f* complex.[28]

Thermodynamics of Redox Linkage

The reduction potentials of the Fe_2S_2 center, cytochrome c1, the heme b_L, heme b_H and the $(Q/QH_2)_i$ couple are approximately 300, 250, -50, 50 and 60-105 mV, respectively, at physiological pH. The differential binding of ubiquinone and ubiquinol to the protein leads to a "splitting" of the reduction potential of the two one-electron redox couples, Q/Q•- and Q•-/QH2. The difference between the two potentials is determined by the extent to which the protein matrix stabilizes quinone, quinol, and semiquinone. Bifurcation indicates a substantial difference in $E_m(Q/Q^{\bullet}\text{-})_o$ and $E_m(Q^{\bullet}\text{-}/QH2)_o$; it is estimated that this difference is approximately 350 mV. The one-electron Q/Q•- couple associated with the transfer of the first electron from ubiquinol will be higher than 60 mV, and as a result the second will be much less. Therefore, the apparently unfavorable second electron transfer from QH_2 at the Q_i site to heme b_L is actually a thermodynamically reasonable process. In addition, destabilization of the ubisemiquinone at the Q_i center through protein interactions

could increase the driving force for this electron transfer. The result is that the branched electron transfer in cytochrome bc1 is reasonable from a thermodynamic standpoint.

Mandatory Bifurcation

If we consider the overall electron transfer and proton translocation of the bc_1 complex, a simple model suggests that the free energy required for pumping protons across the membrane is slightly greater than the free energy derived from electron transfer through the complex. If we assume that the values are roughly the same within the limits of the calculation, the enzyme must be operating close to the minimum free energy required. This implies that proton translocation should be a reversible process, yet it is not.[1] Therefore, there must be some mechanism that prevents reversal of the reaction. This irreversibility leads to a few notable ideas that may explain the mandatory bifurcation of electrons at the Q_o site: The first is an allosteric argument in which protein dynamics prevent back-communication of electrons from cyt c_1 to the Q_o site (allosterics "gate" the electron transfer reaction); the crystal structures of the enzyme have provided information as to how protein dynamics accomplish bifurcation. The domain movement of the ISP suggests that the second electron transfer from the Qo site is likely more rapid than the time required for the ISP to reach cytochrome c1 and return to the cyt b docking region. Whether this domain movement is purely diffusional vs. energetically tied in to the enzyme turnover remains to be seen. It is possible that the reduced ISP is held at the Qi center until the semiquinone repositions within the pocket. Another possibility is that cytochrome b undergoes structural rearrangement upon reduction/oxidation that affect the location of the ISP. A fundamental piece of information that is needed to further understand this gating mechanism is the kinetics of ubiquinol oxidation at the Q_i site.

The second suggestive factor that should be considered is based on kinetics: This argument considers the relationship of the two outer sphere electron-transfer events in terms of the Marcus theory.[20] A semiclassical expression for the rate constant can be written in the form

$$k = \text{const} \times \exp[-\beta(d - d_o)] \times \exp(-\Delta G^*/kT)$$

$$\Delta G^* = (\lambda + \Delta G^o)^2/4\lambda$$

where d_o is the van der Waals radius (~3 Å, the minimal internuclear distance defined by repulsion of electron clouds), β is the conductivity of the protein matrix through which the electron must pass. This electronic coupling parameter modulates the distance dependence of electron coupling. The reorganization energy (λ) results from the structural changes at the redox site. Alternatively the reorganization energy (λ) can also be associated with more general conformational changes of the protein backbone. There are a number of factors that could contribute to the bifurcation of the second electron, such as a difference in the electron pathway through the protein matrix, electron transfer distances, etc. If the ISP does reorient upon the first electron transfer, the λ term and the relative distances (d) would be dramatically less for the second ET to the b heme.

Section I Focus

In light of the previous discussion, it is apparent that there is a need for the determination of accurate kinetic rates of enzymatic turnover events. In the past fifteen years, methods for photoinduced, one electron input into proteins has been developed to study ET in proteins. To obtain the rates of ET in bc_1, a novel approach will be required that surpasses the time resolution capabilities of current rapid mixing techniques. A further

need is the ability to generate a two electron donating species rapidly and readily. There is no method for photo-initiating a two-electron transfer reaction, to date.

It is the aim of this research to obtain evidence that leads to a unified mechanism for electron transfer and proton translocation in the cytochrome bc_1 complex. To achieve this goal, it will be necessary to measure the individual kinetic steps and the thermodynamics of each event involved in enzyme turnover. The first of these goals will be pursued with the use of a quinol substrate linked to a photolabile-protecting group. If the release of this quinol is fast on the timescale of enzymatic turnover, kinetic resolution should be achieved.

To measure the individual electron transfer events in the bc_1 complex, transient absorption spectroscopy has been employed. By following the spectra of the redox centers throughout single turnover, the rate constants for the individual steps can be discerned. Specifically, the heme soret bands can be used to monitor the rate of initial reduction, as these bands have the highest extinction coefficients. Once the technical details have been worked out, the α bands will be examined as these bands have historically yielded the most information about the individual heme reduction events (the signals from the individual centers can be discerned).

The second section describes the design and synthesis of a "caged" substrate to resolve the kinetic issues of the redox changes during turnover. The final section reports upon the spectroscopic investigations of the chromophoric centers using transient absorption spectroscopy.

References

1)Alberts, B.; Bray, D.; Lewis, J.; Raff, M.; Roberts, K.; Watson, J. D. *Molecular Biology of the Cell*; Garland Publishing: New York, 1994.

2)Hinkle, P. C.; Kumar, M. A.; Resetar, A.; Harris, D. L. *Biochemistry* **1991**, *30*, 3576-82.

3)Iwata, S.; Lee, J. W.; Okada, K.; Lee, J. K.; Iwata, M.; Rasmussen, B.; Link, T. A.; Ramaswamy, S.; Jap, B. K. *Science* **1998**, *281*, 64-71.

4)Iverson, T. M.; Luna-Chavez, C.; Cecchini, G.; Rees, D. C. *Science* **1999**, *284*, 1961-66.

5)Leslie, A. G. W.; Abrahams, J. P.; Braig, K.; Lutter, R.; Menz, R. I.; Orriss, G. L.; van Raaij, M. J.; Walker, J. E. *Biochem. Soc.Trans.* **1999**, *27*, 37-42.

6)Tsukihara, T.; Aoyama, H.; Yamashita, E.; Tomizaki, T.; Yamaguchi, H.; Shinzawa-Itoh, K.; Nakashima, R.; Yaono, R.; Yoshikawa, S. *Science* **1996**, *272*, 1136-44.

7)Grigorieff, N. *J Mol Biol* **1998**, *277*, 1033-46.

8)Hatefi, Y. *Annu Rev Biochem* **1985**, *54*, 1015-69.

9)Brandt, U.; Trumpower, B. *Crit. Rev. Biochem. Mol. Biol.* **1994**, *29*, 165-97.

10)Hatefi, Y.; Haavik, A. G.; Griffiths, D. E. *J. Biol. Chem.* **1962**, *237*, 1681.

11)Schagger, H.; Link, T. A.; Engel, W. D.; von Jagow, G. *Methods Enzymol* **1986**, *126*, 224-37.

12)Iwata, S.; Saynovits, M.; Link, T. A.; Michel, H. *Structure* **1996**, *4*, 567-79.

13)Moser, C. C.; Page, C. C.; Farid, R.; Dutton, P. L. *J Bioenerg Biomembr* **1995**, *27*, 263-74.

14)Zhang, Z.; Huang, L.; Shulmeister, V. M.; Chi, Y. I.; Kim, K. K.; Hung, L. W.; Crofts, A. R.; Berry, E. A.; Kim, S. H. *Nature* **1998**, *392*, 677-84.

15)Xia, D.; Yu, C. A.; Kim, H.; Xia, J. Z.; Kachurin, A. M.; Zhang, L.; Yu, L.; Deisenhofer, J. *Science* **1997**, *277*, 60-66.

16)Crofts, A.; Hacker, B.; Barquera, B.; Yun, C. H.; Gennis, R. *Biochim Biophys Acta* **1992**, *1101*, 162-5.

17)Stonehuerner, J.; O'Brien, P.; Geren, L.; Millett, F.; Steidl, J.; Yu, L.; Yu, C. A. *J Biol Chem* **1985**, *260*, 5392-8.

18)Wikstrom, M.; Krab, K.; Saraste, M. *Annu Rev Biochem* **1981**, *50*, 623-55.

19)Mitchell, P. *J. Theor. Biol.* **1976**, *62*, 327-67.

20)Rich, P. R. *Biochim. Biophys. Acta* **1984**, *768*, 53-79.

21)Ding, H.; Moser, C. C.; Robertson, D. E.; Tokito, M. K.; Daldal, F.; Dutton, P. L. *Biochemistry* **1995**, *34*, 15979-96.

22)Link, T. A.; Schagger, H.; von Jagow, G. *FEBS Lett* **1986**, *204*, 9-15.

23)Matsuno-Yagi, A.; Hatefi, Y. *J Biol Chem* **1997**, *272*, 16928-33.

24)Ding, H.; Robertson, D. E.; Daldal, F.; Dutton, P. L. *Biochemistry* **1992**, *31*, 3144-58.

25)Saribas, A. S.; Ding, H.; Dutton, P. L.; Daldal, F. *Biochemistry* **1995**, *34*, 16004-12.

26)Yun, C. H.; Crofts, A. R.; Gennis, R. B. *Biochemistry* **1991**, *30*, 6747-54.

27)Stowell, M. H.; McPhillips, T. M.; Rees, D. C.; Soltis, S. M.; Abresch, E.; Feher, G. *Science* **1997**, *276*, 812-6.

28)Ullmann, G. M.; Hauswald, M.; Jensen, A.; Kostic, N. M.; Knapp, E. W. *Biochemistry* **1997**, *36*, 16187-96.

Chapter 3:

Rapid Photochemical Generation of Ubiquinol Through a Radical Pathway: An Avenue for Probing Submillisecond Enzyme Kinetics

Abstract

The carbonate ester of *N*-hydroxypyridine-2-thione and ubiquinol-2 (PTOC-Q_2H_2) was synthesized as a photoreleaseable substrate for quinol-oxidizing enzymes. Steady-state photolysis of PTOC-Q_2H_2 in acetonitrile and aqueous detergent solution yielded ubiquinone-2, ubiquinol-2, and 2,2'-dithiobispyridine in equimolar amounts. Transient absorbance spectroscopy revealed the generation of semiquinone on a submicrosecond time scale, with disproportionation of the semiquinone in acetonitrile occurring with a second-order rate constant of 2.2×10^8 M^{-1} s^{-1}. In the presence of the hydrogen atom donor 2-mercaptoethanol at 1 M concentration, the semiquinone decayed at a rate approximately four times that of the disproportionation reaction. In aqueous detergent solution, yield of semiquinone was decreased, but the rate of semiquinone decay was greater than that in acetonitrile. Photolysis of PTOC-Q_2H_2 in the presence of the quinol oxidase cytochrome bo_3 resulted in electron input to the enzyme, but with a substoichiometric yield.

Introduction

The use of photoreleasable protecting groups ("cages") on bioactive molecules provides a means for the rapid initiation of bimolecular reaction chemistry in biological systems.[1,2] In this approach, the protecting group renders an otherwise biologically active molecule inert, so that the molecule can be mixed with an enzyme or other biological target molecule without any reaction taking place. Irradiation of the "caged" molecule leads to the release of the protecting group, so that the biological substrate is

free to react with its target biomolecule. Because the bimolecular chemistry can be initiated by a laser pulse, the time frame over which the reaction can be probed is determined by the photochemistry leading to the release of substrate. This time frame can be much shorter than the time scale of milliseconds associated with stopped-flow and other rapid-mixing techniques. For some caged substrates, such as carboxylic acids and phosphates derivatized with benzoin moieties,[3-6] release of active substrate is essentially instantaneous upon irradiation. For alcoholic substrates such as quinols, however, release of free substrate has been limited by chemistry that occurs subsequent to photocleavage of the cage molecule. When protecting groups such as α-carboxynitrobenzyl[7] and 3',5'-bis(carboxymethoxy)benzoin[8] are used to derivatize quinols, a carbonate linker is required. Upon irradiation, the quinol is released as a carbonate monoester, and the slow decarboxylation of this species is rate-limiting in generating free quinol.

An alternative approach to the photochemical generation of quinol involves the photolysis of a precursor molecule to generate free semiquinone, which can then be reduced rapidly to a quinol. The use of the photolabile protecting group *N*-hydroxypyridine-2-thione makes this approach possible. Esters based on *N*-hydroxypyridine-2-thione have been used in the photochemical generation of alkyl radicals as well as nitrogen- and oxygen-based radicals.[9-16] Herein we report the extension of this methodology with the synthesis of the carbonate ester of ubiquinol-2 and *N*-hydroxypyridine-2-thione (PTOC-Q_2H_2, **1**). We present the characterization of this compound, and demonstrate the release of ubisemiquinone upon photolysis of PTOC-Q_2H_2 in acetonitrile and aqueous detergent solution, the formation of ubiquinol by both disproportionation and reduction of semiquinone, and electron transfer from the

photogenerated ubiquinol to a quinol-oxidizing enzyme, cytochrome bo_3 from *Escherichia coli*.

Results and Discussion

The synthesis of PTOC-Q_2H_2 (**1**) followed standard methodology for the synthesis of *N*-hydroxypyridine-2-thione esters, using a one-pot synthesis. Ubiquinol-2 was reacted with diphosgene and pyridine in THF, and the thallium salt of *N*-hydroxypyridine-2-thione was added to generate the carbonate ester. Purification yielded compound **1** as a mixture of two isomers, arising from esterification of the quinol at the 1-position or at the 4-position of the quinol ring. These two isomers were resolvable by chromatography, but their chemical and photophysical properties were sufficiently similar that it was deemed unnecessary to separate the two prior to the reactivity studies. The synthesis gave an overall yield of 61%.

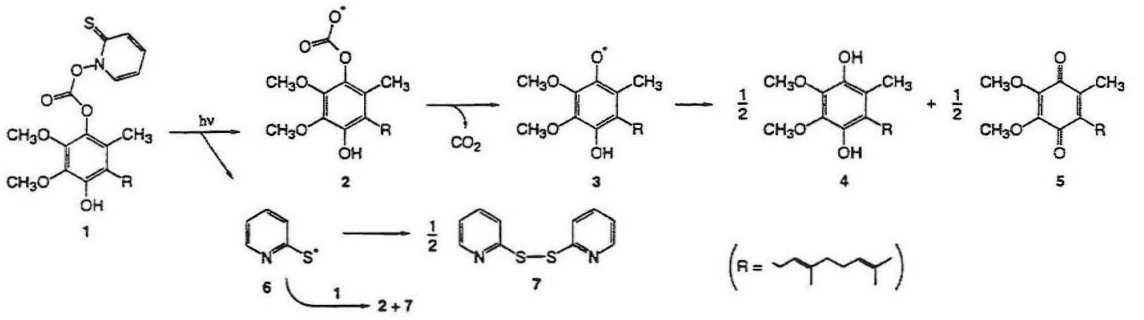

Figure 1. Proposed photolysis pathway for PTOC-Q_2H_2.

Photolysis of PTOC-Q_2H_2 in either acetonitrile or 100 mM sodium phosphate, 0.1% Brij-35 (a non-denaturing detergent used in protein studies), pH 7.4 with a mercury arc lamp under anaerobic conditions yielded equimolar amounts of 2,2'-dithiobispyridine, ubiquinol-2, and ubiquinone-2, as determined by HPLC analysis. On the basis of the

known photochemistry of *N*-hydroxypyridine-2-thione esters,[17,18] the photolysis of PTOC-Q_2H_2 was assumed to follow the sequence diagrammed in Scheme 2. Irradiation of PTOC-Q_2H_2 (**1**) led to the homolytic cleavage of the N-O bond to yield the 2-pyridylthiyl radical and the oxygen-based radical **2**. Rapid decarboxylation of **2** yielded free ubisemiquinone (**3**), which disproportionated to form quinone (**4**) and quinol (**5**). The 2-pyridylthiyl radical dimerized to form 2,2'-dithiobispyridine (**6**) or reacted with starting material **1** to make 2,2'-dithiobispyridine and **2**.

Formation and decay of ubisemiquinone in acetonitrile and aqueous detergent solution following photolysis of PTOC-Q_2H_2 were monitored using transient absorption spectroscopy. Photolysis was achieved using a 308 nm pulse from a XeCl excimer laser with pulse width of 25 ns, and the semiquinone concentration was monitored at 420 nm,

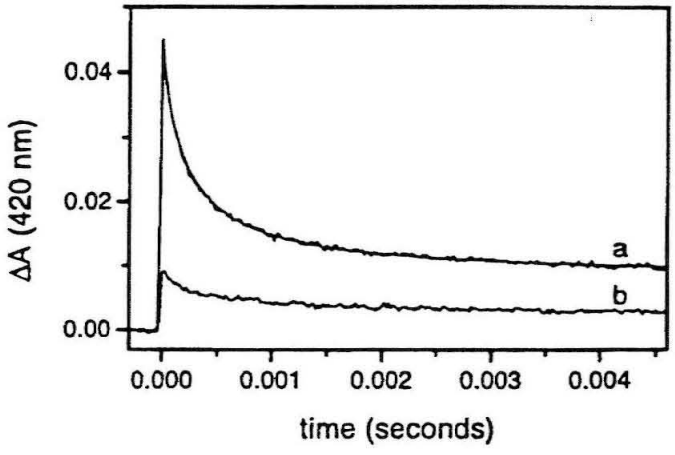

Figure 2. (a) Absorption transient following photolysis of 50 μM PTOC-Q_2H_2 in acetonitrile, measured at 420 nm, and the fit of the data by a second-order decay model. (b) Absorption transient following the photolysis of 50 mM PTOC-Q_2H_2 in 100 mM sodium phosphate, 0.1% Brij-35, pH 7.4. For both traces a single 308 nm pulse from a XeCl excimer laser, with a pulse energy of 2.1 mJ, was used for the photolysis.

the λ_{max} for protonated semiquinone. Trace (a) in figure 2 shows an absorption transient following the irradiation of 50 μM PTOC-Q_2H_2 in acetonitrile. An immediate increase in absorbance at 420 nm was followed by a decay of the signal on a millisecond time scale. The wavelength dependence of this decay over the wavelength range 390 nm to 500 nm was consistent with the spectrum of protonated ubisemiquinone reported by Land and Swallow,[19] confirming the identity of the species responsible for the signal. A kinetic model that assumed only a second-order disproportionation reaction of semiquinone fit the transient at 420 nm. The fit, which used an extinction coefficient of 3000 M^{-1} cm^{-1} for the semiquinone,[19] gave a rate constant of 2.2×10^8 M^{-1} s^{-1} for semiquinone decay. This fit is included in figure 2. The high quality of the fit suggests that disproportionation of semiquinone was the dominant if not exclusive decay pathway for this species. Trace (b) in figure 2 shows an absorption transient that arose from the photolysis of PTOC-Q_2H_2 in 100 mM sodium phosphate, 0.1% Brij-35, pH 7.4. Both the maximum yield of semiquinone and the final concentration of photoproducts were significantly lower than those in acetonitrile. A second-order kinetic model did not fit the data in a satisfactory fashion, and thus a rate constant was not calculated. Nevertheless, formation of the photoproducts was complete within 400 μs.

In order to measure the extent to which an exogenous one-electron reductant can increase the rate of reduction of ubisemiquinone to ubiquinol, the photolysis of PTOC-Q_2H_2 was performed in acetonitrile in the presence of varying concentrations of 2-mercaptoethanol. A thiol was used because thiols have a relatively low S-H bond strength (~88.5 kcal/mol)[20] and have been used previously for the trapping of alkyl

radicals.[21-23]. In addition, thiols such as glutathione serve as reductants in biological systems. 2-Mercaptoethanol has a high solubility in both acetonitrile and water, and it will not perform the two-electron reduction of quinone to quinol in a kinetically facile manner. Control experiments on the steady-state photolysis of PTOC-Q_2H_2 in acetonitrile in the presence of 2-mercaptoethanol, using a mercury arc lamp, revealed that reduction of semiquinone by thiol can compete effectively with the disproportionation of semiquinone, leading to a higher yield of quinol (data not shown). Figure 3 shows absorption transients that monitored the decay of ubisemiquinone following laser photolysis of PTOC-Q_2H_2 in the presence of different concentrations of 2-mercaptoethanol. In the absence of thiol, the semiquinone signal decayed cleanly via the disproportionation reaction. As the concentration of thiol was increased, the semiquinone decayed more rapidly as a result of the reaction with the thiol. This decay was expected to follow a rate law arising from competing first- and second-order processes. However,

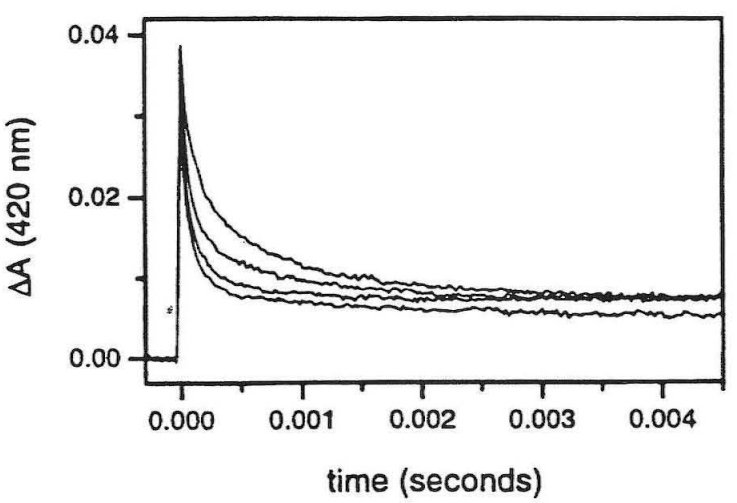

Figure 3. Absorption transients following the photolysis of 50 μM PTOC-Q_2H_2 in acetonitrile in the presence of 2-mercaptoethanol. Top→bottom: 0 M, 10 mM, 100 mM, 1M 2-mercaptoethanol. The lower absorbance with 1M 2-mercaptoethanol arose from a lower yield of semiquinone during photolysis.

the data were not adequately fit using this model, suggesting more complex kinetics. In light of this inability to extract fundamental rate constants from the transient absorption data, the time taken for the absorption signal to decay to (1/e) times the amplitude of the decay curve was used as an indicator of reaction rate. Using this criterion, the presence of 1M 2-mercaptoethanol resulted in approximately a four-fold increase in the rate of semiquinone decay, with a characteristic decay time of approximately 80 μs. This time scale is more rapid than that of standard turbulent mixing (e.g., stopped-flow) by a factor of ten.

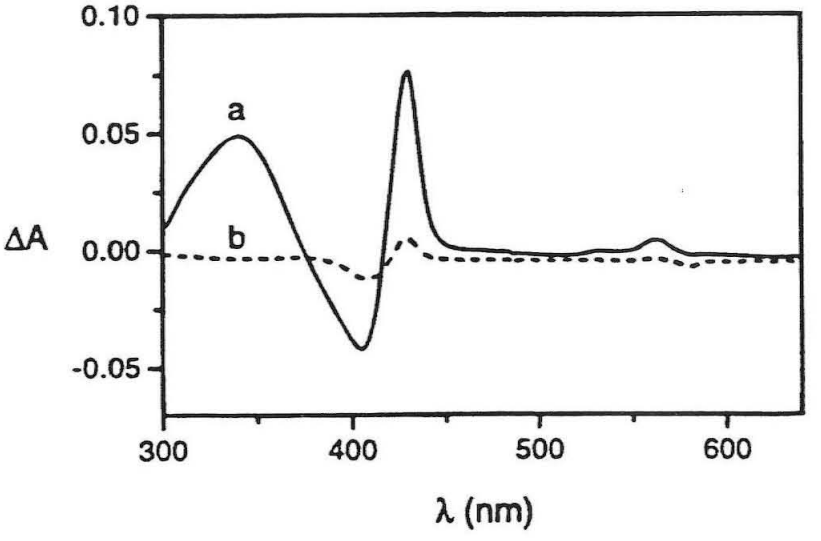

Figure 4. (a) Optical difference spectrum from the irradiation of 25 μM PTOC-Q_2H_2 in the presence of 1.2 μM cytochrome *bo*$_3$ in 100 mM sodium phosphate, 0.1% Brij-35, pH 7.4 for 20 s using a mercury arc lamp. The solution contained 100 μg/mL glucose oxidase, 50 μg/mL catalase, and 50 mM glucose to scavenge dioxygen from the solution. The reaction was performed under an argon atmosphere. (b) Optical difference spectrum from the irradiation of 1.2 μM cytochrome *bo*$_3$ in the absence of PTOC-Q_2H_2. Other reaction conditions are identical to those in (a).

Photolysis of PTOC-Q_2H_2 was performed under strictly anaerobic conditions in the presence of cytochrome *bo*$_3$, a ubiquinol-oxidizing respiratory enzyme from *Escherichia coli*, in order to demonstrate electron transfer from released substrate into the enzyme. The results of this experiment are shown in Figure 4. The solid trace (a) shows the photolyzed minus unphotolyzed difference spectrum that arose from the steady-state irradiation of 25 μM PTOC-Q_2H_2 for 20 seconds (check) in the presence of 1.2 μM enzyme. The peak at 340 nm was characteristic of the photolysis products of PTOC-Q_2H_2 and the spectral features at higher wavelengths showed reduction of cytochrome *bo*$_3$. The difference spectrum revealed the photolysis of 17 μM PTOC-Q_2H_2 with the associated reduction of 0.4 μM heme. Assuming that the heme reduction was indicative

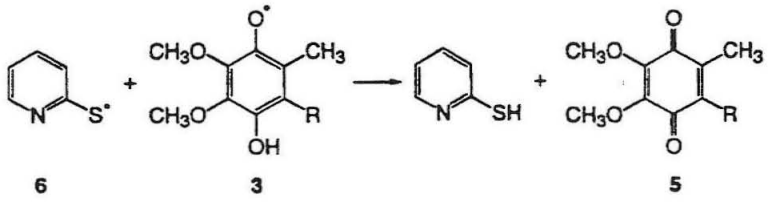

Figure 5. Oxidation of ubisemiquinone by the 2-pyridylthiyl radical.

of full enzyme reduction (five electrons per enzyme molecule), only 6% of the electrons available upon photolysis reduced the enzyme. The loss of reducing equivalents likely occurred from the reaction of released semiquinone with either lipid molecules or amino acid residues on the proteins.

In order to demonstrate that the enzyme reduction did not arise from direct photoreduction, cytochrome *bo*$_3$ was irradiated in the absence of PTOC-Q_2H_2 under the

same conditions as described above. The results of this experiment are shown as the dotted trace (b) in figure 4. Photoreduction of 0.06 μM heme was calculated on the basis of the difference spectrum in the Soret region, a significantly lower value than was observed during the irradiation of enzyme in the presence of caged substrate. Thus, the reducing equivalents in the latter reaction arose primarily from the photoreleased substrate.

Following photolysis of PTOC-Q_2H_2, the reaction of photogenerated ubiquinol with enzyme is a second-order process in the concentration regime studied in this work. However, the low yield of ubiquinol in these experiments led to slow kinetics of enzyme reduction, such that significant electron transfer to cytochrome *bo*$_3$ was not observed in the 100 ms time window of the transient absorbance experiments.

Conclusions

The use of *N*-hydroxypyridine-2-thione as a protecting group for quinols has led to a system in which semiquinone can be produced on a submicrosecond time scale, and formation of quinol from the semiquinone can occur on a submillisecond time scale, almost an order of magnitude more rapidly than reagents can be mixed in traditional rapid mixing techniques. As demonstrated with *E. coli* cytochrome *bo*$_3$, photolysis of PTOC-Q_2H_2 leads to the reduction of enzyme, with the actual reduction rate determined by the amount of substrate released in the photolysis reaction. Thus, as long as the biochemical system of interest can tolerate the short-term presence of radical species, the radical-based mechanism for photochemical generation of quinol constitutes a rapid

methodology for the initiation of bimolecular chemistry of alcohols in biological systems on a submillisecond time scale.

Experimental Section

General: Anhydrous THF was prepared by refluxing over sodium and benzophenone, and was distilled prior to use. All other solvents were of reagent grade. Glassware was oven-dried. The thallium salt of *N*-hydroxypyridine-2-thione was prepared according to the literature procedure.[18] Synthesis of ubiquinone-2 is described elsewhere.[24] 2-Mercaptoethanol was distilled under argon prior to use. All other reagents were from commercial sources and used as received. Type VII glucose oxidase from *Aspergillus niger* and bovine liver catalase were purchased from Sigma. Cytochrome bo_3 from *Escherichia coli* was prepared as described previously.[25]

Synthesis of 1: A solution of ubiquinone-2 (~1.3 g) in 10 ml of diethyl ether was treated with an excess of sodium dithionite in 10 ml of water and vortexed for 10 minutes under nitrogen gas to give ubiquinol-2. The organic layer was rinsed twice with 8 ml of water to remove any remaining reductant, and the solvent was removed under reduced pressure overnight. The ubiquinol that resulted (1.25 g, 3.90 mmol) was redissolved in dry THF. The reaction mixture was cooled to -78°C and 2.5 M *n*-butyl lithium in hexanes (0.594 ml, 1.48 mmol) was added dropwise. After 30 minutes the temperature was adjusted to 0°C and diphosgene (0.220 g, 1.11 mmol) was added, followed by the slow addition of dry pyridine in THF. After one hour the temperature was again decreased to -78°C and the thallium salt of *N*-hydroxypyridine-2-thione was added (0.486 g, 1.475 mmol). The extent of reaction was monitored by tlc. Upon completion of the

reaction, the reaction mixture was filtered and the solvent was removed under reduced pressure. The resulting yellow oil was purified by flash chromatography on a silica column using 1/1 hexane/EtOAc. Yield 440 mg (61%). R_f = 0.25 (1/1 hexane/EtOAc). ^{1}H NMR ($CDCl_3$, 300 MHz) δ 8.363 (m, 1 H), δ 8.204 (1, 1 H), δ 7.354 (t, J = 7.20 Hz, 1 H), δ 7.218 (m, 1 H), δ 5.049 (q, J = 5.70 Hz, 2 H), δ 3.914 (s, 3 H), δ 3.857 (s, 3 H), δ 3.337 (d, J = 6.60 Hz, 2 H), δ 2.074 (m, 7 H), δ 1.747 (s, 3 H), δ 1.637 (s, 3 H), δ 1.565 (s, 3 H). HRMS (FAB) *m/z* (MH^+) calcd 474.1950, obsd 474.1938.

Steady state photolysis: Samples were placed in a quartz cuvette and irradiated using an Oriel 66011 Hg vapor arc lamp operating at 450 W and equipped with water-cooled Schott glass UG11 and WG320 filters. The optical absorbance was monitored with an HP 8452 diode array spectrophotometer. The photolysis was judged to be complete when no further spectral changes occurred upon continuing illumination. HPLC analysis was performed using a Shimadzu LC-6A system equipped with a Vydac C-18 reverse phase column.

Laser spectroscopy: The laser setup for transient absorbance spectroscopy has been described previously.[26] Photolysis was performed with a Lambda-Physik LPX201I XeCl excimer laser (308 nm) with pulse energies of 2.0-2.2 mJ at the sample. The probe beam came from a 75 W xenon arc lamp. When possible, a 385 nm high-pass filter was used between the probe lamp and the sample to minimize adventitious photolysis. An Instruments SA 1690B double monochromator in conjunction with a photomultiplier tube was used for signal detection.

References

(1) Adams, S. R.; Tsien, R. Y. *Annu. Rev. Physiol.* **1993**, *55*, 755-784.

(2) Corrie, J. E. T.; Trentham, D. R. In *Bioorganic Photochemistry Volume 2: Biological Applications of Photochemical Switches*; Morrison, H., Ed.; John Wiley & Sons: New York, 1993, p 243-305.

(3) Sheehan, J. C.; Wilson, R. M.; Oxford, A. W. *J. Am. Chem. Soc.* **1971**, *93*, 7222-7228.

(4) Baldwin, J. E.; McConnaughie, A. W.; Moloney, M. G.; Pratt, A. J.; Shim, S. B. *Tetrahedron* **1990**, *46*, 6879-6884.

(5) Givens, R. S.; Athey, P. S.; Kueper, L. W., III; Matuszewski, B.; Xue, J.-y. *J. Am. Chem. Soc.* **1992**, *114*, 8708-8710.

(6) Givens, R. S.; Athey, P. S.; Matuszewski, B.; Kueper, L. W., III; Xue, J.-y.; Fister, T. *J. Am. Chem. Soc.* **1993**, *115*, 6001-6012.

(7) Rossi, F. M.; Kao, J. P. Y. *J. Biol. Chem.* **1997**, *272*, 3266-3271.

(8) Hansen, K. C.; Schultz, B. E.; Wang, G.; Chan, S. I. *BBA* **2000**, *1456,* 121-137.

(9) Barton, D. H. R.; Crich, D.; Motherwell, W. B. *Tetrahedron* **1985**, *41*, 3901-3924.

(10) Crich, D.; Quintero, L. *Chem. Rev.* **1989**, *89*, 1413-1432.

(11) Newcomb, M.; Park, S.-U.; Kaplan, J.; Marquardt, D. J. *Tetrahedron Lett.* **1985**, *26*, 5651-5654.

(12) Newcomb, M.; Deeb, T. M. *J. Am. Chem. Soc.* **1987**, *109*, 3163-3165.

(13) Barton, D. H. R.; Jaszberenyi, J. C.; Morrell, A. I. *Tetrahedron Lett.* **1991**, *32*, 311-314.

(14) Newcomb, M.; Kumar, M. U.; Boivin, J.; Crépon, E.; Zard, S. Z. *Tetrahedron Lett.* **1991**, *32*, 45-48.

(15) Togo, Y.; Nakamura, N.; Iwamura, H. *Chem. Lett.* **1991**, 1201-1204.

(16) Burdi, D.; Aveline, B. M.; Wood, P. D.; Stubbe, J.; Redmond, R. W. *J. Am. Chem. Soc.* **1997**, *119*, 6457-6460.

(17) Bohne, C.; Boch, R.; Scaiano, J. C. *J. Org. Chem.* **1990**, *55*, 5414-5418.

(18) Aveline, B. M.; Kochevar, I. E.; Redmond, R. W. *J. Am. Chem. Soc.* **1995**, *117*, 9699-9708.

(19) Land, E. J.; Swallow, A. J. *J. Biol. Chem.* **1970**, *245*, 1890-1894.

(20) Janousek, B. K.; Reed, K. J.; Brauman, J. I. *J. Am. Chem. Soc.* **1980**, *102*, 3125-3129.

(21) Newcomb, M.; Park, S. U. *J. Am. Chem. Soc.* **1986**, *108*, 4132-4134.

(22) Franz, J. A.; Bushaw, B. A.; Alnajjar, M. S. *J. Am. Chem. Soc.* **1989**, *111*, 268-275.

(23) Ha, C.; Horner, J. H.; Newcomb, M.; Varick, T. R.; Arnold, B. R.; Lusztyk, J. *J. Org. Chem.* **1993**, *58*, 1194-1198.

(24) Stowell, M. H. B.; Wang, G.; Day, M. W.; Chan, S. I. *J. Am. Chem. Soc.* **1998**, *120*, 1657-1664.

(25) Musser, S. M.; Stowell, M. H. B.; Lee, H. K.; Rumbley, J. N.; Chan, S. I. *Biochemistry* **1997**, *36*, 894-902.

(26) DiMagno, T. J.; Stowell, M. H. B.; Chan, S. I. *J. Phys. Chem.* **1995**, *99*, 13038-13047.

Chapter 4:
A Water-Soluble "Caged" Decylubiquinol for the Reduction of Quinol-Oxidizing Enzymes

Abstract

In order to probe the reaction chemistry of respiratory quinol-oxidizing enzymes on a rapid time scale, a photoreleasable quinol substrate was synthesized by coupling decylubiquinol with the water-soluble protecting group 3',5'-bis(carboxymethoxy)benzoin (BCMB) through a carbonate linkage. The resulting compound, DQ-BCMB, was highly soluble in aqueous detergent solution, and showed no reactivity with quinol-oxidizing enzymes prior to photolysis. Upon photolysis in acetonitrile, 5,7-bis(carboxymethoxy)-2-phenylbenzofuran, carbon dioxide, and decylubiquinol were formed. In aqueous media, free 3',5'-bis(carboxymethoxy)benzoin was also produced. Photolysis of DQ-BCMB with a 308 nm excimer laser led to the release of the BCMB group in less than 10^{-6} s. Decylubiquinol was released in the form of a carbonate monoester, which decarboxylated with an observed first order rate constant of 195-990 s^{-1}, depending on the reaction medium. Yields of decylubiquinol as high as 35 μM per laser pulse were attained readily. The solubility, photolysis, and reactivity properties of DQ-BCMB make it a useful tool for the photoinitiation of the enzymatic reactions of decylubiquinol on a time scale as fast or faster than traditional rapid mixing or other photolysis reactions. This work suggests that the use of BCMB as a photolabile protecting group for enzyme substrates can be applied to the study of many other biological systems as well.

Introduction

Respiratory chains in most aerobic organisms include enzymes that catalyze the oxidation of quinols, using the energy from this oxidation to promote the generation of an electrochemical gradient across the cytoplasmic or mitochondrial membrane in order to

produce ATP [1]. The complexity of these quinol-oxidizing enzymes makes study of the proton translocation apparatus difficult. The electron input from quinol to the enzyme plays a substantial role in enzyme function, and yet this reaction is difficult to study under single-turnover conditions on account of the rapidity of the electron transfer. While in principle the rate of quinol oxidation by these enzymes can be determined at low substrate concentrations on account of the second-order kinetic process involved, a thorough understanding of electron transfer through the enzymes requires that the time scale for substrate oxidation be comparable to or more rapid than that of subsequent electron transfers through the enzyme, and thus that the substrate concentration be sufficiently high. The time frame of traditional rapid-mixing techniques is limited by the mixing time of the reagents, with dead times typically on the order of milliseconds. While inroads are being made into submillisecond rapid mixing techniques [2], an alternative method for the rapid initiation of reaction chemistry is through the use of substrates that contain photolabile protecting groups ("cages"). By removing a photolabile protecting group with a laser pulse, reaction chemistry can be initiated on a time scale dictated by the rate of the photolysis reaction, which can be much more rapid than the mixing of reagents through turbulent flow. The use of such photoreleasable substrates in the study of biological systems has been reviewed elsewhere [3, 4].

Our interest in quinol-oxidizing enzymes led us to explore the possibility of using photoreleasable substrates to probe the reaction chemistry of these enzymes. We chose an approach based on the use of the 3'-5'-dimethoxybenzoin (DMB) moiety as a protecting group. In early work by Sheehan and coworkers, *O*-acetyl-3',5'-dimethoxybenzoin was shown to photolyze with the concomitant release of acetate, with

a rate constant estimated at $>10^{10}$ s^{-1} [5]. Pirrung and coworkers extended the methodology to derivatize alcohols using a carbonate linkage [6]. The rapid photolysis rate and a facile synthesis of the DMB group made its use desirable. In prior work from this laboratory, a ubiquinol-2 substrate derivatized with the 3',5'-dimethoxybenzoin group was synthesized and studied [7]. However, poor solubility of the caged ubiquinol in aqueous media prevented full characterization of the compound and precluded its use in enzymatic reactions.

Recent work in our laboratory has led to the development of a derivative of the 3',5'-dimethoxybenzoin group in which the water solubility is dramatically increased by replacing the methoxy groups with carboxymethoxy groups [8]. This new protecting group, 3',5'-bis(carboxymethoxy)benzoin (BCMB), has the potential to allow the water-solubility of otherwise insoluble substrates. In this work we present the synthesis of a water-soluble caged decylubiquinol based on the BCMB protecting group (hereafter referred to as DQ-BCMB), characterization of its reactivity and photolysis properties, and an evaluation of the compound as a potential substrate for studying the reaction of ubiquinol with respiratory enzymes. The use of DQ-BCMB in the study of two respiratory enzymes, mitochondrial cytochrome bc_1 and *Escherichia coli* cytochrome bo_3, is presented in the following chapter.

Materials and Methods

1. General

Anhydrous THF was distilled from sodium/benzophenone ketyl prior to use. Anhydrous acetonitrile and methylene chloride were purchased from Aldrich. All other

solvents were of reagent grade. Decylubiquinone was purchased from Sigma and purified by reverse phase HPLC to greater than 99% purity. The synthesis of the water-soluble BCMB cage is reported elsewhere [8].

2. Synthesis of Silylated Decylubiquinol (1)

A solution of decylubiquinone (0.30 g, 0.93 mmol) was placed into a solution of ether/water (1/1) and excess sodium dithionite was added. The reaction vessel was capped and purged with argon. After five minutes of vigorous mixing, the solution became clear. The organic layer was filtered through a small plug of $MgSO_4$ and transferred to a stoppered round bottom flask. Solvent was removed in vacuo and the nearly colorless oil was redissolved in dry acetonitrile and purged with dry argon. The flask was charged with a stir bar and 86 μL of triethylamine (0.76 mmol). Chlorotriethylsilane (0.093 g, 0.90 mmol) in acetonitrile was added dropwise using a syringe pump over a four hour period. The solvent was removed under reduced pressure and the resultant oil was purified by flash chromatography using 9/1 hexane/EtOAc. Isomeric resolution was achieved under these conditions. The product was isolated as a clear oil. Yield 0.28 g (71%). ^{1}H NMR ($CDCl_3$) δ 5.370 (s, 1 H), δ 3.887 (s, 3 H), δ 3.762 (s, 3 H), δ 2.569 (t, J = 8.4 Hz, 2 H), δ 2.107 (s, 3 H), δ 1.442 (m, 4 H), δ 1.256 (m, 11 H), δ 0.950 (t, J = 7.8 Hz, 9 H), δ 0.874 (t, J = 6.9 Hz, 4 H), δ 0.743 (q, J = 8.1,8.7 Hz, 6 H).

3. Synthesis of Bis(2-nitrophenyl)carbonate (2)

A round bottom flask equipped with a stir bar was charged with 2-nitrophenol (13.91 g, 100 mmol), 250 mL of dry methylene chloride, and phosgene (6.43 g, 21.7 mmol) at room temperature under dry argon. To this solution 14.03 ml of triethylamine was added. The solution was allowed to stir for 4 hours at room temperature and the solvent was removed under reduced pressure to give an off-white solid. Recrystallization was performed with ethyl acetate/petroleum ether to give white, flat crystals. Yield: 14.50g (94%). ^{1}H NMR ($CDCl_3$) δ 8.191 (dd, J = 6.60 Hz, 1.60 Hz, 2H), δ 7.762 (t, J = 5.93, 2H), δ 7.519 (m, 4H).

4. Synthesis of Carbonate Ester of 2-Nitrophenol and Silylated Decylubiquinol (3)

A solution of **1** (0.235 g, 0.52 mmol) and **2** (0.264 g, 0.85 mmol) was prepared in 100ml dry methylene chloride under dry argon. To this solution was added 6.4 mg of 4-(dimethylamino)pyridine (DMAP) (0.052 mmol) in 10ml of dry methylene chloride under argon. The reaction was allowed to run for 18 hours. The reaction mixture was poured into 25 ml of 0.1 M HCl and extracted with 2×50 ml of methylene chloride. The organic phases were combined and filtered through a plug of $MgSO_4$ and the solvent was removed under reduced pressure. The resulting oil was purified by flash chromatography using 4/1 hexane/EtOAc. Yield 2.10g (92%). R_f = 0.33 (4/1 hexane/EtOAc); ^{1}H NMR ($CDCl_3$) δ 8.219 (dd, J = 1.5, 6.0 Hz, 1 H) δ 7.697 (t, J = 7.8 Hz, 1 H), δ 7.439 (t, J = 6.0 Hz, 2 H), δ 3.911 (s, 3 H), δ 3.776 (s, 3 H), δ 2.623 (t, J = 8.2 Hz, 2 H), δ 2.143 (s, 3 H), δ 1.417 (m, 4 H), δ 1.253 (m, 11 H), δ 0.956 (t, J = 7.8 Hz, 9 H), δ 0.865 (t, J = 6.8 Hz, 4 H), δ 0.763 (q, J = 8.1, 8.7 Hz, 6 H).

5. Carbonate Ester of Protected BCMB and Silylated Decylubiquinol (5)

A round bottom flask was charged with **3** (280 mg, 0.461) and *tert*-butyl-protected BCMB **4** (237 mg, 0.55 mmol) in 30 ml of dry methylene chloride. To this solution was added a solution of 0.43 mg of DMAP in dry CH_2Cl_2 via syringe pump over 8 hours. The reaction was kept at room temperature, under argon, and allowed to run for 48 hours. The product was purified by flash chromatography using 9/1 hexane/EtOAc. Yield 310 mg (73%). R_f = 0.40 (4/1 hexane/EtOAc). ^{1}H NMR ($CDCl_3$) δ 7.912 (d, *J* = 7.20 Hz, 2 H), δ 7.509 (t, *J* = 8.7 Hz, 1 H), δ 7.383 (t, *J* = 7.20 Hz, 2 H), δ 6.711 (d, *J* = 5.40 Hz, 2 H), δ 6.686 (s, 1 H), δ 6.466 (t, *J* = 2.10 Hz, 2 H), δ 4.462 (s, 4 H), δ 3.786 (s, 3 H), δ 3.744 (s, 3 H), δ 2.524 (m, 2 H), δ 2.106 (s, 3 H), δ 1.473 (s, 18 H) δ 1.367 (m, 4 H), δ 1.249 (m, 11 H), δ 0.942 (t, J = 8.4 Hz, 9 H) δ 0.870 (t, 4 H), δ 0.729 (q, *J* = 8.1, 8.7 Hz, 6 H).

6. Synthesis of Carbonate Ester of Decylubiquinol and 3',5'-Bis(carboxymethoxy)benzoin (DQ-BCMB, 6)

To a round bottom flask containing 25 mL neat trifluoroacetic acid (TFA) in an ice bath was added 280 mg of **5**. Under stirring ~0.1 ml of water was added to the reaction mixture. After one hour the reaction was frozen with liquid N_2, and the solvent removed under reduced pressure for 24 hours. Final purification was achieved using reverse-phase HPLC, using a gradient of 75%-100% MeCN in water with 0.1% TFA over 30 minutes. Upon removal of solvent, the product was isolated as a white powder. Yield 195 mg (91%). R_f = 0.05 (2/1 hexane/EtOAc); ^{1}H NMR (acetone-d_6) δ 8.086 (dd, *J* = 8.10, 0.90 Hz, 2 H), δ 7.604 (t, *J* = 6.30 Hz, 1 H), δ 7.487 (t, *J* = 7.50 Hz, 2 H), δ

7.004 (s, 1 H), δ 6.887 (d, J = 1.50 Hz, 2 H), δ 6.585 (t, J = 2.40 Hz, 2 H), δ 4.726 (s, 4 H), δ 3.781 (s, 6 H), δ 2.557 (m, 2 H), δ 2.134 (s, 3 H), δ 1.434 (m, 4 H), δ 1.278 (m, 11 H), δ 0.859 (m, 4 H). ^{13}C NMR (acetone-d_6) δ 193.194, 169.230, 160.173, 146.897, 135.025, 134.090, 129.802, 129.204, 129.157, 108.730, 102.660, 80.708, 65.180, 60.612, 60.488, 32.190, 27.089, 22.856, 13.880, 11.050. MS (FAB) *m/z* calcd 975.0969 ($M+H^+ +2Cs^+$), found 975.0942. The compound was was stored in DMF at -80°C prior to use.

7. Steady-state photolysis

Samples were prepared in a quartz cuvette and irradiated with an Oriel 66011 Hg vapor arc lamp operating at 450 W and filtered through water-cooled Schott glass type UG11 and WG320 filters. A stock solution of **6** was added to acetonitrile; 100 mM sodium phosphate buffer, pH 7.40; or 100 mM sodium phosphate buffer, 0.1% *n*-dodecyl-β-D-maltoside (DDM), pH 7.40 to yield a final concentration of 50 μM. The optical absorption was monitored with an HP 8452 diode array spectrophotometer. Photolysis was judged to be complete when no spectral changes occurred upon further illumination. HPLC analysis was performed using a Shimadzu LC-6A system equipped with a Vydac C-18 reverse-phase column. Analytical runs were performed with 0-100% MeCN in water with 0.1% TFA over 30 minutes.

8. Laser spectroscopy

A complete description of the laser setup for photolysis experiments is given elsewhere [9]. The photolysis was initiated by a 308 nm laser pulse from a Lambda

Physik LPX201I XeCl excimer laser, and the transient absorption was measured at the appropriate wavelength.

9. pH dependence of decarboxylation of the carbonate monoester of decylubiquinol

Aqueous solutions containing 30 μM DQ-BCMB and pH indicator dye were subject to laser photolysis under the conditions given above. Reactions were performed both in the presence and absence of 0.1% DDM. The indicator dyes used, along with the observation wavelength for pH change in water and 0.1% DDM, respectively, were as follows: bromphenol blue (pK_a = 4.0, λ = 590, 596 nm); bromcresol green (pK_a = 4.7, λ = 610, 616 nm); methyl red (pK_a = 4.8, λ = 522, 522 nm); bromcresol purple (pK_a = 6.3, λ = 588, 592 nm); bromthymol blue (pK_a = 7.0, λ = 614, 620 nm); *m*-cresol purple (pK_a = 8.3, λ = 578, 578 nm); and phenolphthalein (pK_a = 9.5, λ = 552, 552 nm). The solutions were unbuffered except by the indicator dye itself. The pH of the solutions was determined by measuring the relative amounts of protonated and deprotonated forms of the indicator dye spectrophotometrically. Concentrations of indicator dye were chosen such that the absorbance of the solution at the observation wavelength when poised at the pK_a of the indicator was in the range of 0.3-0.5. The pH changes were measured by the change in intensity of the most intense peak in either the acidic or basic form of the indicator, at the wavelengths listed above.

Results

1. Synthesis of Caged Decylubiquinol

The caged decylubiquinol used in this work, DQ-BCMB (**6**), consists of the decylubiquinol enzyme substrate (**8**) linked to the photolabile BCMB group (**10**) by means of a carbonate linkage. The synthesis is presented in Scheme 1. The carbonate diester was synthesized in a two-step process, the first of which was the coupling of monosilylated decylubiquinol (**1**) with bis(2-nitrophenyl)carbonate (**2**) to generate compound **3**. A second transesterification step led to the replacement of the nitrophenyl

Scheme 1. Synthesis of DQ-BCMB.

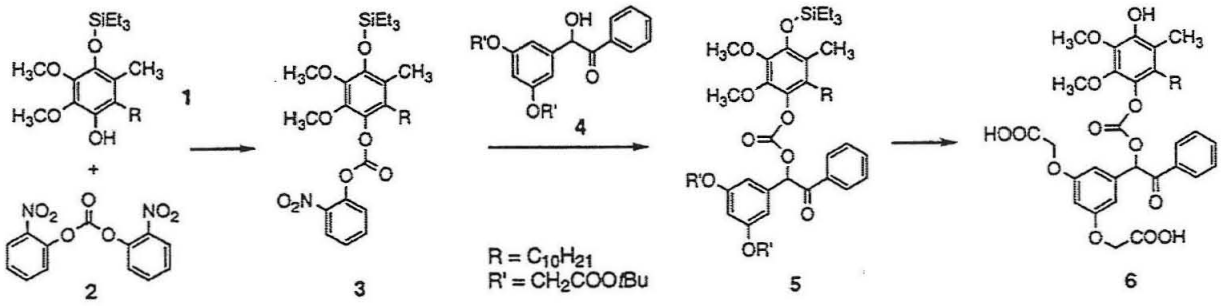

group with the *tert*-butylated BCMB cage (**4**) to yield the protected caged quinol **5**. Deprotection of this compound was achieved with neat TFA, to give the final product **6**.

The synthesis of the caged complex was complicated by the presence of the carbonate linkage. This linkage would hydrolyze in basic solutions, and was sensitive to heat and light. Bis(2-nitrophenyl)carbonate was chosen as the reagent for generating this linkage, as its reactions were found to give much higher yields and fewer side products than those involving reagents such as phosgene or 2-nitrophenylchloroformate. The acidic conditions used in the final deprotection step were found to be incompatible with the presence of double bonds in the hydrophobic side chain of the ubiquinol. Initial

attempts to produce a caged substrate using the quinols ubiquinol-1 and ubiquinol-2, both of which contain isoprenoid side chains, yielded a white, insoluble solid during the deprotection step. This material was believed to be a polymer formed from the intermolecular reactions of the carboxylate groups on the BCMB moiety and the activated double bonds of the ubiquinol. Decylubiquinol, which contains a saturated hydrocarbon tail, was used as a substrate in order to eliminate this side reaction. This quinol is commercially available and is commonly used to obtain the steady state kinetics of quinol-oxidizing enzymes.

2. Steady-State Photolysis of DQ-BCMB

Steady-state photolysis reactions of DQ-BCMB were performed in the following solvents: acetonitrile; 100 mM Na-PO_4, pH 7.4; and 100 mM Na-PO_4, 0.1% DDM, pH 7.4. On the basis of prior reports [6, 8, 10, 11] and results presented below, the photolysis reactions appear to have proceeded as diagrammed in Scheme 2. Upon photolysis of DQ-BCMB, the quinol was released as a carbonate monoester (**7**), and subsequent decarboxylation yielded free quinol **8**. Figure 1 shows the spectrum of intact DQ-BCMB in 100 mM Na-PO_4, 0.1% DDM, pH 7.4 (1a), as well as the spectra of the products of the photolysis reaction in the above solvents. The photolysis in MeCN (1c) was typical of the photolytic reactions of the BCMB group. A peak at 292 nm arose during the photolysis; on the basis of earlier studies [7, 8], it was assigned as arising from the cyclization of the BCMB group to form the substituted benzofuran **9**. No significant

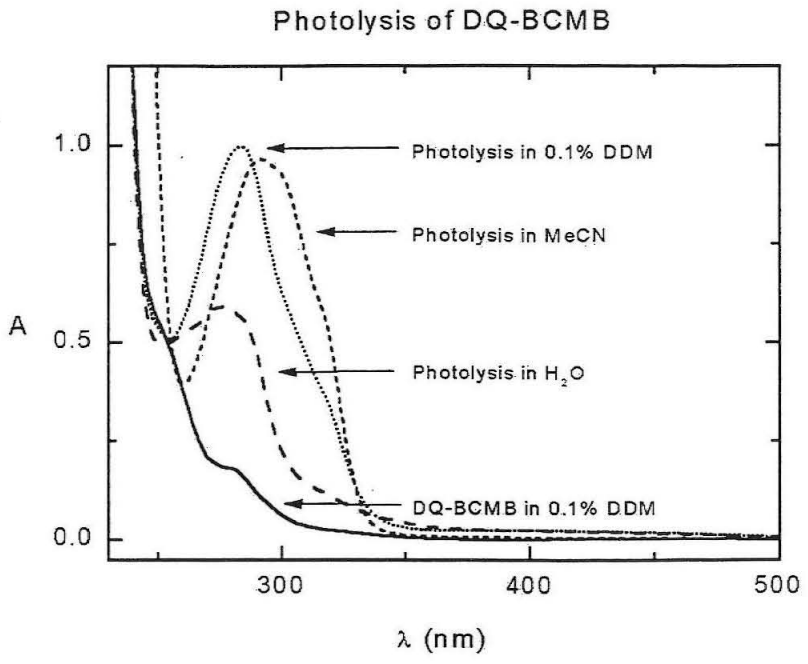

Figure 1. Absorption spectra of 50 μM DQ-BCMB in 100 mM Na-PO_4, 0.1% DDM, pH 7.4 (a); and the products of the photolysis of 50 μM DQ-BCMB in 100 mM Na-PO_4, pH 7.4 (b); acetonitrile (c); and 100 mM Na-PO_4, 0.1% DDM, pH 7.4 (d).

spectral changes occurred as a result of the release of the quinol molecule. In aqueous phosphate buffer solution (1b), photolysis of DQ-BCMB gave rise to a broad peak with a λ_{max} at 276 nm and an intensity much lower than is observed in acetonitrile. Prior work from this laboratory has shown that a competition exists in aqueous solution between cyclization of the BCMB group to form the benzofuran and the attack of water on one of the intermediates of the photolytic process to regenerate the parent benzoin **10** [8]. As free BCMB has a spectrum similar to that of unphotolyzed DQ-BCMB, the low intensity seen at 276 nm suggests that the yield of benzofuran product is in fact lower in aqueous solution than in acetonitrile. In accord with this, HPLC analysis of the photolysis products revealed the presence of both the substituted benzofuran and BCMB, in a ratio of 30:70. Photolysis of DQ-BCMB in phosphate buffer with 0.1% DDM (1d) gave rise to a spectral peak at 284 nm, with an intensity slightly higher than that in acetonitrile.

This result was observed consistently for DQ-BCMB at DDM concentrations in the range of 0.05%-0.5% (data not shown). HPLC analysis showed that in addition to the release of decylubiquinol, the benzofuran photoproduct was formed in >80% yield. The high yield of substituted benzofuran observed in DDM solution suggested that the DQ-BCMB was localized in detergent micelles, so that it was shielded from water during photolysis.

3. Laser photolysis of DQ-BCMB

To determine the rate of photolysis of DQ-BCMB and the photolysis yield under conditions compatible with enzymatic study, transient absorption spectra of 50 μM DQ-BCMB were taken in 100 mM Na-PO_4, 0.1% DDM, pH 7.4. As shown in Figure 1, the photolysis products of DQ-BCMB have a small but non-zero absorbance at wavelengths as high as 500 nm. Control experiments with organic acids derivatized with the BCMB group showed that the absorbance change at high wavelengths arose from the benzoin and benzofuran products, not the quinol substrate. The change in absorbance at 400 nm was used to monitor the photolysis reaction, as there is negligible absorption by DQ-BCMB at this wavelength, and thus no photolysis of the sample by the probe beam, and this wavelength lies below the Soret band in heme spectra. An extinction coefficient for the photolyzed minus unphotolyzed difference spectrum of 0.5 mM^{-1} cm^{-1} was calculated on the basis of the spectra in Figure 1. At a concentration of 50 μM DQ-BCMB, photolysis yield was linear with laser power, generating 10 μM of quinol at a laser power of 3.5 mJ/pulse. Transient absorption was also monitored at 310 nm to measure benzofuran formation specifically. As has been shown with the 3',5'-dimethoxybenzoin

group [7], photolysis occurred within the instrument response time of the laser setup, setting a lower bound of 10^6 s^{-1} for benzofuran formation.

4. Decarboxylation of the caged ubiquinol

As diagrammed in Scheme 2, the overall photolysis reaction of DQ-BCMB involves two processes: the cyclization or hydrolysis of the BCMB group with concomitant release of substrate, and a decarboxylation of the released substrate. While the former reaction is readily observable by optical spectroscopy, the decarboxylation step is more difficult to observe. During experiments in which transient absorption spectroscopy was used to monitor the reaction of photoreleased decylubiquinol with *E. coli* cytochrome bo_3, we found the rates of enzyme reduction by the released substrate to be slower than the enzyme turnover, which suggested that decarboxylation of the substrate was rate-limiting in this process. These results are presented in the following paper. In other recent experiments in which amines were linked to photolabile protecting groups using a carbamate linkage, decarboxylation of substrate was shown to be significantly slower than the primary photolytic process [10]. The availability of a water-

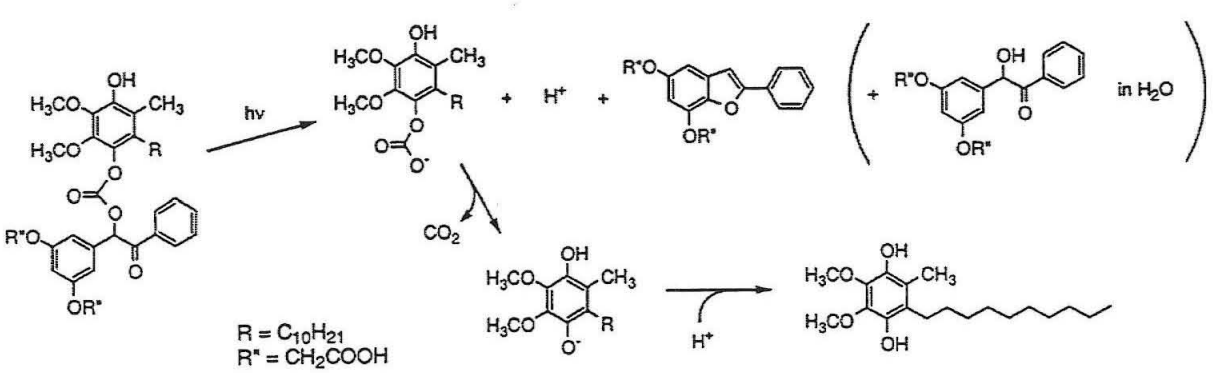

Scheme 2. Photolysis reaction of DQ-BCMB.

soluble BCMB cage allowed us to explore the decarboxylation reaction of quinol carbonate monoesters in more depth.

The photolysis of DQ-BCMB contains two steps that involve the uptake or release of protons (see Scheme 2). In the actual photolysis event, the BCMB group will either cyclize to form benzofuran and release a proton, or will be hydrolyzed with the associated release of a proton. The carbonate monoester of the quinol will remain deprotonated in normal pH ranges, but upon decarboxylation, the quinol anion will pick up a proton if the solution pH is less than the pK_a for the quinol. Thus, upon photolysis of the caged decylubiquinol, there will be a rapid acidification of the solution and a subsequent alkalinization that should occur at the rate of decarboxylation of the quinol carbonate monoester.

In order to monitor the decarboxylation reaction, laser photolysis reactions were performed in aqueous solution in the presence of pH indicator dyes, so that the pH changes during the reaction could be measured by the absorbance change of the indicator. Reactions were performed both in the presence and in the absence of 0.1% DDM, in the pH range of 3.9-9.6. Figure 2 summarizes the results of these reactions over the pH range 3.9-8.1. The inset shows a typical absorption transient, following the photolysis of DQ-BCMB in 0.1% DDM in the presence of bromcresol purple. The rapid decrease in absorbance following the laser flash indicated an acidification of the solution. This was followed by a biexponential rise corresponding to realkalinization of the solution, in which the rapid phase contributed most of the increase in intensity. The slower phase likely arose from a slow protonation of a small subset of the quinol molecules, or a reaction of the indicator dye itself. In either case, the phase was sufficiently slow and of

low enough intensity that it was not expected to have a significant effect on subsequent enzyme chemistry. Because of photobleaching of the dye, the absorbance did not return

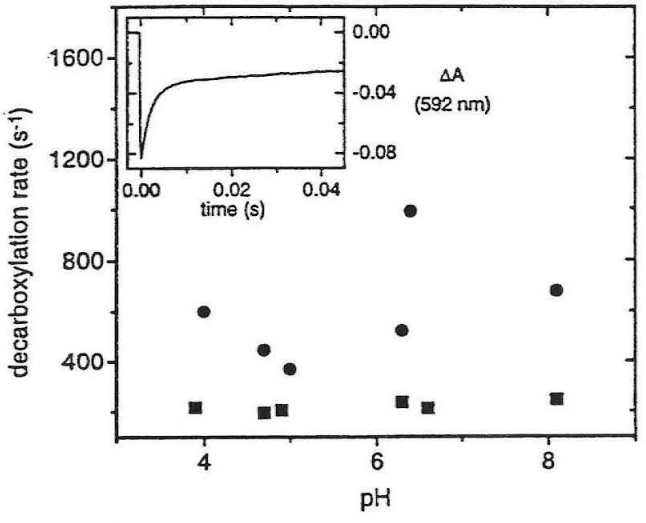

Figure 2. Rates of decarboxylation of the carbonate monoester of decylubiquinol in the presence (circles) or absence (squares) of 0.1% DDM as a function of pH. Inset: Time course of the reaction of 32 μM DQ-BCMB in 11 μM bromcresol purple, 0.1% DDM, pH 6.3 following photolysis by a 308 nm laser pulse. The absorption was monitored at 592 nm. See text for details.

to the baseline at the end of the reaction, as the reaction stoichiometry would predict. At all pH values, the acidification was instantaneous on the time scale of the experiment. In the absence of detergent, the alkalinization reaction occurred over the pH range with first order rate constants of 195-250 s^{-1}. At pH values > 9, little alkalinization was observed, most likely because the ubiquinol remained deprotonated. As a result, kinetic data in this pH range are not included in Figure 2. In 0.1% DDM solution, the decarboxylation rates were significantly more rapid than those in its absence. Over the range of indicators used, the rates varied from 370 s^{-1} to 990 s^{-1}. The variation in rates showed no correlation with pH, demonstrating that the decarboxylation step is not acid- or base-

assisted. The generally more rapid decarboxylation in detergent solution likely arose because the caged quinol molecules were localized within detergent micelles, an environment that would tend to destabilize the charged carbonate formed during photolysis of the starting material.

5. Reaction of DQ-BCMB with Cytochrome bc_1 and Cytochrome bo_3

Decylubiquinol released upon photolysis of DQ-BCMB was shown to react with the quinol-oxidizing enzymes mitochondrial cytochrome bc_1 and *E. coli* cytochrome bo_3 on a time scale of milliseconds. Full details of these experiments are given in the following paper.

Discussion

1. Evaluation of DQ-BCMB as a Photoreleasable Enzyme Substrate

The caged decylubiquinol, DQ-BCMB, was designed and synthesized for use as a substrate for quinol-oxidizing respiratory enzymes. Compatibility of DQ-BCMB with biological systems and its utility in enzymological studies require several chemical and physical properties, which are assessed below.

In previous work on ubiquinol protected with a 3',5'-dimethoxybenzoin moiety, the photolysis properties of this compound could not be evaluated completely on account of the insolubility of this compound in water [7]. Solubility problems of this sort are common for photolabile protecting groups, which usually contain aromatic chromophores that decrease the aqueous solubility of the molecules they protect. The BCMB cage has overcome this problem through the presence of two carboxylate groups that provide

water solubility without significantly affecting the photochemical properties of the protecting group. We have measured the solubility of DQ-BCMB as > 300 μM in 0.1% DDM solution, a concentration that is much higher than that necessary for enzymological studies. Although the compound is water-soluble, it has the desirable feature of partitioning preferentially into the detergent phase of solution, as demonstrated by the steady-state photolysis experiments described above. Localization of the substrate in a hydrophobic environment is ideal in that the carbonate linkage of the substrate is less prone to hydrolysis in the hydrophobic environment, and in that the enzymes of interest to us are membrane-bound, and thus the reaction chemistry should be facilitated by the proximity of substrate and enzyme.

Two other criteria for an optimal caged substrate are the inactivity of the caged substrate with respect to the enzyme and the formation of inert by-products from the photolysis reaction. Through the use of control reactions, we have demonstrated the first property with respect to cytochrome bc_1 and cytochrome bo_3. The by-products of the reaction, the substituted phenylbenzofuran and CO_2, do not possess any functional groups that are likely to react with these enzymes, and neither product has shown inhibition of enzyme turnover.

The quantum yield of the photolysis products of DQ-BCMB is quite high as well, another requirement for a useful photocage. Sheehan et al. reported a quantum yield of 0.64 for DMB-acetate [5], and a similar value has been estimated for alcohols protected with the DMB group using a carbonate linkage [6]. We expect the quantum yield for DQ-BCMB to be the same. From a practical standpoint, laser photolysis of 100 μM DQ-

BCMB was capable of releasing 35 μM of substrate in one pulse using acceptable laser power (~5.5 mJ/pulse), a value sufficiently high for enzyme studies.

The BCMB cage was chosen for use on the basis of the rapid photochemistry of the benzoin group. However, the rate-determining step for release of active quinol is the decarboxylation of the carbonate that arises upon photolysis of the caged substrate. Sauers et al. have found an empirical relationship between the pK_a of aliphatic alcohols and the rate of decarboxylation of the corresponding alkyl carbonates [12]. Rossi and Kao have utilized the *o*-nitromandelyloxycarbonyl group to cage 2,5-di(*tert*-butyl)hydroquinone, and on the basis of the above relationship, they calculated an approximate $t_{1/2}$ for the decarboxylation of the carbonate of 5 ms [11]. Further, Papageorgiou and Corrie have reported a $t_{1/2}$ of 4.5 ms for decarboxylation of a carbamate that was generated photochemically [10]. The values reported herein are comparable to or faster than these.

Although the potential rates of decylubiquinol release that may have been predicted on the basis of the rate of benzoin cyclization were not realized, the BCMB cage still allows a rapid release of this substrate. In detergent solution, decarboxylation rates as high as 990 s^{-1} were observed for decylubiquinol, making substrate release comparable to or faster than traditional rapid-mixing/stopped-flow techniques. The photorelease of quinol substrate can serve as a complementary technique to more traditional methods of studying rapid kinetics. It has potential use in situations where the turbulent mixing associated with stopped flow may disrupt the integrity of liposomes, and for techniques such as Laue diffraction in which rapid mixing cannot be used to initiate reaction chemistry.

2. General Utility of BCMB as a Photolabile Protecting Group

While the primary focus of this work has been the caging of quinol molecules, it also reveals the general utility of BCMB as a photolabile protecting group for enzyme substrates. The solubility and photochemical reactivity of the BCMB group and the inertness of the benzofuran photoproduct of this protecting group are characteristics of the cage itself that will apply to any substrates that can be derivatized with this group. As has been shown in previous studies with DMB-, BCMB- and benzoin-protected compounds [5, 8, 13], substrates which are good leaving groups (e.g., organic acids and phosphates) can be deprotected at the rate of benzofuran formation (< 100 ns). Further, it is expected that the observed inertness of the BCMB cage with respect to the integrity and activity of cytochrome bc_1 and cytochrome bo_3 will apply to a broad range of enzymes. Thus, we feel that BCMB-caged substrates can be an excellent tool in the study of the rapid bimolecular reactions of enzymes with their substrates, particularly those in which the substrate is hydrophobic.

Conclusions

In this work we have characterized the caged decylubiquinol DQ-BCMB and demonstrated that it possesses many properties that make it highly suitable as a photoreleasable enzyme substrate. It has good solubility in aqueous solution, excellent reactivity characteristics, a high photolysis yield, and a release time comparable to or better than traditional mixing techniques or photolysis of other "caged" alcohols. In the following paper, we present the use of this protected ubiquinol in the study of the

enzymes cytochrome bc_1 and cytochrome bo_3. From the standpoint of general utility, the availability of a caged alcohol substrate with a release rate on the microsecond time scale would expand the range of topics that could be addressed though the use of photoreleasable substrates and allow a complete study of the rapid bimolecular kinetics of many other enzymes. Further work is in progress to extend the methodology to this rapid time scale.

References

1) B.L. Trumpower, R.B. Gennis, Annu. Rev. Biochem. 63 (1994) 675-716.

2) M.C.R. Shastry, S.D. Luck, H. Roder, Biophys. J. 74 (1998) 2714-2721.

3) S.R. Adams, R.Y. Tsien, Controlling cell chemistry with caged compounds, Annu. Rev. Physiol. 55 (1993) 755-784.

4) J.E.T. Corrie, D.R. Trentham, Caged nucleotides and neurotransmitters, in: H. Morrison (Ed.), Bioorganic Photochemistry Volume 2: Biological Applications of Photochemical Switches, John Wiley & Sons, New York, 1993, pp. 243-305.

5) J.C. Sheehan, R.M. Wilson, A.W. Oxford, The photolysis of methoxy-substituted benzoin esters. A photosensitive protecting group for carboxylic acids, J. Am. Chem. Soc. 93 (1971) 7222-7228.

6) M.C. Pirrung, J.-C. Bradley, Dimethoxybenzoin carbonates: Photochemically-removable alcohol protecting groups suitable for phosphoramidite-based DNA synthesis, J. Org. Chem. 60 (1995) 1116-1117.

7) M.H.B. Stowell, G. Wang, M.W. Day, S.I. Chan, Design, synthesis, and photochemical properties of a photoreleasable ubiquinol-2: A novel compound for studying rapid electron-transfer kinetics in ubiquinol-oxidizing enzymes, J. Am. Chem. Soc. 120 (1998) 1657-1664.

8) R.S. Rock, S.I. Chan, Preparation of a water-soluble "cage" based on 3'-5'-dimethoxybenzoin, J. Am. Chem. Soc. 120 (1998) 10766-10767.

9) T.J. DiMagno, M.H.B. Stowell, S.I. Chan, Photoreduction of cytochrome *c* and other heme proteins by new nitrobenzene derivatives: A general approach to

studying intermolecular electron transfer reactions in proteins, J. Phys. Chem. 99 (1995) 13038-13047.

10) G. Papageorgiou, J.E.T. Corrie, Synthesis and properties of carbamoyl derivatives of photolabile benzoins, Tetrahedron 53 (1997) 3917-3932.

11) F.M. Rossi, J.P.Y. Kao, Nmoc-DBHQ, a new caged molecule for modulating sarcoplasmic/endoplasmic reticulum Ca^{2+} ATPase activity with light flashes, J. Biol. Chem. 272 (1997) 3266-3271.

12) C.K. Sauers, W.P. Jencks, S. Groh, The alcohol-bicarbonate-water system. Structure-reactivity studies on the equilibria for formation of alkyl monocarbonates and on the rates of their decomposition in aqueous alkali, J. Am. Chem. Soc. 97 (1975) 5546-5553.

13) R.S. Givens, P.S. Athey, L.W. Kueper, III, B. Matuszewski, J.-y. Xue, Photochemistry of α-keto phosphate esters: Photorelease of a caged cAMP, J. Am. Chem. Soc. 114 (1992) 8708-8710.

Chapter 5:

Reaction of Mitochondrial Cytochrome *bc*1 and *Escherichia coli* Cytochrome *bo*3 With a Photoreleasable Decylubiquinol

Abstract

The electron transfer from decylubiquinol to the respiratory enzymes *Escherichia coli* cytochrome bo_3 and mitochondrial cytochrome bc_1 was studied using a decylubiquinol molecule derivatized with the 3',5'-bis(carboxymethoxy)benzoin (BCMB) protecting group. As described in the previous paper, irradiation of the protected decylubiquinol (DQ-BCMB) with a 308 nm laser pulse led to the rapid release of decylubiquinol. In the presence of cytochrome bo_3, photolysis of DQ-BCMB led to the oxidation of quinol by the enzyme with a rate that was limited by the rate of the decylubiquinol release. Cytochrome bc_1 reacted with photoreleased decylubiquinol with distinct kinetic phases corresponding to rapid *b* heme reduction and somewhat slower *c* heme reduction. Oxidation of photoreleased ubiquinol by this enzyme showed saturation kinetics with a K_M of 3.6 μM and a k_{cat} of 210 s^{-1}. The saturation behavior was a result of decylubiquinol being released as a carbonate monoester during the photolysis of DQ-BCMB and interacting with cytochrome bc_1 before decarboxylation of this intermediate yielded free decylubiquinol. The reaction of cytochrome bc_1 and photoreleased decylubiquinol in the presence of antimycin A led to monophasic *b* heme reduction, but also yielded slower quinol oxidation kinetics. The discrimination of kinetic phases in the reaction of cytochrome bc_1 with ubiquinol substrates has provided a means of exploring the bifurcation of electron transfer that is central to the operation of the Q-cycle in this enzyme.

Introduction

Quinol oxidation is a common feature of respiration in mitochondria and aerobic bacteria [1]. Quinol-oxidizing enzymes utilize the energy released in the electron transfer from quinols to electron-accepting substrates in order to promote the translocation of protons across the inner mitochondrial or cytoplasmic membrane. The resulting electrochemical gradient is utilized for the production of ATP. The fundamental component of the coupling of electron transfer to proton translocation is the ability of the enzyme to direct the electron transfer through the protein in a precise manner, in terms of both the sequence of electron carriers and the rates of electron transfer, so that redox-linked proton translocation is achieved in preference to uncoupled electron transfer that is thermodynamically favored but non-productive with respect to proton translocation. Thus, a complete description of the electron transfer mediated by proton-translocating enzymes is necessary to understand the mechanism of these proteins. In the case of quinol-oxidizing enzymes, the initial electron input to the enzyme is expected to play a crucial role in proton translocation. Yet, this has been a difficult area of study on account of the rapid kinetics of quinol oxidation.

In our laboratory, we have been interested in two quinol-oxidizing enzymes, mitochondrial cytochrome bc_1 and *Escherichia coli* cytochrome bo_3, particularly with regard to the mechanistic similarities and differences between the two in terms of proton translocation in each of the proteins. Schematic diagrams of these proteins are shown in Figure 1.

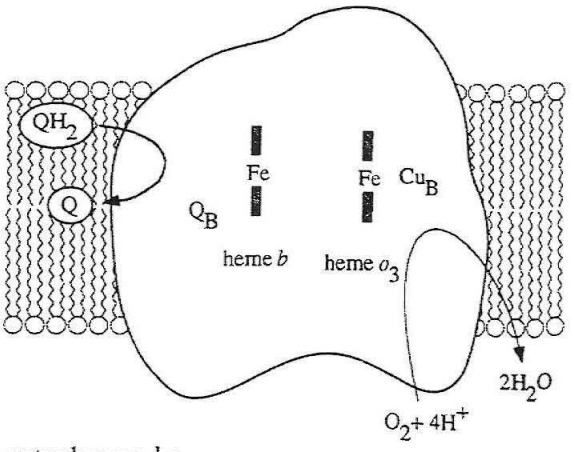

cytochrome bo_3

Figure 1. Schematic diagram of the enzyme cytochrome bo_3 (for cytochrome bc_1 see chapter 2). Abbreviations: Q: ubiquinone; QH_2: ubiquinol. All other redox centers are described in the text.

Cytochrome bo_3 catalyzes the oxidation of ubiquinol to ubiquinone, using the electrons released in this process to promote the four-electron reduction of dioxygen to water. The electron transfer from ubiquinol to dioxygen is coupled to the translocation of protons across the bacterial cytoplasmic membrane. Cytochrome bo_3 contains a low-spin *b* heme involved in electron transfer, and a binuclear site composed of a high spin o_3 heme and a mononuclear copper center (Cu_B). This binuclear site is the location of dioxygen reduction by the enzyme. In addition to the metal centers in the enzyme, there is a tightly bound molecule of quinone (Q_B) near heme *b*, at a site distinct from that of quinol oxidation. The precise location of this quinone and its role in enzyme turnover have not been fully defined to date.

The study of electron transfer through this enzyme has been performed primarily using CO flow-flash methodology [2-9]. Although this type of study can be used to probe electron transfer in pre-reduced enzyme, the utility of this strategy in the study of electron input to the enzyme from quinol under single turnover conditions is limited. Steady-state kinetics of cytochrome bo_3 have revealed a turnover of 1500 molecules of

ubiquinol-2 per second by this enzyme [10], making initiation of single-turnover chemistry difficult. In a previous freeze-quench EPR study from our laboratory in which cytochrome bo_3 was reacted with a substoichiometric amount of ubiquinol-2, the resulting electron distribution in the enzyme suggested that heme *b* and Cu_B were the electron acceptors from quinol [11]. However, the enzyme reduction occurred in the 10 ms dead time of the apparatus used in the study, and therefore the kinetics of the electron input could not be studied. Thus, verification of which redox centers are the initial electron acceptors from ubiquinol, the rate of electron input to the enzyme, and the sequence of electron tranfers following quinol oxidation remain unresolved issues.

Mitochondrial cytochrome bc_1 is an eleven-subunit enzyme embedded in the inner mitochondrial membrane. Three of the subunits, cytochrome *b*, cytochrome c_1, and the iron-sulfur protein, contain redox centers which are involved in electron transfer through the enzyme and constitute the catalytic core of the protein complex. Cytochrome *b* contains two *b* hemes, a low-potential heme b_L and a higher potential heme b_H. The iron-sulfur protein contains an Fe_2S_2 cluster, and cytochrome c_1 contains a single *c* heme. In addition to these four redox centers, the enzyme contains two quinone/quinol binding sites. The P center lies near the cytoplasmic side of the membrane, and is the site of ubiquinol oxidation. The N center is near the matrix side of the membrane; quinone reduction occurs at this site, as described below. Recent crystal structures of cytochrome bc_1 have defined the location and orientation of these centers [12-14].

The reaction mechanism of cytochrome bc_1 is described by a Q-cycle model, originally formulated by Mitchell [15]. At the heart of this model is a branched electron transfer pathway through the enzyme controlled at the P center of the enzyme. The cycle

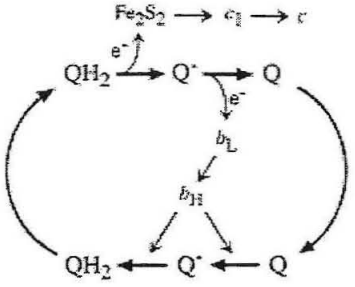

Figure 2. Schematic diagram of the Q-cycle of mitochondrial cytochrome bc_1. Solid arrows denote chemical transformations or diffusion of substrate. Dashed arrows indicate electron transfer. Abbreviations: Q: ubiquinone; $Q^{\bullet}$: ubisemiquinone; QH_2: ubiquinol. b_L, b_H, and c_1 denote the heme

is shown schematically in Figure 2. Full turnover of the enzyme requires the oxidation of two molecules of quinol. Upon the oxidation of the first molecule of ubiquinol, one electron from this oxidation is transferred to the Rieske iron-sulfur cluster, and the other is passed to heme b_L and then on to heme b_H. The electron at the iron-sulfur cluster is then passed to cytochrome c_1, and on to the water-soluble protein ferricytochrome *c*. The electron in cytochrome *b* is transferred to a quinone at the N center of the enzyme, reducing the quinone to its ubisemiquinone form. Reaction of a second molecule of quinol at the P center again leads to the transfer of one electron to the iron-sulfur cluster and one to cytochrome *b*. The electron at the iron-sulfur cluster is transferred through cytochrome c_1 to a second molecule of ferricytochrome *c*, and the electron in cytochrome *b* is used to reduce the semiquinone at the N center to its fully reduced quinol form. This quinol can then dissociate and diffuse back into the membrane-bound ubiquinone pool. The result of this reaction is the oxidation of two molecules of ubiquinol with the release of four protons on the cytoplasmic side of the mitochondrial membrane, the reduction of one molecule of ubiquinone with the associated uptake of two protons from the matrix side of the mitochondrial membrane, and the reduction of two molecules of ferricytochrome *c*. The $(([QH_2]/[Q])_{pool}$ / ([cyt c^{3+}]/[cyt c^{2+}])) ratio provides the driving force for the vectorial proton translocation. In terms of the efficiency of proton

translocation, the reaction cycle leads to the release of four protons on the cytoplasmic side of the inner mitochondrial membrane with a *net* oxidation of only one ubiquinol molecule and the transfer of two electrons to ferricytochrome *c*. In contrast, if there was no branched electron transfer, and all of the electrons from quinol oxidation were transferred to cytochrome *c*, bypassing the N center, only two scalar protons would be deposited in the cytosol for every two electrons passing to cytochrome *c*. Thus, the Q-cycle doubles the efficiency of proton translocation arising from ubiquinol oxidation.

The branched electron transfer at the P center of cytochrome bc_1 is kinetically controlled, since the thermodynamically more favored reaction is the transfer of all of the electrons from quinol oxidation to ferricytochrome *c*. The precise means of this control is not understood at this time. Models of the branched electron transfer pathway include a "catalytic switch" model in which electron transfer is controlled by differential binding of quinol and semiquinone in the P center of the enzyme [16, 17], P center dual-occupancy models [18-20], a "proton-gated affinity change" mechanism in which electrostatic interactions between the iron-sulfur cluster and bound semiquinone prevent the transfer of an electron from the iron-sulfur cluster to cytochrome c_1 prior to the oxidation of semiquinone [21], and structure-based models involving domain motion of the iron sulfur protein after it accepts an electron from ubiquinol [13, 14]. The validity of these possibilities depends on the identity of the rate-determining step in the reduction of enzyme. With regard to the Q-cycle model in Figure 2, the most likely rate determining steps are the oxidation of the first molecule of quinol in the turnover cycle (equation 1), domain movement of the iron-sulfur cluster in its electron transfer to cytochrome c_1 (equation 2), and the oxidation of the second molecule of quinol in the reaction cycle

(equation 3). These three possibilities give different predictions with respect to the kinetics of heme reduction by ubiquinol in cytochrome bc_1. If the oxidation of the first molecule of quinol is rate-limiting (equation 1), all three hemes in the enzyme should have identical reduction rates. If electron transfer from the iron-sulfur protein to cytochrome c_1 is rate-limiting (equation 2), a fast *b* heme reduction should be observed, followed by a second phase in which *b* heme and *c* heme reduction occur at equal rates. Finally, if the oxidation of the second molecule of quinol is rate-limiting (equation 3), a rapid reduction of *b* and *c* hemes, followed by a slower phase of *b* heme reduction, would be predicted. In this connection, it is important to note that the oxidation of quinol by cytochrome bc_1 is a bimolecular reaction, whereas the electron transfer from the iron-sulfur cluster to cytochrome c_1 is intramolecular. Therefore, depending on the reaction conditions, either quinol oxidation or intramolecular electron transfer may be rate-limiting. Factors which may control which step is rate-limiting include the concentration of the quinol substrate, the identity of the quinol substrate, and the presence of enzyme inhibitors.

$$QH_2 + \text{Fe-S(ox)} + \text{cyt } b\text{(ox)} \rightarrow Q + \text{Fe-S(red)} + \text{cyt } b(1e^-\text{-red}) \quad (1)$$

$$\text{Fe-S(red)} + \text{cyt } c_1\text{(ox)} \rightarrow \text{Fe-S(ox)} + \text{cyt } c_1\text{(red)} \quad (2)$$

$$QH_2 + \text{Fe-S(ox)} + \text{cyt } b(1e^-\text{-red}) \rightarrow Q + \text{Fe-S(red)} + \text{cyt } b(2e^-\text{-red}) \quad (3)$$

A full mechanistic understanding of the turnover of both cytochrome bo_3 and cytochrome bc_1 requires the ability to initiate the reaction with ubiquinol on a suitably

rapid time scale. In order to study the electron transfer from ubiquinol to cytochrome bo_3 and cytochrome bc_1, we have synthesized decylubiquinol molecules derivatized with the photolabile protecting group 3',5'-bis(carboxymethoxy)benzoin (BCMB). The carbonate ester of decylubiquinol and BCMB, hereafter referred to as DQ-BCMB, undergoes rapid photolysis to release decylubiquinol, which is then free to react with enzyme. The synthesis and characterization of DQ-BCMB and its photochemical properties are presented in the previous paper. In this work we describe the reaction of DQ-BCMB with cytochrome bo_3 and cytochrome bc_1 following the rapid initiation of reaction chemistry with a laser pulse.

Materials and Methods

1. General

The caged quinol DQ-BCMB was synthesized as described in the previous paper. Antimycin A was purchased from Sigma and used as received. *n*-Dodecyl-β-D-maltopyranoside (DDM) was purchased from Anatrace. Cytochrome bc_1 from bovine heart mitochondria and *Escherichia coli* strain GO105/pJRHisA were generous gifts from Dr. C. A. Yu of the Department of Biochemistry, Oklahoma State University, and Dr. R. B. Gennis of the Department of Biochemistry, University of Illinois, respectively. Cytochrome bo_3 was prepared as described previously [10].

2. Laser spectroscopy

Transient absorption spectroscopy was performed using a laser setup described elsewhere [22]. The photolysis was initiated by a 308 nm laser pulse from a Lambda

Physik LPX201I XeCl excimer laser. Transient absorption was measured at individual wavelengths.

3. Reaction of cytochrome bo_3 with DQ-BCMB

A solution of 1.2 μM cytochrome bo_3 and 100 μM DQ-BCMB in 1 mL of 100 mM sodium phosphate buffer (Na-PO4), 0.1% DDM, pH 7.4 was subjected to irradiation at 308 nm. The laser power was measured prior to each experiment. Transient absorption was measured at individual wavelengths from 400-450 nm. For any given sample, a maximum of 20 pulses (25 ns pulse width, 500 ns total irradiation) was used, with stirring in between each pulse, before the sample was replaced, so as to prevent excessive depletion of starting material. Control experiments were performed on 1.2 μM cytochrome bo_3 in the absence of DQ-BCMB, and on 100 μM DQ-BCMB in the absence of cytochrome bo_3, over the same wavelength range and using identical conditions as above.

4. Reaction of cytochrome bc_1 with DQ-BCMB

Solutions of 1.7 μM or 3.4 μM mitochondrial cytochrome bc_1 and 100 μM DQ-BCMB in 100 mM Na-PO_4, 0.1% DDM, pH 7.4 were irradiated with 308 nm laser pulses. Energies of the laser pulses were measured for each experiment. Absorption transients were acquired over the wavelength ranges 400-450 nm (heme Soret bands) and 540-580 nm (α-bands). Samples were replaced after a maximum of six pulses. For the power dependence studies, a flow cell was used and the sample replaced after each pulse.

Control experiments on cytochrome bc_1 in 100 mM Na-PO_4, 0.1% DDM, pH 7.4 in the absence of DQ-BCMB, and inhibition studies utilizing antimycin A were performed under identical conditions.

Results

1. Reaction of DQ-BCMB with cytochrome bo_3

The reaction of *E. coli* cytochrome bo_3 was studied following photolysis of the caged decylubiquinol by measuring the changes in the optical absorption spectra of hemes *b* and o_3. Figure 3 shows absorption transients at 404 nm and 430 nm following the photolysis of DQ-BCMB in the presence of 1.2 μM cytochrome bo_3. These wavelengths correspond to the minimum and maximum, respectively, of the reduced minus oxidized difference spectrum of the enzyme. At 404 nm, there was a nearly

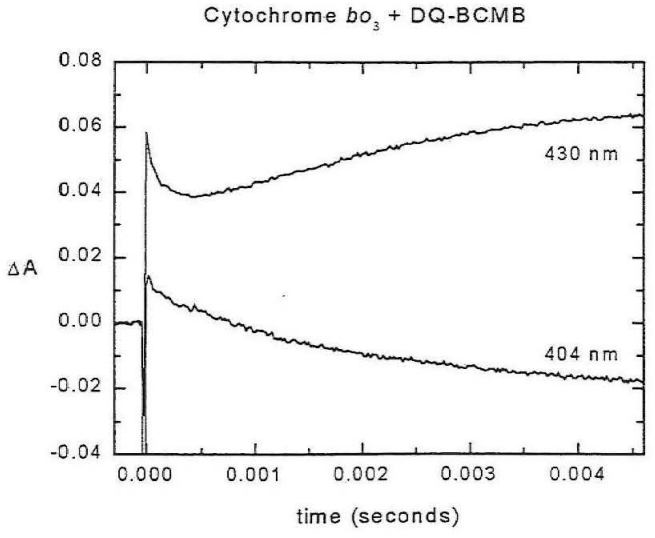

Figure 3. Time course of the reaction of 1.2 μM cytochrome bo_3 with 100 μM DQ-BCMB following photolysis, measured at 404 nm and 430 nm. The excitation wavelength was 308 nm, with energy of 5 mJ/pulse. The traces are an average of five absorption transients.

instantaneous increase in absorbance followed by a biphasic decay in intensity. At 430 nm, the initial increase in absorbance was followed by a rapid decay of the signal and a slower rise in absorbance at this wavelength. The first phase was assigned on the basis of the wavelength dependence of its magnitude. Through comparison of this phase with the spectrum of the photolysis products of DQ-BCMB (see previous paper) and the reduced-minus-oxidized spectrum of cytochrome bo_3 (see figure 4), the phase was assigned as the photolysis of 23 μM DQ-BCMB and the photoreduction of 0.05 μM cytochrome bo_3 (0.1 μM heme). In control experiments in which the cytochrome bo_3 and DQ-BCMB were subjected to laser irradiation independently, photoreduction of cytochrome bo_3 and photolysis of DQ-BCMB were observed at levels slightly higher than those listed above. The second phase of the reaction of cytochrome bo_3 with DQ-BCMB, extending from t =

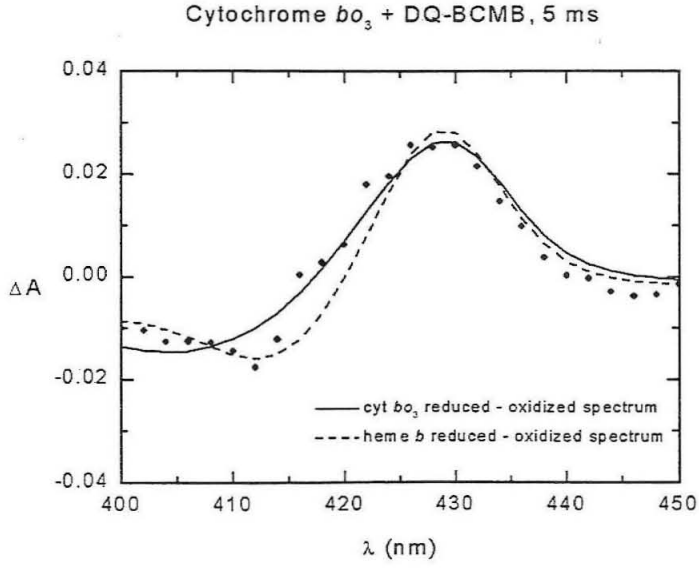

Figure 4. Wavelength dependence of the reaction of 1.2 μM cytochrome bo_3 with 100 μM DQ-BCMB following photolysis. Data points are the magnitude of the kinetic phase corresponding to electron transfer from decylubiquinol to cytochrome bo_3 (the slowest phase in figure 3). Values were calculated from biexponential fits of the transient absorption at each wavelength, ignoring the initial rise in absorbance.

0 to approximately 500 μs, was assigned primarily to reoxidation of the hemes, again on the basis of multiple wavelength measurements. Decay arising from amplifier ringing in the instrumental setup was also observed during this phase.

The final phase corresponded to the electron transfer from photoreleased decylubiquinol to cytochrome bo_3. This phase was not observed in control experiments in which cytochrome bo_3 or DQ-BCMB was irradiated by itself. A biexponential fit to the transient absorption data at both 404 nm and 430 nm gave an observed rate constant of 450 s^{-1} for the final electron transfer phase. Figure 4 shows the wavelength dependence of the magnitude of this phase over the wavelength range 400-450 nm. Also included are a reduced minus oxidized difference spectrum for cytochrome bo_3 and a difference spectrum for heme *b* alone, measured as described in prior literature [3]. Comparison with these two spectra suggests that the absorption change for this phase arose from a general reduction of the enzyme, with a slightly larger reduction level for heme *b* than for heme o_3. Reduction of both *b* and *o* hemes was verified on the basis of α-band absorbance as well (data not shown). The magnitude of the absorbance change corresponded to a reduction of 0.11 μM enzyme (0.22 μM heme).

The dependence of the rate of reduction of cytochrome bo_3 on the concentration of photoreleased decylubiquinol was determined over the range 3 μM - 35 μM quinol. Decylubiquinol was released as a carbonate upon photolysis of DQ-BCMB (see previous paper), and because neither the carbonate nor the free quinol had a significant optical absorption at the wavelengths used to monitor cytochrome bo_3 reduction, the concentration of the benzofuran and benzoin photoproducts of the photolysis was used to quantify the amount of decylubiquinol released, with the understanding that the

calculated decylubiquinol concentration was the sum of the concentrations of carboxylated and free quinol. The decylubiquinol concentration was varied by changing the laser pulse energy at the sample. The variation of the observed enzyme reduction rate constant k_{obs} with decylubiquinol concentration is shown in figure 5. This concentration dependence was characteristic of pre-steady-state saturation kinetics. Fitting the data using a Michaelis-Menton treatment yielded a K_M value of 7 μM and a k_{cat} of 580 s^{-1}. The decarboxylation rate constant of the caged decylubiquinol in detergent solution has been determined to be on the order of 500-600 s^{-1} (see previous paper), very similar to the observed k_{cat} for cytochrome bo_3 reduction. From this we conclude that the kinetics of cytochrome bo_3 reduction were dictated by the chemistry of the carboxylated decylubiquinol, as described in equations 4 and 5. Photolysis of DQ-BCMB yielded the carboxylated decylubiquinol, which rapidly formed a tight Michaelis complex with cytochrome bo_3. Electron transfer into the enzyme did not happen until decarboxylation of the decylubiquinol occurred. Therefore, the decarboxylation of the substrate was rate-limiting in the reduction of enzyme. This reaction chemistry was a peculiarity of the photochemical system used to initiate the chemistry; nevertheless, it dominated the intended reaction chemistry for this system shown in equations 4 and 6, decarboxylation of decylubiquinol followed by reaction of the free decylubiquinol with the enzyme.

Of the redox centers in cytochrome bo_3, the Cu_B center has the highest reduction potential. The observed electron distribution in cytochrome bo_3 following reduction by photoreleased decylubiquinol showed comparable reduction levels of heme *b* and heme o_3. Since copper will undoubtedly accept one electron from decylubiquinol during its oxidation, reduction of both hemes requires either the reaction of the enzyme with more

than one molecule of substrate or the equal sharing of one electron between the two hemes. We prefer the former explanation in that there was invariably an excess of decylubiquinol released in the photolysis reactions, and most reported redox studies of cytochrome bo_3 have shown that the reduction potentials of the two hemes differ by at least 60 mV [23-28].

In earlier work, we showed that a significantly higher level of heme *b* was reduced relative to heme o_3 when a substoichiometric amount of ubiquinol was employed in the reaction of ubiquinol with cytochrome bo_3 [11]. In the current study, the different electron distribution observed lends further support to the idea that more than one quinol molecule reacted with each enzyme molecule. In addition, the results presented here suggest that two or more molecules of quinol can react with enzyme on a two-millisecond time scale, in accord with the known steady-state kinetics of cytochrome bo_3. In spite of the apparent four-electron reduction of enzyme, we did not observe signs of dioxygen chemistry in this time range. Experiments performed after incubating the enzyme and substrate under an argon atmosphere gave comparable reduction rates and reduction levels for cytochrome bo_3.

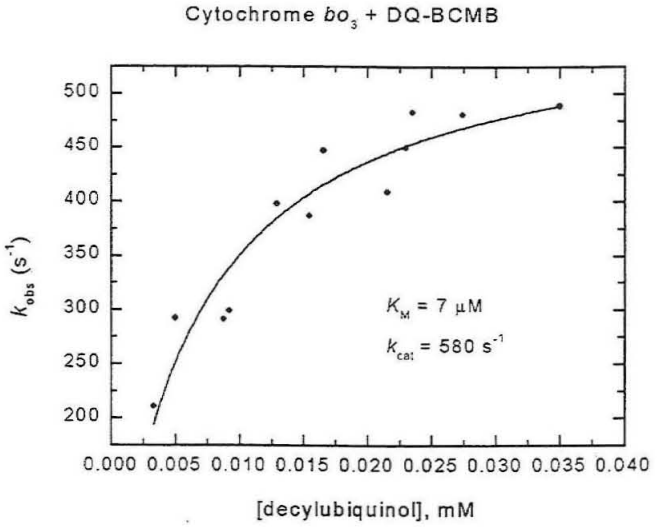

Figure 5. Observed rate constant for reduction of 1.2 μM cytochrome bo_3 as a function of the concentration of photoreleased decylubiquinol. The initial concentration of DQ-BCMB was 100 μM.

2. Reaction of DQ-BCMB with cytochrome bc_1

Following photolysis of DQ-BCMB in the presence of 1.7 μM cytochrome bc_1, the electron transfer from decylubiquinol to cytochrome bc_1 was monitored by following the absorption changes over the range 400-450 nm. Figure 6 shows absorption transients at 410 nm and 430 nm, the minimum and maximum in the reduced minus oxidized difference spectrum of cytochrome bc_1, following irradiation of the reaction mixture with a laser pulse of 5.5 mJ. Upon irradiation of the sample, a sharp increase in absorbance at 430 nm and a slight increase in absorbance at 410 nm occurred. This phase was assigned as a combination of the photoreduction of 0.14 μM cytochrome bc_1 (0.42 μM heme) and the formation of the photoproducts of DQ-BCMB at a concentration of 21 μM, on the

basis of multiple wavelength measurements. However, unlike in cytochrome bo_3, no subsequent reoxidation of the hemes was observed. Following the first phase, we observed an exponential decay at 410 nm and rise at 430 nm, which were indicative of reduction of the heme groups in the enzyme by the photoreleased decylubiquinol. Single exponential fits to this phase gave an observed first order rate constant of 200 s^{-1} for the reduction. The wavelength dependence of the magnitude of this reduction phase is shown in Figure 7 (left). Also included is a scaled, reduced minus oxidized difference spectrum of cytochrome bc_1. The data were fit in a satisfactory manner by the difference spectrum, clearly showing reduction of enzyme, but the relative reduction levels of the *b* and *c* hemes could not be measured accurately from these data. Assuming reduction of all of the redox centers, 0.22 μM of enzyme was reduced from a single laser pulse.

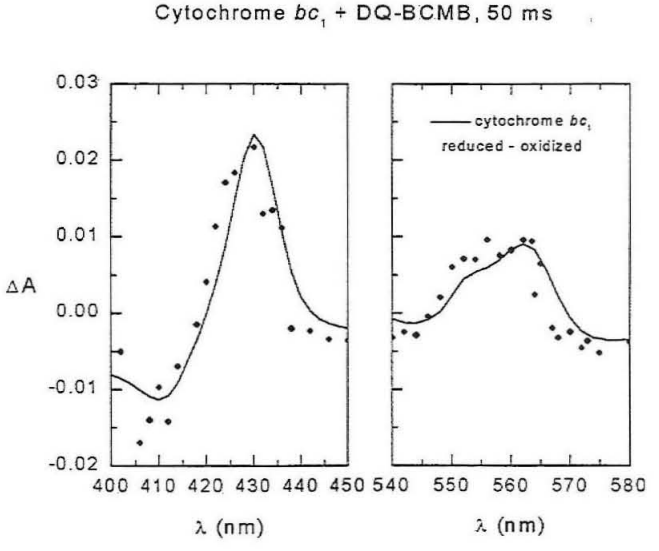

Figure 7. Wavelength dependence of the reaction of cytochrome bc_1 with 100 μM DQ-BCMB following photolysis. Data points are the magnitude of the kinetic phase corresponding to electron transfer from decylubiquinol to cytochrome bc_1. Left: Soret band absorption changes, 1.7 μM cytochrome bc_1, 5 mJ/pulse. Right: Absorbance changes in the α-band region, 3.4 μM cytochrome bc_1, 4 mJ/pulse.

In a parallel experiment, DQ-BCMB was photolyzed in the presence of 3.4 μM cytochrome bc_1 in order to study the wavelength dependence of the reaction in the α-band region. Figure 7 (right) shows the magnitude of the absorbance change from this reaction over the wavelength range 540-580 nm. Also included is the reduced minus oxidized spectrum of cytochrome bc_1 in this spectral range. The α-band data reveal reduction of both cytochrome *b* and cytochrome c_1. However, the proportionally higher absorbance at 552 nm, the absorption maximum of cytochrome c_1, relative to that at 565 nm, the absorption maximum for cytochrome *b*, shows a higher average level of *c* heme reduction than *b* heme reduction. This difference is attributed to *b* heme oxidation by quinone at the N center of cytochrome bc_1.

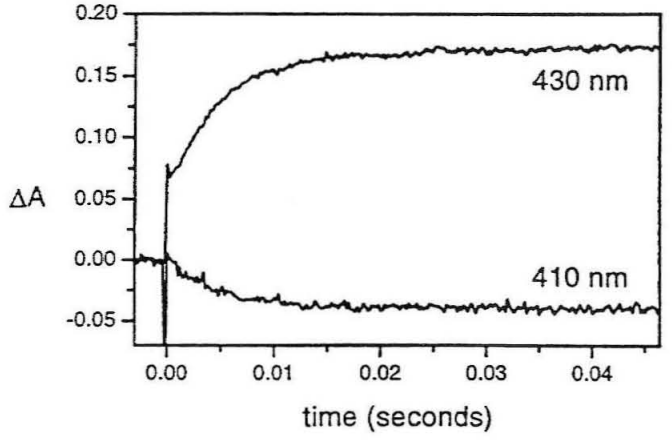

Figure 6. Time course of the reaction of 1.7 μM cytochrome bc_1 with 100 μM DQ-BCMB following photolysis, measured at 410 nm and 430 nm. The excitation wavelength was 308 nm, with an energy of 5 mJ/pulse. Each trace resulted from a single laser pulse.

In the reaction of 1.7 μM cytochrome bc_1 with 100 μM DQ-BCMB, the dependence of the electron transfer rate into cytochrome bc_1 on the concentration of photoreleased decylubiquinol was measured using the absorbance change at 430 nm following photolysis. The concentration was varied by changing the laser pulse energy, and was measured in a parallel experiment in which 100 μM DQ-BCMB was photolyzed under identical laser pulse energies in the absence of enzyme. Unlike in prior literature reports [29, 30], the expected linear dependence of the rate on decylubiquinol concentration was not observed. Rather, a concentration dependence indicative of saturation kinetics was seen. Fitting the data with a Michaelis-Menton model yielded a K_M of 3.6 μM and a k_{cat} of 210 s^{-1}.

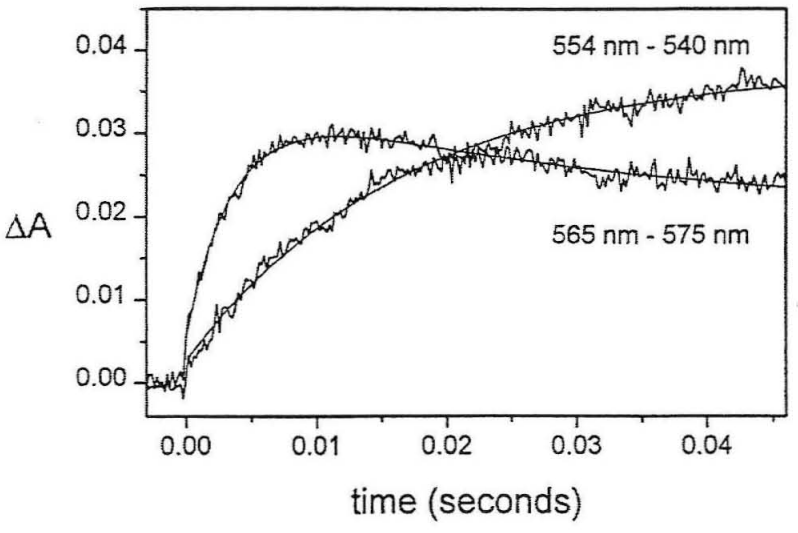

Figure 8. Time course of the reaction of 3.4 μM cytochrome bc_1 with 100 μM DQ-BCMB. Photolysis was initiated with a 4.5 mJ laser pulse. The traces show the difference spectrum of the absorbance at 565 nm minus 575 nm, with a biexponential fit to the data, and the difference spectrum at 554 nm minus 540 nm, with a single exponential fit to the data. The trace at each wavelength resulted from a single laser pulse.

Monitoring the reaction of cytochrome bc_1 with DQ-BCMB through the α-bands in the absorption spectra allowed the distinction between *b* heme and *c* heme reduction. The wavelength pairs 565-575 nm and 554-540 nm were used for this purpose. Figure 8 shows the time course of the reaction of 3.4 μM cytochrome bc_1 with 100 μM DQ-BCMB, irradiated with a laser pulse energy of 4.5 mJ. The trace with the more rapid initial rise shows the time course of the difference spectrum at 565 nm minus 575 nm, a pair that isolates the redox chemistry of the *b* hemes in the enzyme. An initial rise in absorbance corresponding to *b* heme reduction was followed by a slower decay assigned as electron transfer from the *b* hemes to ubiquinone at the N center of the enzyme. A biexponential fit to the data gave an observed rate constant of 270 s^{-1} for the reduction of the *b* hemes and a rate constant of 34 s^{-1} for the subsequent oxidation. The other trace is that from the difference of the transients at 554 nm and 540 nm, characteristic of *c* heme reduction. The trace reveals a reduction of cytochrome c_1 that was slower than that of the *b* hemes, with an exponential fit yielding a reduction rate constant of 60 s^{-1}. The magnitudes of the absorbance changes corresponded to a reduction of 1.1 μM *b* heme (0.54 μM cytochrome *b*) and 1.2 μM *c* heme. The higher maximal reduction level of *c* heme was attributed to loss of electrons from cytochrome *b* through the N center.

In order to eliminate the loss of electrons from the N site of cytochrome bc_1, the reaction of 3.4 μM cytochrome bc_1 with 100 μM DQ-BCMB in the presence of the respiratory inhibitor antimycin A was performed in conjuction with the above reactions. Figure 10 shows the difference transients from the reaction of cytochrome bc_1 with DQ-BCMB in the presence of 10 μM antimycin A. The upper trace shows the difference in

absorbance at 565 nm minus 575 nm. The reduction was monophasic, with an absorbance change corresponding to reduction of 1.24 μM *b* heme. The rate of *b* heme reduction was slower than that in the absence of inhibitor, with an observed rate constant of 53 s^{-1} for this phase. This slower rate of *b* heme reduction cannot be explained by a lower quinol concentration. Thus, we attribute the slower rate at least in part to inhibition of quinol oxidation by antimycin. The lower trace in Figure 9 follows the reduction of the *c* heme in the enzyme. A reduction rate of 56 s^{-1} was observed, essentially identical to that of *b* heme reduction and very similar to that of *c* heme reduction in the absence of inhibitor. The absorbance change corresponded to a reduction of 0.98 μM *c* heme. The coincidence of the reduction rates for *b* and *c* heme reduction are in accord with

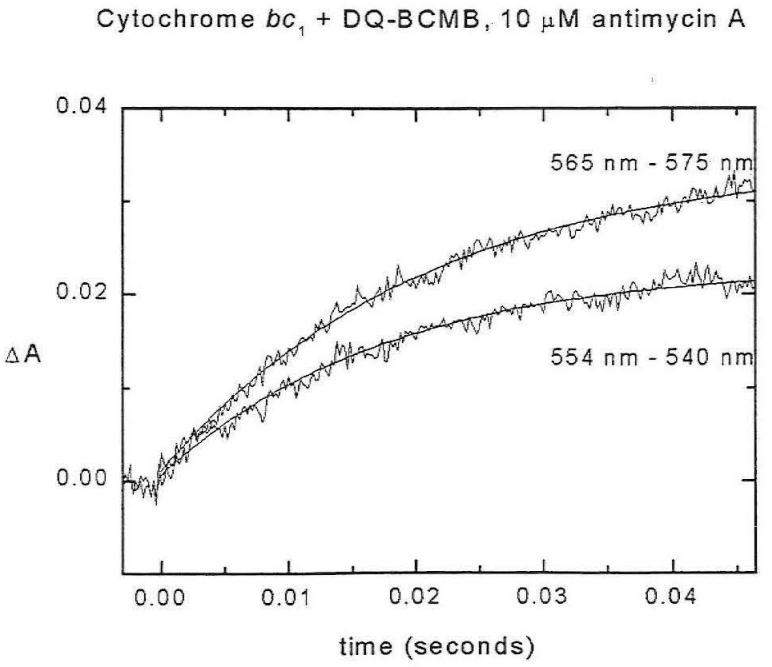

Figure 9. Time course of the reaction of 3.4 μM cytochrome bc_1 with 100 μM DQ-BCMB in the presence of 10 μM antimycin A. Photolysis was initiated with a 4 mJ laser pulse. Upper trace: Difference spectrum of the absorbance at 565 nm minus 575 nm, with a single exponential fit to data. Lower trace: Difference spectrum at 554 nm minus 540 nm, with a single exponential fit to data. The trace at each wavelength arose from a single laser pulse.

inhibition of quinol oxidation by antimycin. When an antimycin concentration of 2 μM was used, rate constants of 70 s^{-1} and 57 s^{-1} were observed for *b* heme and *c* heme reduction, respectively, demonstrating an easing of the inhibition.

Discussion

1. Reaction chemistry of cytochrome bo_3 with photolyzed DQ-BCMB

As mentioned above, the reduction of cytochrome bo_3 was rate-limited by the reaction chemistry leading to the release of decylubiquinol. The expected sequence of events in this system was the release of decylubiquinol followed by the reaction of the quinol with cytochrome bo_3, as shown in equations 4 and 6. Although the rate constant for decarboxylation of the photoreleased quinol was measured at approximately 600 s^{-1}, photolysis of a large amount of DQ-BCMB would be expected to produce an excess of decylubiquinol with respect to cytochrome bo_3 on a submillisecond time scale, so that enzyme reduction rates of greater than 600 s^{-1} would be observed. However, the apparent maximum reduction rate of 580 s^{-1} for the enzyme and the concentration dependence of the rate suggested that the enzyme substrate formed a Michaelis complex prior to the decarboxylation reaction. The apparent K_M of 7 μM for the substrate is somewhat lower than the K_M value of 42 μM reported for the reaction of cytochrome bo_3 with decylubiquinol under steady-state conditions [31], suggesting that the carboxylated decylubiquinol did in fact out-compete the free decylubiquinol at the binding site. Prior to the decarboxylation of the photoreleased decylubiquinol, the observed chemistry was non-physiological, and the release of free quinol was too slow to yield useful mechanistic

data. Thus, further methodology development will be necessary to probe fully the quinol oxidation by this enzyme.

Because of the low concentration of enzyme used in these studies, the photolysis of DQ-BCMB invariably produced an excess of quinol with respect to cytochrome bo_3. The wavelength dependence of the absorption changes in this process and the monophasic kinetics at all wavelengths showed that the reduction of both heme groups was rate-limited at the level of substrate release. As mentioned above, the reduction of both heme groups required that the enzyme react with more than one molecule of substrate. If only one molecule of substrate was to react with the enzyme, information regarding electron distribution in the enzyme on a millisecond time scale could be determined, even if the electron transfer to the enzyme was too rapid to study directly. Specifically, the electron distribution resulting from the reaction of enzyme with substoichiometric amounts of substrate would represent a quasi-equilibrium arising from the interplay of the reduction potentials of the redox centers in the enzyme and the kinetic barriers to internal electron transfer. Our prior work in this area, using freeze-quench methodology to study the reaction of cytochrome bo_3 with ubiquinol-2, showed that if only one molecule of quinol was allowed to react with enzyme, the electrons transferred in this reaction ended up primarily on Cu_B and heme *b* in the enzyme [11]. In principle, the photolysis of DQ-BCMB with low laser power could reproduce this experiment with an almost ten-fold increase in time resolution, so that more rapid electron transfers leading to the final electron distribution could be detected. This prospect represents a further line of study for this enzyme.

2. Reaction chemistry of cytochrome bc_1

Through the use of DQ-BCMB as a photoreleasable enzyme substrate, we have been able to probe the reaction of cytochrome bc_1 with a ubiquinol substrate under pre-steady-state conditions. Although the decarboxylation of photoreleased decylubiquinol had to be taken into account in interpreting the kinetics of the reaction, the kinetics were well-defined, so there was no dead time as such for this experimental setup. Reduction of cytochrome bc_1 by decylubiquinol was observed in both the Soret and α-bands in the optical spectra of the enzyme, and kinetic phases corresponding to *b* and *c* heme reduction were distinguished. These observations have demonstrated the utility of DQ-BCMB as a photoreleasable enzyme substrate, and have shown that the methodology has been sufficiently refined to probe all of the kinetic phases in the pre-steady-state reaction of this enzyme.

The resolution of *b* heme and *c* heme reduction rates has allowed us to explore the nature of the electron transfer at the P center of cytochrome bc_1, as described above. In the reaction of cytochrome bc_1 with decylubiquinol in the absence of inhibitors, cytochrome *b* reduction occurred at a more rapid rate than that of cytochrome c_1. This is in accord with the view that the first molecule of quinol to be oxidized in the reaction cycle of cytochrome bc_1 reduces the iron-sulfur cluster and cytochrome *b*, but not cytochrome c_1. The slower reduction of cytochrome c_1 relative to cytochrome *b* showed that electron transfer from the iron-sulfur protein to cytochrome c_1 was slower than the oxidation of the quinol substrate, and thus that the initial oxidation reaction of quinol (equation 1) was not rate-limiting in the full reduction of the enzyme. As no distinct second phase of *b* heme reduction was observed on the time scale of these experiments, it

cannot be confirmed whether motion of the iron-sulfur protein (equation 2) or subsequent quinol oxidation (equation 3) was rate-limiting under these conditions. In the presence of antimycin A, the *b* heme reduction level was increased relative to that of cytochrome c_1 and no phase corresponding to *b* heme oxidation was seen, as expected from the known inhibitory properties of antimycin. However, we found that the rate of *b* heme reduction was decreased and was nearly identical to that of *c* heme reduction in the presence of antimycin. We interpret this result to mean that antimycin was able to affect the reaction chemistry at the P center of the enzyme as well as the N center, although the role of the N center in electron input to cytochrome *b* has not been defined fully. The inhibition showed that the reaction rates of the various steps in the reduction of cytochrome bc_1 are sufficiently close that small changes in the reaction conditions can result in changes in the rate-determining step. This suggests that more than one factor is involved in directing electron transfer through the enzyme.

The saturation kinetics observed in the reaction of photoreleased decylubiquinol stand in stark contrast to the second order behavior noted in the pre-steady-state reaction of cytochrome bc_1 with comparable concentrations of ubiquinol-10 [29] and menaquinol [30] in previous studies. Also, the observed reaction rates in this study are significantly higher than in the previous work. As with the reaction of photolyzed DQ-BCMB with cytochrome bo_3, we attribute this behavior to the reaction of carboxylated decylubiquinol with cytochrome bc_1.

Decylubiquinol, ubiquinol-8, and menaquinol have sufficiently similar chemical properties that the saturation kinetics observed in this study cannot be attributed to any features of decylubiquinol itself. Therefore, one must conclude that the carboxylated

decylubiquinol is responsible for the kinetic behavior observed in the reaction of DQ-BCMB with cytochrome bc_1. The fact that saturation behavior is observed in this reaction implies that the carboxylated quinol binds much more tightly to the enzyme than does the natural ubiquinol substrate. The most distinguishing feature of the carboxylated decylubiquinol which could explain this observation is the charge of this species. At physiological pH, the carboxylated ubiquinol is anionic. Its chemical structure is similar to that of deprotonated ubiquinol and ubisemiquinone anion, both of which are presumed intermediates in quinol oxidation by cytochrome bc_1. As stabilization of the latter two species is an expected feature of quinol-oxidizing enzymes, adventitious stabilization of the carboxylated decylubiquinol is not unreasonable. From biochemical evidence and the recently published crystal stuctures of cytochrome bc_1, the most likely residues that would be involved in an electrostatic stabilization of these anionic species are the histidine residues associated with the iron-sulfur cluster, specifically His161 of the mitochondrial enzyme [13, 14, 21].

The value of k_{cat}/K_M for the reaction of cytochrome bc_1 with photolyzed DQ-BCMB, 5.8×10^7 M^{-1} s^{-1}, provides a measure of the rate enhancement achieved by the use of DQ-BCMB as a substrate. Over the concentration range studied, the observed rates arising from the saturation kinetics of this system would exceed those of a second-order kinetic process with a rate constant of 1×10^7 M^{-1} s^{-1}. By way of comparison, a second-order rate constant of 1.3×10^6 M^{-1} s^{-1} was reported for the reaction of menaquinol with cytochrome bc_1 [30], and a value of 3×10^5 M^{-1} s^{-1} published for the reaction of ubiquinol with cytochrome bc_1 in which the reaction was initiated by irradiation of photosynthetic reaction centers [29]. Thus, if the second-order kinetic

process diagrammed in equation 6 was to play a significant role in the reaction of photolyzed DQ-BCMB with cytochrome bc_1, a very rapid reaction of free decylubiquinol with cytochrome bc_1 would be necessary. In spite of the fact that the carboxylated decylubiquinol controlled the reaction kinetics in this system, the reaction chemistry following the decarboxylation of the quinol was expected to be identical to that of native ubiquinol with enzyme. Therefore, the conclusions regarding relative electron transfer rates and mechanisms of branched electron transfer should still be applicable.

Two other methodologies have been employed to study the electron input to cytochrome bc_1. As mentioned above, ubiquinol has been generated photochemically in bacterial chromatophores containing photosynthetic reaction centers and cytochrome bc_1, and the subsequent electron transfer to cytochrome bc_1 has been observed [19, 29, 32-34]. This technique has been used successfully to measure second-order rate constants for the reduction of cytochrome *b* by ubiquinol-10. In spite of the rapid time scale that has been probed using this technique, the complexity of the technique limits its general utility. Changing the concentration of substrate requires adjustment of the redox poise to levels at which the redox centers in cytochrome bc_1 are partially or fully reduced. The presence of multiple *c*-type cytochromes in the samples has made the kinetics of cytochrome c_1 reduction difficult to quantitate. In addition, a time lag corresponding to the release of ubiquinol from the photosynthetic reaction center is observed in this chemistry. Finally, the use of chromatophores makes quantitation of protein and quinone concentrations difficult. While this technique has provided much information with respect to pathways of electron transfer in cytochrome bc_1 and mechanistic details relating to the Q-cycle model, a simpler technique should be able to address the

ambiguities and uncertainties in the measurements. The use of photoreleasable substrates as described in this work has the advantage of yielding a better defined system with a more direct method of initiating and probing the reaction chemistry.

The reaction of quinol with cytochrome bc_1 has also been studied using stopped-flow spectrophotometry. A recent stopped-flow, rapid-scanning optical spectrophotometry study explored the reaction of yeast cytochrome bc_1 with menaquinol, a non-physiological substrate of cytochrome bc_1 [30]. This study demonstrated the basic features of the Q-cycle in the reaction of cytochrome bc_1 with menaquinol, but measurements of reaction rates were only made in the presence of unspecified amounts of enzyme inhibitors. Also, the slower phases of enzyme reduction in this study were significantly slower than enzyme turnover. These features limit the interpretation of the results with respect to physiological turnover of enzyme. However, the turbulent mixing associated with the stopped-flow technique gives a dead time of at least a few milliseconds, a time scale in which the most rapid cytochrome *b* reductions occurred in our experiments with cytochrome bc_1 and DQ-BCMB.

Conclusions

In this work we have demonstrated the use of the BCMB protecting group as a means of photoinitiating bimolecular enzyme chemistry. With a BCMB-derivatized decylubiquinol, we have probed the electron input kinetics of mitochondrial cytochrome bc_1 on a millisecond time scale. The improvement in time resolution gained over more traditional stopped-flow techniques allowed us to observe even the most rapid electron transfers from ubiquinol to this enzyme using substrate concentrations as high as 35 μM.

Resolution of *b* heme and *c* heme reductions on this time scale has provided an avenue for the exploration of the events that occur at the P center during the oxidation of quinol molecules, and hopefully will allow an accurate description of the means by which the bifurcation of electron transfer in this enzyme takes place. We hope that further methodology development with photolabile protecting groups will allow an equally complete description of electron transfer into cytochrome bo_3 and other quinol-oxidizing enzymes.

References

1) B.L. Trumpower, R.B. Gennis, Energy transduction by cytochrome complexes in mitochrondrial and bacterial respiration: The enzymology of coupling electron transfer reactions to transmembrane proton translocation, Annu. Rev. Biochem. 63 (1994) 675-716.

2) M. Svensson, T. Nilsson, Flow-flash study of the reaction between cytochrome *bo* and oxygen, Biochemistry 32 (1993) 5442-5447.

3) J.E. Morgan, M.I. Verkhovsky, A. Puustinen, M. Wikström, Intramolecular electron transfer in cytochrome *o* of *Escherichia coli*: Events following the photolysis of fully and partially reduced CO-bound forms of the bo_3 and oo_3 enzymes, Biochemistry 32 (1993) 11413-11418.

4) Y. Orii, T. Mogi, M. Kawasaki, Y. Anraku, Facilitated intramolecular electron transfer in cytchrome *bo*-type ubiquinol oxidase initiated upon reaction of the fully reduced enzyme with dioxygen, FEBS Lett. 352 (1994) 151-154.

5) Y. Orii, T. Mogi, M. Sato-Watanabe, T. Hirano, Y. Anraku, Facilitated intramolecular electron transfer in the *Escherichia coli bo*-type ubiquinol oxidase requires chloride, Biochemistry 34 (1995) 1127-1132.

6) M. Svensson, S. Hallén, J.W. Thomas, L.J. Lemieux, R.B. Gennis, T. Nilsson, Oxygen reaction and proton uptake in helix VIII mutants of cytochrome bo_3, Biochemistry 34 (1995) 5252-5258.

7) J. Wang, J. Rumbley, Y.-C. Ching, S. Takahashi, R.B. Gennis, D.L. Rousseau, Reaction of cytochrome bo_3 with oxygen: Extra redox center(s) are present in the protein, Biochemistry 34 (1995) 15504-15511.

8) M.I. Verkhovsky, J.E. Morgan, A. Puustinen, M. Wikström, The "ferrous-oxy" intermediate in the reaction of dioxygen with fully reduced cytochromes aa_3 and bo_3, Biochemistry 35 (1996) 16241-16246.

9) A. Puustinen, M.I. Verkhovsky, J.E. Morgan, N.P. Belevich, M. Wikström, Reaction of the Escherichia coli quinol oxidase cytochrome bo_3 with dioxygen: The role of a bound ubiquinone molecule, Proc. Natl. Acad. Sci. USA 93 (1996) 1545-1548.

10) S.M. Musser, M.H.B. Stowell, H.K. Lee, J.N. Rumbley, S.I. Chan, Uncompetitive substrate inhibition and noncompetitive inhibition by 5-*n*-undecyl-6-hydroxy-4,7-dioxobenzothiazole (UHDBT) and 2-*n*-nonyl-4-hydroxyquinoline-*N*-oxide (NQNO) is observed for the cytochrome bo_3 complex: Implications for a $Q(H_2)$-loop proton translocation mechanism, Biochemistry 36 (1997) 894-902.

11) B.E. Schultz, D.E. Edmondson, S.I. Chan, Reaction of *E. coli* cytochrome bo_3 with substoichiometric ubiquinol-2: A freeze-quench EPR investigation, Biochemistry 37 (1998) 4160-4168.

12) D. Xia, C.-A. Yu, H. Kim, J.-Z. Xia, A.M. Kachurin, L. Zhang, L. Yu, J. Deisenhofer, Crystal structure of the cytochrome bc_1 complex from bovine heart mitochondria, Science 277 (1997) 60-66.

13) Z. Zhang, L. Huang, V.M. Shulmeister, Y.-I. Chi, K.K. Kim, L.-W. Hung, A.R. Crofts, E.A. Berry, S.-H. Kim, Electron transfer by domain movement in cytochrome bc_1, Nature 392 (1998) 677-684.

14) S. Iwata, J.W. Lee, K. Okada, J.K. Lee, M. Iwata, B. Rasmussen, T.A. Link, S. Ramaswamy, B.K. Jap, Complete structure of the 11-subunit bovine mitochondrial cytochrome bc_1 complex, Science 281 (1998) 64-71.

15) P. Mitchell, Possible molecular mechanisms of the protonmotive function of cytochrome systems, J. Theor. Biol. 62 (1976) 327-367.

16) U. Brandt, G. von Jagow, Analysis of inhibitor binding to the mitochondrial cytochrome *c* reductase by fluorescence quench titration: Evidence for a 'catalytic switch' at the Q_O center, Eur. J. Biochem. 195 (1991) 163-170.

17) U. Brandt, U. Haase, H. Schägger, G. von Jagow, Significance of the "Rieske" iron-sulfur protein for formation and function of the ubiquinol-oxidation pocket of mitochondrial cytochrome *c* reductase (bc_1 complex), J. Biol. Chem. 266 (1991) 19958-19964.

18) H. Ding, D.E. Robertson, F. Daldal, P.L. Dutton, Cytochrome bc_1 complex [2Fe-2S] cluster and its interaction with ubiquinone and ubihydroquinone at the Q_o site: A double-occupancy Q_o site model, Biochemistry 31 (1992) 3144-3158.

19) H. Ding, C.C. Moser, D.E. Robertson, M.K. Tokito, F. Daldal, P.L. Dutton, Ubiquinone pair in the Q_o site central to the primary energy conversion reactions of cytochrome bc_1 complex, Biochemistry 34 (1995) 15979-15996.

20) U. Brandt, Bifurcated ubihydroquinone oxidation in the cytochrome bc_1 complex by proton-gated charge transfer, FEBS Lett. 387 (1996) 1-6.

21) T.A. Link, The role of the 'Rieske' iron sulfur protein in the hydroquinone oxidation (Qp) site of the cytochrome bc_1 complex: The 'proton-gated affinity change' mechanism, FEBS Lett. 412 (1997) 257-264.

22) T.J. DiMagno, M.H.B. Stowell, S.I. Chan, Photoreduction of cytochrome *c* and other heme proteins by new nitrobenzene derivatives: A general approach to studying intermolecular electron transfer reactions in proteins, J. Phys. Chem. 99 (1995) 13038-13047.

23) J.C. Salerno, B. Bolgiano, W.J. Ingledew, Potentiometric titration of cytochrome-*bo* type quinol oxidase of *Escherichia coli*: evidence for heme-heme and copper-heme interaction, FEBS Lett. 247 (1989) 101-105.

24) H.K. Withers, P.D. Bragg, Potentiometric and spectroscopic properties of the cytochrome *o* complex of *Escherichia coli*, Biochem. Cell Biol. 68 (1990) 83-90.

25) J.C. Salerno, B. Bolgiano, R.K. Poole, R.B. Gennis, W.J. Ingledew, Heme-copper and heme-heme interactions in the cytochrome *bo*-containing quinol oxidase of *Escherichia coli*, J. Biol. Chem. 265 (1990) 4364-4368.

26) B. Bolgiano, I. Salmon, W.J. Ingledew, R.K. Poole, Redox analysis of the cytochrome *o*-type quinol oxidase complex of *Escherichia coli* reveals three redox components, Biochem. J. 274 (1991) 723-730.

27) B. Bolgiano, I. Salmon, R.K. Poole, Reactions of the membrane-bound cyotchrome *bo* terminal oxidase of *Escherichia coli* with carbon monoxide and oxygen, Biochim. Biophys. Acta 1141 (1993) 95-104.

28) B.E. Schultz, S.I. Chan, Thermodynamics of electron transfer in *Escherichia coli* cytochrome bo_3, Proc. Natl. Acad. Sci. USA 95 (1998) 11643-11648.

29) A.R. Crofts, S.W. Meinhardt, K.R. Jones, M. Snozzi, The role of the quinone pool in the cyclic electron-transfer chain of *Rhodopseudomonas sphaeroides*: A modified Q-cycle mechanism, Biochim. Biophys. Acta 723 (1983) 202-218.

30) C. Snyder, B.L. Trumpower, Mechanism of ubiquinol oxidation by the cytochrome bc_1 complex: pre-steady-state kinetics of cytochrome bc_1 complexes containing site-directed mutants of the Rieske iron-sulfur protein, Biochim. Biophys. Acta 1365 (1998) 125-134.

31) J.N. Rumbley, E.F. Nickels, R.B. Gennis, One-step purification of histidine-tagged cytochrome bo_3 from *Escherichia coli* and the demonstration that associated quinone is not required for the structural integrity of the oxidase, Biochim. Biophys. Acta 1340 (1997) 131-142.

32) A.R. Crofts, Z. Wang, How rapid are the internal reactions of the ubiquinol:cytochrome c_2 oxidoreductase, Photosynth. Res. 22 (1989) 69-87.

33) D.E. Robertson, F. Daldal, P.L. Dutton, Mutants of ubiquinol-cytochrome c_2 oxidoreductase resistant to Q_0 site inhibitors: Consequences for ubiquinone and ubiquinol affinity and catalysis, Biochemistry 29 (1990) 11249-11260.

34) S.R. Van Doren, R.B. Gennis, B. Barquera, A.R. Crofts, Site-directed mutations of conserved residues of the Rieske iron-sulfur subunit of the cytochrome bc_1

complex of *Rhodobacter sphaeroides* blocking or impairing quinol oxidation, Biochemistry 32 (1993) 8083-8091.

Section II

Chapter 6:

The Protein Folding Problem

Introduction

One of the fundamental processes of living cells is the synthesis of proteins. The folding of proteins must take place for the proper three-dimensional structure to be reached and hence, their biological function to be realized. In some cases, the cell has devised elaborate chaperone proteins to facilitate this process; however, in many proteins the folding is driven exclusively by thermodynamic forces and/or kinetic pathways that are not completely understood at this time. Elucidation of these protein folding pathways and forces can shed light on how proteins obtain their unique structures and also aid in the design of novel proteins with tailored functions. To study protein folding or unfolding, a triggering event that perturbs a protein from its equilibrium state is required. At the same time this triggering event needs to be faster than the events that will be studied; in the case of protein folding, the earliest events occur in the hundred of nanoseconds time regime. One of the reasons that it is important to understand the folding of proteins is that misfolding of proteins can lead to disease.

Protein Folding and Human Disease

In the cell proteins are in constant dynamic equilibrium. Many times after the folding process is complete, proteins will go in the reverse direction and unfold. This unfolding process is an important aspect of cellular control, because it provides a means of removing proteins when their activity is no longer required. The ability to fold, unfold, degrade and remove proteins rapidly is of particular importance in the regulation of many cellular events. A consequence of loss of these control processes is usually cellular malfunctioning and hence disease. Many diseases are associated with the failure

of proteins to fold correctly or to remain folded when they shouldn't be under a given physiological state.

The discovery that amyloid deposits recovered from human tissues represent fibrillar forms of specific protein fragments revealed that protein aggregation was associated with a number of human diseases.[1,2] In parallel, the discovery that heat-shock proteins include chaperones that aid in protein folding, established that failure of protein folding is a general phenomenon, at least under stressful conditions such as elevated temperatures.[3] There are two general classifications of diseases that arise from the conformational state of a protein. The first are diseases associated with the loss of active protein. These include Sickle-cell and other haemoglobin anaemias which arise from a single amino acid substitution. This substitution changes the conformational state of the protein and causes the protein to polymerize into large, insoluble fibers.[4] Other conformational disorders involve the serpins,[5] or serine protease inhibitors, defects in p53 tumor suppression (over 50% of cancers are associated with p53 defects),[6,7] cystic fibrosis,[8] and collagen deficiency diseases.[9] The second category includes those diseases that are associated with the accumulation of mis- or unfolded protein aggregates. The amyloid disorders fall into this classification; these involve build up of fibril protein plaques that cause neurodegenerative damage as seen in Alzheimer's disease and infectious fatal prion diseases.[10-12] Other non-amyloid aggregation disorders include Huntington's disease which results from N-terminus polyglutamine repeats of the Huntington protein,[13] amyotropic lateral sclerosis,[14,15] cataracts[16] and Parkinson's disease.[17] To help understand, treat, and prevent these and other as of yet unidentified

diseases associated with protein structure, we need to better understand the process of protein folding.

General Aspects of Protein Folding

Protein folding is directed by a set of interatomic interactions that guide the polypeptide to its native protein state. The strongest of these interactions is the covalent structure of the amino acid chain. The protein folding event is a torsional search process of all bonds where rotation is permitted, and this search is directed by a large sum of nonbonded interactions and limited by sterics. A fact that most simple folding models overlook is that the conformation space is smaller than the number of possible bond rotation states due to the sterics (a low energy state with self-crossing of the backbone is not possible). A dominant force in folding, and one that plays an important role in the early events of folding, is hydrophobic interactions. This interaction causes the nonpolar side chains to collapse to form a hydrophobic core; this collapse is driven by the entropically unfavorable interactions between ordering water molecules around the side chains. The patterning of the hydrophilic and hydrophobic residues in core formation greatly limits the phase space and, thus, dictates the range of topologies possible and accelerates the folding process.

Hydrogen bonding interactions are critical for the organization of several secondary structural elements and ultimately tertiary and quaternary structure. The electrostatic forces between charged side chains, as well as the C-terminal carboxylates and N-terminal amine groups, are prevalent in protein structures. Electrostatic forces are also present in certain organized structures such as the dipole moment in the α-helix.

Also, the intrinsic secondary structure propensities of the individual amino acid residues play an important role. And, finally, the tight packing arrangement of the final structure is further guided by Van der Waals interactions.

The collections of weaker interactions are most likely responsible for impart, both, nucleation events early in the folding process and also for annealing of the final folded state. These interactions are also the hardest to observe from an experimental standpoint and provide a major challenge for future folding experiments. The physical nature of noncovalent interactions between atoms are understood fairly well for individual atoms in the gas phase and in a regular solid, but not in liquids. This is a consequence of the complexity of the liquid system with its constantly changing interactions between many molecules in transient ensembles.

The free-energy barriers between the energetically favored conformations of a single residue in a polypeptide favored conformation by rotations of ϕ and ψ are only on the order of 0.5 to 1.5 kcal/mol. As a result, these rotations are expected to occur on the order of 10^{12} s^{-1}.[18] However, because these bonds are part of a larger polymer, their rotation is not independent and therefore slower and more concerted. Measurements of relaxation times by ^{13}C nuclear magnetic resonance indicates that the average rates at which individual bonds in disordered polypeptides change conformations to be ~1 – 2 nanoseconds.[19]

The protein folding funnel was introduced in 1992 by Peter Leopold and Jose Onuchic.[20] It is a conceptual model for understanding the self-organizition of a protein. The width of the funnel represents the conformational entropy, and the height represents the internal energy of a given conformation (figure 1). At the top of the funnel, the

protein exists in a large number of random fluctuating states that have relatively high enthalpy and high entropy. Progress down the funnel is accompanied by an increase in native-like structure that is reflected in the value Q, the fraction of native contacts made in the state i. Our understanding of ensemble in the upper region of the funnel is relatively poor, and for the most part we do not know the level of heterogeneity involved. As the protein reaches the bottom of the folding funnel, the heterogeneity is dramatically decreased, but not completely, as it has been shown that conformational sub-states are thermally accessible to the native protein. This is the folding model which, in some variation, has been accepted by most researchers. In some cases the information that has been obtained about a specific proteins folding funnel will need to be re-evaluated, taking into account the effects of the specific experimental conditions and how they may change the shape of the funnel.

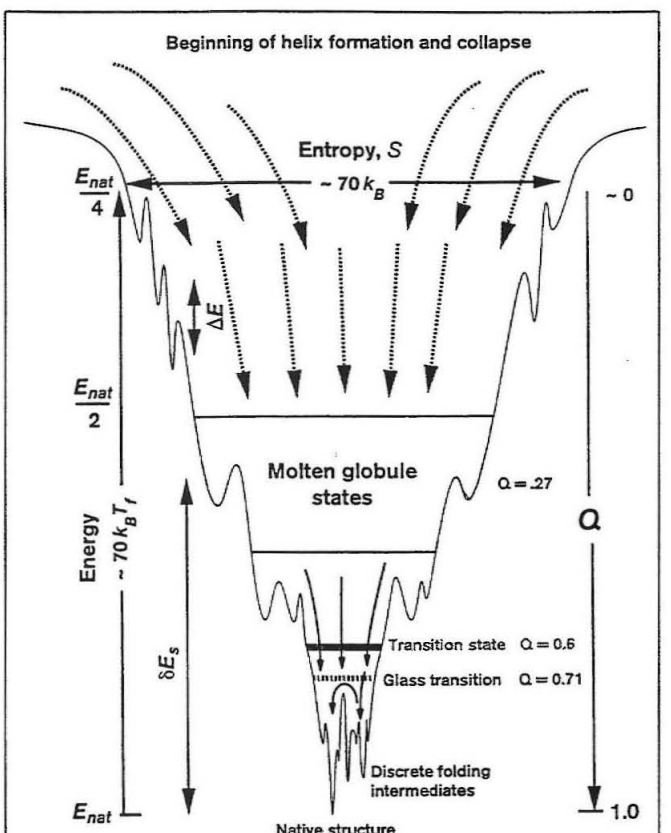

Figure 1. Protein folding funnel initially proposed by Peter Leopold and Jose Onuchic in 1992. The width of the funnel represents the conformational entropy, and the height represents the interna energy of a given conformation.

The Unfolded State

The denatured state is often presumed to be a random coil, partially due to results of Tanford.[21] They showed that the intrinsic viscosities of 11, 6M guanidine hydrochloride denatured proteins depended only on chain length and not sequence which points to an extended conformation. However, a growing body of evidence casts doubt on the universality of this assumption.

Flory's isolated-pair hypothesis states that the backbone conformation of every amino acid residue, described by its ϕ and ψ backbone angles, is independent of the conformations of neighboring residues.[22] If this theory is valid, then the random coil protein in these conditions has no structure characteristic of the native protein, which could be used to guide the first steps of the refolding process. This view would point to hydrophobic collapse as being solely responsible for initiation of folding. Several investigators have found that this is not the case. Tanford and coworkers have used a number of biophysical methods to show that thermally denatured proteins in water have residual secondary structure that is possibly that of the native state.[21] More recently, Hennig *et al.* have used NMR to show that there are hydrophobic clusters in pH 2.0, 8 M urea denatured lysozyme.[23] Calculations by Pappu have shown that steric clashes among residues separated by 3-6 peptide bonds greatly limit the large number of backbone conformations in certain regions of the Ramachandran plot.[24] Ribonuclease A was found by fourier transform infrared spectroscopy (FTIR) to have significant secondary structure upon heat denaturation.[25] Studies by Shortle and Engelman have shown that the radius of a denatured staphylococcus nuclease fragment, determined by small-angle X-ray scattering (SAXS), changes greatly in response to mutations, behavior

not expected for a random coil.[26,27] The result of these findings is that the denatured protein is sampling contacts, some of them native, and that the folding space is limited by self-crossing sterics. This predisposes a protein to adopt a much narrower set of specific backbone conformations in the unfolded state than would be predicted by Flory's isolated pair hypothesis.

At the global level, the random coil state of a polypeptide consists of a wide distribution of conformers, some of which are highly extended but others of which are extremely compact, with the majority in between. In a random coil there will be a statistical distribution between the various possible formations, weighted according to their given energies. It is predicted that the probability of a given region of five residues in a sequence being α-helix or a β-strand at any given time is approximately 3% of the time on average.[28] Using more sophisticated analysis that take into account the secondary structure propensities for the different amino acids and the influence on the conformational distribution of neighboring residues results in the prediction that some sequences in proteins will have populations of secondary structure of up to 10% in the random-coil state.[28] Thus, not only are some proteins predicted to be as compact as the native state, but some regions of the sequence are predicted to have a significant population of the secondary structure that they occupy in the native structure. As one might imagine this can have a major impact on the folding process. These sites of ordered structure could very well be nucleation sites in the folding event.

The unfolded state is a crucial part of the protein folding problem, and without a sound modeling framework from which to formulate questions, understanding denatured protein behavior will be delayed. There is a need for experiments that probe the

molecular detail of the unfolded state; this data will be the first step in the direction of achieving such a framework.

Experimental Protein Folding

Experiments are needed to guide and test the concepts and theories used in simulations. The methods for doing so are not straightforward due to the extremely heterogeneous population of polypeptide chains in the critical early stages of the folding process. Another difficulty is that, although overall protein folding is in general slow compared with many simple reactions, it is still fast (typically milliseconds) and individual events can occur much faster (nanoseconds to picoseconds). Even the slowest of these times make traditional macromolecular structural methods difficult if not impossible to use. However, there are a number of biophysical techniques that have overcome this problem by following the development of different aspects of the formation of protein structure over time. For example, fluorescence spectroscopy has been used to follow the local environment around Trp and Tyr residues, exposure of hydrophobic residues, and formation of active site and inter-residue distances with FRET.[29] NMR has been used to detect the environment of individual residues on the millisecond time scale and longer while line-shape analysis has provided folding-unfolding rates close to equilibrium[30] (For a complete review on techniques used to study the structure of folding species, see 31, 32). Such methods have lead to further insight into the folding problem by providing a global description of structural changes that take place during the folding reaction of several relatively slow folding proteins. Until fairly recently, these approaches have been limited to events on the millisecond

Table 1. Methods for initiating protein folding reaction.

Triggering Method	*Time Window*	*Back Reaction*	*Use of Denaturant*	*Comment*
Rapid mixing	>ms	No	Yes	Turbulent flow
Ultrafast mixing	>50 μs	No	Yes	Flow can damage proteins, mixing artifacts
Electron Transfer	<ns	Yes*	Yes	Metal center required
Photodissociation of heme ligands	~ns	Yes	Yes	Heme group required
Aryl-Disulfide dissociation	NA	Yes	Yes	Low quantum yield (<5%), requires two aminothiotyrosines to be incorporated into protein
Temperature Jump	~ns	Yes	Yes*	Few proteins cold denature, heating artifacts
pH Jump	>μs	No	Yes	Requires proteins that exhibit conformational transition over a narrow pH range.
Pressure Jump	>50 μs	No*	Yes	Only small changes in equilibrium can be measured (>1000 bar is required)

timescales or longer. To obtain more detailed information and to study faster folding proteins, new methods for triggering the protein folding reaction are necessary.

In order to unravel the complexity of the protein folding process, a host of techniques have been developed over the last thirty years. Unfortunately, the most accessible method for triggering conformational changes, the rapid dilution of a protein into or out of a denaturant solution, is often too slow to measure the earliest kinetic phases due to the dead time of the mixing apparatus. Techniques to overcome this limitation include means for triggering proteins based on perturbations of temperature,[33] pressure,[34] pH,[35] heme-ligation,[36] and modified side-chain disulfides[37] (table 1). These methods have allowed for observation of shorter time scales but are limited in that

they require different initial and final environments, such as denaturant concentration, pH and temperature. Another problem is the reversibility associated with these techniques so that at any given data point the sum of forward and reverse reactions are being observed. These disadvantages make interpretation of collected data complicated and often very speculative.

It is important to keep in mind that the folding reaction of an amino acid sequence is not a simple chemical kinetics problem with a single reactant and product. The unfolded state is generally thought to be vastly inhomogeneous, composed of an ensemble of different conformations of the polypeptide. For a more informative study to be carried out it will be important to deconvolute the folding pathways based on differences in starting conditions. This will greatly facilitate the mapping of the folding energy landscape.

Modern folding experiments use a variety of methods to denature a protein as described previously. An often-overlooked distinction of the various initiation methods is that the unfolded states can be different based on the method used for denaturation.

The Overlooked Effect of Using Denaturants

The most widely studied proteins are those that fold by apparent two-state folding kinetics (For a recent review see 38). In this section we will discuss the possibility of missed intermediates in the experimental study of proteins with apparent two-state folding kinetics.

Intermediates that are present at equilibrium at low concentration will not be detected by most spectroscopic methods. In addition, they will not be detected by calorimetry if they do not build up during the thermal transition. There are many

examples of proteins that have stable intermediates present in water, but are not observed in a denaturation transition. Extrapolation of equilibrium data will result in thermodynamic properties of the denatured state.

If we assume that the free energy of transfer of a peptide chain from water to solutions of denaturant is linearly proportional to the concentration of denaturant, the free energy at any particular concentration of denaturant can be given by $\Delta G_{D\text{-}N} = {}^{H2O}\Delta G_{D\text{-}N} - m_{D\text{-}N}[\text{denaturant}]$ where m is a constant of proportionality (= $-\partial(\Delta G_{D\text{-}N})/\partial[\text{denaturant}]$).[Pace, 1989 #53] The result is that the denatured state is preferentially stabilized by denaturant; this is because the D state is more exposed to solvent than the N state. An example of this can be seen in the common practice of adding denaturant to solubilize aggregated unfolded proteins. The plot of $m_{D\text{-}N}$ is shown in red and $m_{I\text{-}N}$ is shown in purple. In this example, the highest energy species in the transition state region is I and so is not observed at equilibrium. This is also true when heat is used to denature the protein. The arrows in figure 1 depicts the ideal situation for a folding experiment. The denatured state at point C is rapidly converted to point B by the loss of the majority of the denaturant-protein binding interactions. Once the protein is in state B the protein folding

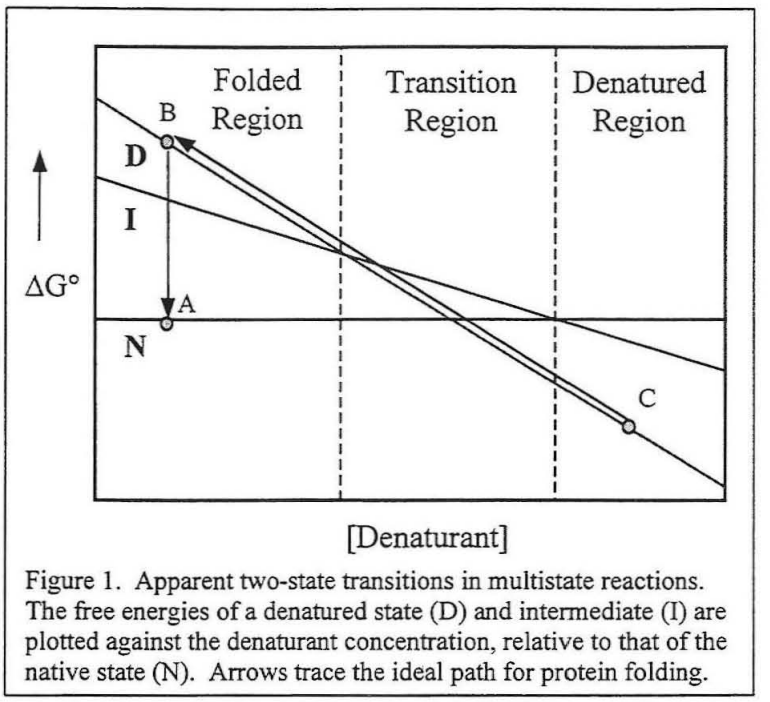

Figure 1. Apparent two-state transitions in multistate reactions. The free energies of a denatured state (D) and intermediate (I) are plotted against the denaturant concentration, relative to that of the native state (N). Arrows trace the ideal path for protein folding.

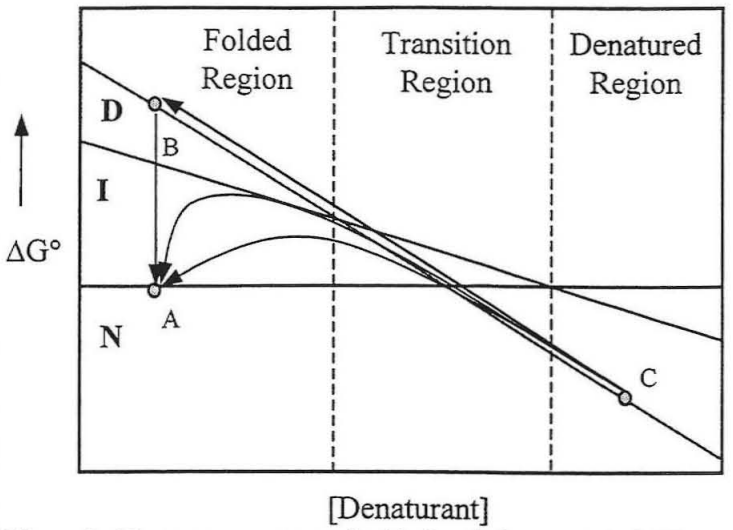

Figure 2. The top arrows trace the ideal path for a protein folding experiment. The lower two are cases when the time for C → B is not >> than B → A resulting in a false folding pathway.

initiation events begin and the protein will pass through intermediate states on the way to the native point A. This process would give an accurate representation of a protein traveling down its folding funnel. For this to occur the denaturant off rate constant needs to be much less than the initiation rate constant. In titration experiments, the path A-to-C and C-to-A would always be observed. An important consequence of figure 2 is that for many proteins it is an artifact that they appear to follow two-state transitions, as under more renaturing conditions (B-to-A pathway) intermediates would accumulate. As folding experiments are usually carried out at the transition region, measurements will give information on the transition between D and N; thus, extrapolation of equilibrium data will give the thermodynamic properties of the denatured state. If calorimetry is used as a control, the same error will be present and the I state will never be detected. Many proteins have stable intermediate states in water, but are not observed during the denaturation transition. An example is barnase that has an I state that is more stable than the D state but only at low concentrations of denaurant.[Sanz, 1993 #52] Figure 2 shows possible folding trajectories in the cases where denaturant off rates compete with folding initiation rates.

Throughout the process of studying protein folding and the building of hypotheses and theories, it is important to keep the final goal in mind. The general application is to be able to predict the three-dimension fold of a protein based on its primary sequence. More specifically, we would like to know what the fold would be of an expressed or synthesized protein when placed in aqueous or other solution. This will be important in the design of engineered proteins and reconstitution of proteins into *in vitro* environments. Eventually, we would like to know the mechanism at the molecular level of what occurs when a protein is synthesized in the cell and passed into the endoplasmic reticulum and on to other cellular environments. This will be important in structure prediction from genomic sequence data. These two are not the same questions. The initiation events in the two could be very different. In the case of *in vitro* folding, proper folding will require rapid kinetic pathways that initiate the proper fold before aggregation occurs. In the cell, folding is more likely to be directed by local nucleation and hierarchic assembly due to the sequential nature of synthesis, accessory protein interactions and possibly a more accommodating environment in general. This environment may change the thermodynamic driving force and relax the kinetic requirements to acquire a proper fold with respect to the *in vitro* case. Thus, even for the same protein sequence, folding mechanism may be different based on local environments. In fact, many proteins that are found folded in cells cannot fold *in vitro*. Solving the more fundamental *in vitro* problem will be a prerequisite to understanding the more complex *in vivo* protein folding problem.

Ab Initio Protein Folding

Among the goals of computer simulations on protein systems are to understand the mechanism and kinetics of folding and to predict the correct native structure form the primary sequence. Computational prediction of the three-dimensional structure of proteins from their sequences is referred to as ab initio protein structure prediction. The development of such a computational algorithm was first addressed by Nemethy and Scheraga in 1965[39] and has been gaining momentum in interest and efforts ever since.

A simulation technique that will play a key role in understanding protein systems is molecular dynamics. Increases in computing speed have enabled studies on the early stages of the mechanism of protein folding reaction for the small villin headpiece using all-atom, explicit solvent model,[40,41] an accomplishment that just a few years ago was prohibitively unrealistic. The ability to discriminate between the correct native structure and other misfolds has been a major difficulty in the goal of predicting protein structures. Because native protein structures are determined by their free energies, which consist of competing enthalpic and entropic terms, standard gas-phase energies alone are unlikely to be effective for this purpose.

A denatured protein makes many interactions with water and other molecules such as ions, small molecules and even biomolecules such as other proteins or peptides. As the protein begins to fold, it exchanges these solvent interactions with intramolecular ones. These include hydrophobic interactions, salt bridges, and formation of hydrogen bonds. The relative stabilization energy of a protein is difficult to calculate because its value is very small relative to the sum of the overall energetics. Opposing the forces that direct protein folding is the conformational entropy of the polypeptide chain. Organization of the polypeptide chain and side chains incurs a significant entropic

penalty. This penalty is only slightly offset by the favorable interactions. As a result, proteins are only marginally stable with the free energy of folding typically around –4 to –16 kcal mol^{-1}.

To determine the stability of a protein, we have to calculate not only the interaction energy between any two atoms within a protein, but also this energy relative to the interactions that the individual atoms make with water, ions, and other molecules in the denatured and native states. Currently potential functions and computing power are not sufficient for this purpose. In order to develop the framework that will be required to calculate these energetics we need a better understanding of the unfolded state, kinetics and protein energetics.

An alternative method is to model the protein structure by homology. Significant progress has been made in predicting protein structure from sequence.[42] Homology modeling based methods have seen some of the best results in the CASP competitions. The basic assumption is that the unknown and the homologous template protein of known structure have nearly identical backbone structure in the aligned regions. Of course, the success of this method depends on the level of homology. With >70% homology this method works very well and <50% the accuracy sharply diminishes. To improve on this method researchers have combined this method with secondary structure threading techniques. However, the success of threading depends on identification of known folds.

A quantitative treatment of folding kinetics is a prerequisite for elucidating mechanisms of protein folding. Even simple kinetics, like single exponential behavior, can be caused by a variety of different folding landscapes. Therefore the interplay between theoretical models and experimental results is essential in the effort to

understand protein folding. The aim of future experimental efforts will be to gain a better understanding of the very early steps of folding reactions and of the complexity of the transition barriers separating native from unfolded protein.

Section II Focus

Our knowledge of the process of protein folding has increased considerably in the recent years and many of the underlying principles are beginning to surface. Likewise, there is still much advancement needed to develop a full understanding of this complex process, particularly with respect to folding in complex environment such as those found *in vivo*. For future progress investigators will need to give more attention to the denatured state and how it effects the observed folding pathways.

Computational methods are becoming more accurate at predicting the rates of folding and progress is being made towards the goal of structure prediction. Methods that rely on first principles require the type of information that will be obtained in this work to improve to a level where prediction would become accurate and consistent. With the advancing human genome project, the need for accurate structure prediction is apparent. The technological and medical advancements will be far reaching if we can decode the language relating the primary amino acid sequence to a protein's native tertiary fold. Likewise, better force fields will be important for computational predictions in the broader arena of protein dynamics and will be a step towards the very difficult task of determining protein function from structure.

Experimental methods to study protein folding have been evolving since the beginning of the field. Relaxation techniques have opened a time window that was previously inaccessible by rapid-flow methods. Engineering advances have brought

rapid-flow experiments to ultra rapid-flow status. Flash photolysis provided a new means for initiating folding while keeping the denaturant concentrations constant. These improved techniques still do not allow for the study of protein folding from a narrow starting state, in a non-denaturing environment. The following two chapters give two examples of our attempt to achieve this goal. Chapter 7 describes the masking of a charge-charge repulsion in the GCN4-p1 peptide dimmer using the photolabile dimethoxy benzoin group. This novel strategy for initiating protein unfolding is then used to study the folding kinetics using time resolved photoacoustic and photothermal beam deflection. The use of a photolabile linker to denature a protein by intramolecular cyclization is detailed in chapter 8. The Villin Headpiece test protein is cyclized, its photolysis characterized and its folding kinetics followed.

References

1)Glenner, G. G.; Wong, C. W.; Quaranta, V.; Eanes, E. D. *Appl Pathol* **1984**, *2*, 357-69.

2)Glenner, G. G.; Wong, C. W. *Biochem Biophys Res Commun* **1984**, *122*, 1131-5.

3)Hartl, F. U.; Hlodan, R.; Langer, T. *Trends Biochem Sci* **1994**, *19*, 20-5.

4)Ingram, V. M. *Nature* **1957**, *180*, 326.

5)Hekman, C. M.; Loskutoff, D. J. *J Biol Chem* **1985**, *260*, 11581-7.

6)Gorina, S.; Pavletich, N. P. *Science* **1996**, *274*, 1001-5.

7)Anderson, M. E.; Tegtmeyer, P. *Bioessays* **1995**, *17*, 3-7.

8)Qu, B. H.; Thomas, P. J. *J Biol Chem* **1996**, *271*, 7261-4.

9)Baum, J.; Brodsky, B. *Curr Opin Struct Biol* **1999**, *9*, 122-8.

10)Prusiner, S. B. *Proc Natl Acad Sci U S A* **1998**, *95*, 13363-83.

11)Huang, Z.; Prusiner, S. B.; Cohen, F. E. *Fold Des* **1996**, *1*, 13-9.

12)Selkoe, D. J. *Science* **1997**, *275*, 630-1.

13)Rubinsztein, D. C.; Leggo, J.; Coles, R.; Almqvist, E.; Biancalana, V.; Cassiman, J. J.; Chotai, K.; Connarty, M.; Crauford, D.; Curtis, A.; Curtis, D.; Davidson, M. J.; Differ, A. M.; Dode, C.; Dodge, A.; Frontali, M.; Ranen, N. G.; Stine, O. C.; Sherr, M.; Abbott, M. H.; Franz, M. L.; Graham, C. A.; Harper, P. S.; Hedreen, J. C.; Hayden, M. R.; et al. *Am J Hum Genet* **1996**, *59*, 16-22.

14)Beckman, J. S.; Carson, M.; Smith, C. D.; Koppenol, W. H. *Nature* **1993**, *364*, 584.

15)Brown, R. H., Jr. *Curr Opin Neurobiol* **1995**, *5*, 841-6.

16)Benedek, G. B. *Invest Ophthalmol Vis Sci* **1997**, *38*, 1911-21.

17)Polymeropoulos, M. H.; Lavedan, C.; Leroy, E.; Ide, S. E.; Dehejia, A.; Dutra, A.; Pike, B.; Root, H.; Rubenstein, J.; Boyer, R.; Stenroos, E. S.; Chandrasekharappa, S.; Athanassiadou, A.; Papapetropoulos, T.; Johnson, W. G.; Lazzarini, A. M.; Duvoisin, R. C.; Di Iorio, G.; Golbe, L. I.; Nussbaum, R. L. *Science* **1997**, *276*, 2045-7.

18)Ceighton, T. E. *Proteins: Structures and Molecular Properties*; second edition ed.; W. H. Freeman and Co.: New York, 1996.

19)Glushko, V.; Lawson, P. J.; Gurd, F. R. *J Biol Chem* **1972**, *247*, 3176-85.

20)Leopold, P. E.; Montal, M.; Onuchic, J. N. *Proc Natl Acad Sci U S A* **1992**, *89*, 8721

21)Tanford, C. *Adv Protein Chem* **1968**, *23*, 121-282.

22)Flory, P. J. *Statistical Mechanics of Chain Molecules*; Wiley: New York, 1969.

23)Hennig, M.; Bermel, W.; Spencer, A.; Dobson, C. M.; Smith, L. J.; Schwalbe, H. *J Mol Biol* **1999**, *288*, 705-23.

24)Pappu, R. V.; Srinivasan, R.; Rose, G. D. *Proc Natl Acad Sci U S A* **2000**, *97*, 12565

25)Sosnick, T. R.; Trewhella, J. *Biochemistry* **1992**, *31*, 8329-35.

26)Shortle, D.; Meeker, A. K. *Biochemistry* **1989**, *28*, 936-44.

27)Flanagan, J. M.; Kataoka, M.; Fujisawa, T.; Engelman, D. M. *Biochemistry* **1993**, *32*, 10359-70.

28)Smith, L. J.; Fiebig, K. M.; Schwalbe, H.; Dobson, C. M. *Fold Des* **1996**, *1*, R95-106.

29)Eaton, W. A.; Munoz, V.; Hagen, S. J.; Jas, G. S.; Lapidus, L. J.; Henry, E. R.; Hofrichter, J. *Annu Rev Biophys Biomol Struct* **2000**, *29*, 327-59.

30)Dobson, C. M.; Hore, P. J. *Nat Struct Biol* **1998**, *5 Suppl*, 504-7.

31)Callender, R. H.; Dyer, R. B.; Gilmanshin, R.; Woodruff, W. H. *Annu Rev Phys Chem* **1998**, *49*, 173-202.

32)Roder, H.; Shastry, M. R. *Curr Opin Struct Biol* **1999**, *9*, 620-6.

33)Ballew, R. M.; Sabelko, J.; Gruebele, M. *Proc Natl Acad Sci U S A* **1996**, *93*, 5759-64.

34)Jacob, M.; Holtermann, G.; Perl, D.; Reinstein, J.; Schindler, T.; Geeves, M. A.; Schmid, F. X. *Biochemistry* **1999**, *38*, 2882-91.

35)Abbruzzetti, S.; Crema, E.; Masino, L.; Vecli, A.; Viappiani, C.; Small, J. R.; Libertini, L. J.; Small, E. W. *Biophys J* **2000**, *78*, 405-15.

36)Jones, C. M.; Henry, E. R.; Hu, Y.; Chan, C. K.; Luck, S. D.; Bhuyan, A.; Roder, H.; Hofrichter, J.; Eaton, W. A. *Proc Natl Acad Sci U S A* **1993**, *90*, 11860-4.

37)Lu, H. S. M.; Volk, M.; Kholodenko, Y.; Goodling, E.; Hochstrasser, R. M.; DeGrado, W. F. *Journal of the American Chemical Society* **1997**, *119*, 7173-7180.

38)Jackson, S. E. *Fold Des* **1998**, *3*, R81-91.

39)Nemethy, G.; Scheraga, H., A., *Biopolymers* **1965**, *3*, 155.

40)Duan, Y.; Kollman, P. A. *Science* **1998**, *282*, 740-4.

41)Duan, Y.; Wang, L.; Kollman, P. A. *Proc Natl Acad Sci U S A* **1998**, *95*, 9897-902.

42)Simons, K. T.; Ruczinski, I.; Kooperberg, C.; Fox, B. A.; Bystroff, C.; Baker, D. *Proteins* **1999**, *34*, 82-95.

Chapter 7:

Rapid Photochemical Triggering of Protein Unfolding in a Nondenaturing Environment

Abstract

A general, rapid method for triggering protein unfolding is demonstrated using the photolabile protecting group 3',5'-dimethoxybenzoin (DMB). This protecting group is introduced in a site-specific manner to block a mutation known to destabilize the GCN4-p1 coiled-coil. Upon photolysis, the unfavorable interaction is unmasked and the peptide unfolds, as seen in the decrease in α-helical ellipticity. Photothermal beam deflection and photoacoustic calorimetry reveal kinetic processes and associated volume changes with rates of $2 \times 10^5 - 3 \times 10^6$ sec^{-1}, demonstrating that this photochemical technique is capable of triggering rapid protein conformational changes. Furthermore, this system allows conformational triggering under native solvent conditions, in the absence of chemical denaturants.

Introduction

In order to unravel the complexity of the protein folding process, a host of techniques have been developed over the last thirty years to gain insight into the nature of the energy landscape. These techniques include means of examining the interactions that drive the folding process in atomic detail, (1, 2) methods for examining the behavior of individual protein molecules within an ensemble, (3, 4) and even methods that allow the measurement of the force required to unfold a single protein domain (5). In addition to these improved methods for detection of folded structures, much effort has been devoted to improving the techniques used to trigger a conformational change in a protein for kinetic studies (6). For any kinetic study to be successful, the event that perturbs the

equilibrium must occur on a timescale much shorter than the process of interest. Unfortunately, the most accessible method for triggering conformational changes, the rapid dilution of a protein into or out of a denaturant solution, is often too slow to measure the earliest kinetic phases due to the dead time of the mixing apparatus.

To simplify the study of these kinetic processes, a trigger event that is rapid, irreversible, and results in a large change in stability ($\Delta\Delta G°$) is required. In the system described here, the picosecond flash photolysis of small organic chromophores, known as cages, from protein functional groups is employed. Instead of manipulating the external conditions, such as denaturant concentration, pH, or temperature, the covalent structure of the protein is altered in the triggering event. These phototriggers target specific charge-charge interactions in protein side chains. For one peptide test system, a caged GCN4-p1, an unfolding event is initiated on the picosecond timescale, and the subsequent unfolding events are observed on the microsecond timescale. The $\Delta\Delta G°$ upon photolysis is sufficiently large that unfolding may be observed under native conditions (zero denaturant, ambient temperature, neutral pH). Thus difficulties in interpreting the kinetic behavior due to the presence of denaturants are avoided.

Materials and Methods

Synthesis of DMB

The cage 3',5'-dimethoxybenzoin (DMB) was prepared by a one-pot modification of the procedure first reported by Stowell *et al.* (7). A solution of 2-phenyl-1,3-dithiane (4.909 g, 25 mmol) was prepared in 100 mL dry THF. The solution was cooled to 0°C,

and butyllithium (2.5 M in hexanes, 10 mL, 25 mmol) was added dropwise under nitrogen. After 30 min, 3,5-dimethoxybenzaldehyde (4.155 g, 25 mmol) was added. After an additional 30 min, the resulting lithium alkoxyanion was protonated with glacial acetic acid (1.5 mL, 26.3 mmol). The dithiane was then removed by the slow addition of mercuric perchlorate (28.346 g, 62.5 mmol) in 20 mL water. Once precipitation of the mercury-dithiane adduct was complete (15 min), a saturated solution of potassium carbonate (20.7 g, 150 mmol) in water was added. The resulting mixture was filtered through a bed of silica gel, and the filtrate added to ethyl acetate. The organic phase was extracted with a 5% sodium bicarbonate solution, dried with $MgSO_4$, and evaporated, to yield 6.187 g (68%) of white crystals. ^{1}H-NMR ($CDCl_3$, TMS) δ 7.95 (m, 2 H), 7.55 (m, 1 H), 7.41 (m, 2 H), 6.49 (d, J = 2.2 Hz, 2 H), 6.31 (t, J = 2.2 Hz, 1 H), 5.85 (d, J = 4.6 Hz, 1 H), 4.53 (d, J = 4.6 Hz, 1 H), 3.74 (s, 6 H).

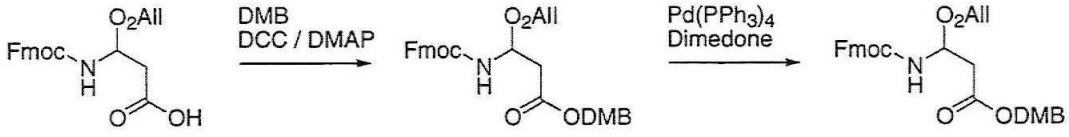

Figure 1. Synthetic scheme for Fmoc-Asp(DMB)-OH.

Synthesis of Fmoc-Asp(DMB)-OH

A solution of Fmoc-Asp-OAll (1.186 g, 3 mmol, Novabiochem) was prepared in 20 mL DCM (figure 1). A sample of DMB (817 mg, 3 mmol) was dried by azeotropic distillation from acetonitrile and added to the Asp solution, followed by DCC (619 mg, 3 mmol) and DMAP (20 mg, 0.16 mmol). The solution was stirred for 12 h, then poured into diethyl ether and extracted with water. The organic phase was then dried with

$MgSO_4$ and evaporated. The resulting oil was redissolved in THF, and $(Ph_3P)_4Pd(0)$ (343 mg, 0.3 mmol) and 3,3-dimedone (1.40 g, 10 mmol) were added under Ar. After stirring for 2 h, the solution was evaporated and the oil purified by flash chromatography (silica gel, 1:1 hexanes / ethyl acetate containing 1% TFA) to yield 1.195 g of a yellow oil (65%). If desired, this oil may be further purified by RP-HPLC (C18, A: water, 0.1% TFA; B: acetonitrile, 0.1% TFA). ^{1}H-NMR ($CDCl_3$, TMS) δ 7.948 (m, 2 H), 7.745 (m, 2 H), 7.573 (m, 4 H), 7.86 (m, 4 H), 7.282 (m, 1 H), 6.996 (m, 0.5 H), 6.832 (d, J = 14.7 Hz, 1 H), 6.558 (m, 2 H), 6.393 (m, 1 H), 6.098 (m, 0.5 H), 4.804 (m, 1 H), 4.387 (m, 2 H), 4.256 (m, 1 H), 3.726 (s, 2 H), 3.708 (s, 2 H), 3.140 (m (br), 2 H) (diastereomeric).

Synthesis of GCN4-p1 (N16D(DMB))

The sequence Ac-RMKQLEDKVEELLSKD(DMB)YHLEVARLKKLVGER-NH_2 was prepared by Fmoc SPPS. The following standard side chain protecting groups were used: Ser(OtBu), Asp(OtBu), Glu(OtBu), Tyr(OtBu), Asn(Trt), Gln(Trt), His(Trt), Lys(Boc), Arg(Pbf). Coupling cycles used a four-fold excess of a 0.3 M Fmoc-amino acid solution, preactivated with 1:1:1.5 HBTU / HOBt / DIEA. Standard coupling cycles were 30 min, with the exception of the following residues in GCN4-p1 peptides, which were coupled for 1 hr: Arg, Asp, Leu, Glu, Val. A 5 min capping cycle using a solution of 0.3 M acetic anhydride, 0.3 M HOBt in 10% (v/v) DCM in DMF was included following each coupling cycle. Fmoc groups were cleaved with 20% (v/v) piperidine in DMF.

The *C*-terminal fragment from residues Tyr17-Arg33 was prepared on a Novasyn TGR Rink amide resin (Novabiochem) on a 0.2 mmol scale (figure 2). After removal of the *N*-terminal Fmoc group, the peptide resin was transferred to a 25 mL manual

synthesis vessel, and rinsed with DCM. The resin was treated with 304 mg 2-hydroxy-4-methoxybenzaldehyde, dissolved in 20 mL 0.1% (v/v) acetic acid in DMF, for 15 minutes. The resin was rinsed with 3 x 20 mL DMF, and the imide was reduced with 128 mg $NaBH_3CN$ in 20 mL of 25% (v/v) MeOH / DMF for 1 h. The resin was transferred to a 10 mL manual synthesis vessel, and rinsed with DCM. The *N*-terminal secondary

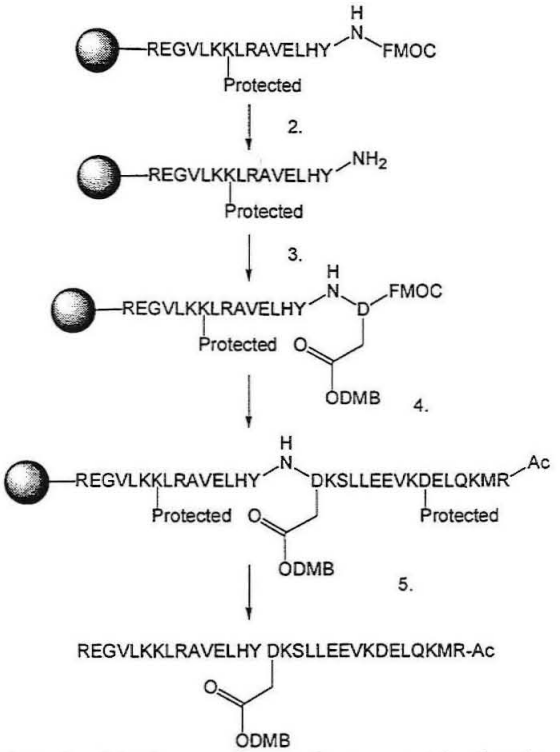

Figure 2. Synthetic scheme for the formation of GCN4-p1 (N16D(DMB)).

amine was acetylated with the preformed symmetrical anhydride of Fmoc-Asp(DMB)-OH, prepared by DCC activation (103 mg, 0.5 mmol) of a solution of Fmoc-Asp(DMB)-OH (609 mg, 1 mmol) in 4 mL DCM. After 12 h, the resin was rinsed with 25 μL DIEA in 5 mL DCM, followed by DCM. Photolysis of a resin sample taken after Asp(DMB) coupling led to formation of the expected phenylbenzofuran photoproduct. The resin was then transferred back to the automated synthesizer for addition of the *N*-terminal

fragment of GCN4-p1, from residues Arg1-Lys15. Finally, the *N*-terminal Arg was acetylated with 10 mL of 20% acetic anhydride in NMP, plus 25 μL of DIEA, for 30 min.

After the synthesis was complete, the resin was rinsed with DCM and dried *in vacuo* for a minimum of 3 hr. Resin cleavage was performed using 92.5% TFA / 2.5% water / 2.5% TIS / 2.5% EDT (v/v), applied to the resin under nitrogen for 1.5 h. The crude peptide was isolated by precipitation in a minimum of five volumes of ice-cold MTBE, followed by four cycles of centrifugation / resuspension in fresh MTBE to remove scavengers. Typically, the crude peptide was dissolved in 50 mM Na phosphate buffer, pH 7.0, and any residual ether was removed under a stream of nitrogen prior to purification by RP-HPLC. All RP-HPLC was performed on a 10 mm x 250 mm C18 column (Vydac), using a gradient of 0.1% (w/v) TFA in water (solvent A), and 0.1% TFA in acetonitrile (solvent B), to yield 16 mg (1.9%) of GCN4-p1 (N16D(DMB)). MALDI-TOF MS $[M+H]^+$ exp. 4293.98, found 4293.12.

MALDI-TOF MS of Caged Peptide Photoproducts

Stock solutions of GCN4-p1 (N16D(DMB)) were prepared in deionized water. One-half of each stock solution was photolyzed for 120 sec using a 500 W high-pressure Hg vapor arc lamp, with a combination of Schott glass UG11 and WG320 filters. The following *m/z* $[M+H]^+$ were found: GCN4-p1 (N16D(DMB)) exp. 4293.98, found 4293.22; GCN4-p1 (N16D(DMB)) (photolyzed 180 s) exp. 4039.70, found 4039.65.

Peptide Preparations for Spectroscopy

Stock solutions, prepared from dissolving lyophilized aliquots of peptide (~ 0.5-1 mg) in 200 μL buffer (50 mM Na phosphate, 150 mM NaCl, pH 7.00), were prepared. Spectral overlap of the benzoinyl cage with the aromatic absorbtion bands of the protein

prevented concentration measurements using A_{260}. Therefore, peptide concentrations were determined by BCA assays, and the peptide concentration was adjusted to 50 μM for all CD and fluorescence studies. For GCN4-p1 (N16D(DMB)), this stock solution gave an A_{260} of 0.618, or an A_{320} of 0.149, and future peptide stock concentrations were adjusted accordingly.

Steady-State Circular Dichroism Studies

Circular dichroism studies were performed on an Aviv 62A DS CD spectrophotometer, equipped with a Peltier thermal control unit. Wavelength scans were performed on freshly prepared peptide samples, followed by thermal melts. The spectrometer slits were closed between temperature points, to prevent photolysis of the sample during equilibration. A second wavelength scan following the thermal melt verified that no significant photolysis occurred during the experiment. The sample was then photolyzed to completion, as determined by the phenylbenzofuran UV absorbtion band at 300 nm. A second set of wavelength scans and temperature melts was performed after photolysis.

Photoacoustic Calorimetry and Photothermal Beam Deflection

Peptide concentrations were 50 μM for both PAC and PBD. PAC was performed as previously described (8). All photoacoustic waves were normalized by the sample absorbance at the excitation wavelength of 337 nm.

For PBD, the photochemistry was initiated by a pulse from a pulsed nitrogen laser (LSI Inc., 337 nm, 7 ns pulse width, ~400 μJ/pulse) passing nearly collinear with a continuous wave diode laser probe (Edmond Scientific, LDL 175, 820 nm, 3 mW). The probe beam emerging from the sample was focused onto a split photodiode bicell

detector (Centronics LD2-5T, coupled to an Analog Devices AD844 amplifier operating in a difference mode). The generated signal was then digitized using a Tektronix RTD710A 200 MHz transient digitizer coupled to an IBM-based PC. Sample temperature was varied between 17 and 35°C in increments of ~5°C with a constant temperature block regulated by a circulating water bath. Generally, the PBD system can resolve volume/enthalpy changes with lifetimes ranging from roughly 1 μs to 50 ms.

The PBD data were analyzed by fitting (Sigmaplot™ software) to the following equation:

$$F = \alpha 0 + \Sigma\, \alpha_i\,(1\text{-}exp[-k/\tau_i]) \qquad (1)$$

where the α_i's equal S of equation 4 for each intermediate step in the PBD studies (see below). The total enthalpy of reaction is obtained by the PBD parameters where $\Delta H = E_{hv} - Q$ for α_0 and for the subsequent α_i's, $\Delta H = Q$.

Results and Discussion

Photochemical Triggering System

The ideal conformational trigger for protein folding and unfolding studies would have the following properties. First, the trigger must involve a large stability change, i.e., a large ΔΔG°. Such a large change in stability allows a wide variety of conditions to be examined, especially strongly native, zero-denaturant conditions. Second, the trigger event must be rapid. The rapid triggering studies described above suggested that some conformational changes might be detected on timescales as rapid as 100 ps, depending on the system. As a result, the ideal trigger event would be complete in less than this time. Third, in order to be of general applicability, the trigger must not rely on protein

prosthetic groups, such as hemes or metal ions that are not present in all proteins. Hemes in particular are to be avoided, since a heme is a significant fraction of the protein mass and may be expected to contribute interactions that would dominate the conformational change. Finally, and perhaps most importantly, the trigger must be irreversible. All current rapid conformational triggers (with the exception of capillary mixing) suffer from reversibility to a greater or lesser extent. Protein conformational changes can be enormously complex, with events spanning timescales from picoseconds to seconds. It is simply too difficult to construct an accurate kinetic framework by combining data from different triggering methods, each with its own observation window, when a single, rapid, irreversible trigger would provide the same information. Some have claimed that reversibility is a desired property of a conformational trigger, in that signal averaging from multiple triggering events is allowed (9). This would be true, if the reverse reaction occurred on the timescale of seconds or more, after all relevant conformational changes were complete. However, with the current systems, timescales spanning at most three orders of magnitude may be studied, due to reverse reactions that are too rapid. On the other hand, with an irreversible trigger, signal averaging may always be achieved with larger quantities of protein.

One triggering technique that can meet all of the above requirements is the flash photolysis of a class of organic protecting groups known as cages. Irradiation of a cage chromophore leads to specific, irreversible bond-cleavage. Carefully placed, a cage group will block the reaction of interest until a photolysis pulse is applied. A number of cages, with a variety of photochemical properties, are candidates for protein conformational triggers (10, 11). One that is particularly suited for the applications

examined here is 3',5'-dimethoxybenzoin (DMB), first studied in depth by Sheehan, Wilson, and Oxford (12, 13). DMB forms carboxylate and phosphate esters that may be cleaved to form the free acid when irradiated from 300-360 nm. The sole photoproducts are 5,7-dimethoxy-2-phenyl benzofuran, and the parent acid. The photolysis of DMB cannot be quenched by triplet quenchers such as piperylene or napthalene, while unsubstituted benzoinyl esters which photolyze to yield the same products are quenched. Stern-Volmer analysis therefore suggests that the photolysis rate is in excess of 10^{10} sec^{-1}, (13) and may be as high as 10^{12} sec^{-1} (14). The quantum yield of photolysis is high (0.64), allowing short photolysis laser pulses as multiple excitation of the DMB chromophore is not required. Finally, the phenylbenzofuran photoproduct is inert, so further reactions with polypeptide functional groups are not expected.

Since DMB esters are uncharged, while photolysis liberates a charged side-chain, DMB cages may be used to target charge-charge interactions in protein side chains. If a particular salt bridge is critical to the stability of a protein, the carboxylate may be protected by a DMB cage, and then rapidly liberated by a photolysis pulse to restore the key interaction. In an opposite strategy, as outlined below, an unfavorable charge-charge repulsion may be masked by a DMB cage. The caged peptide is therefore folded; upon photolysis the unfavorable interaction is unmasked to commence an unfolding reaction.

Protein System

One peptide that serves as an ideal caging test system is the GCN4-p1 leucine zipper (15-18). GCN4-p1 is the 33-residue peptide derived from the bZIP class of yeast transcription factors, that forms a homodimeric coiled-coil in solution. The solid-phase synthesis of GCN4-p1 is facile, which allows caged side chains to be introduced in a site-

Figure 3. Ribbon diagram of GCN4-p1 dimer.

specific manner. In addition, GCN4-p1 contains a site within the hydrophobic interface that is a potential target for a caged side chain. Although the coiled-coil interface (the a- and d-positions in the heptad repeat) consists of primarily hydrophobic residues, it also contains a single polar residue in Asn16 that forms a buried interstrand hydrogen bond. This internal hydrogen bond may either help to set the register of the two helices, preventing overhanging ends, or it may help to regulate the dimeric state of GCN4-p1, preventing the formation of trimers and tetramers (19-22).

Recently, DeGrado and coworkers examined Asn16 in GCN4-p1 as a potential site for a designed, buried salt-bridge (23). In the proposed design, the Asn16 in one strand is mutated to an Asp residue (GCN4-p1 (N16D)), while the Asn16 in the neighboring strand is converted to a diaminopropionic acid (Dap) or diaminobutyric acid (Dab). As expected, homodimers do not form for these peptides due to charge repulsion. Homodimers do form, however, at a pH where the buried residue is neutral. In the strategy applied here, the mutant GCN4-p1 (N16D) is examined for rapid unfolding studies. The unfavorable charge-charge repulsion at Asp16 is blocked by a DMB ester, allowing the formation of GCN4-p1 (N16D(DMB)) homodimers. Photolysis results in rapid conversion to the charged GCN4-p1 (N16D) species, with concomitant unfolding of the homodimer.

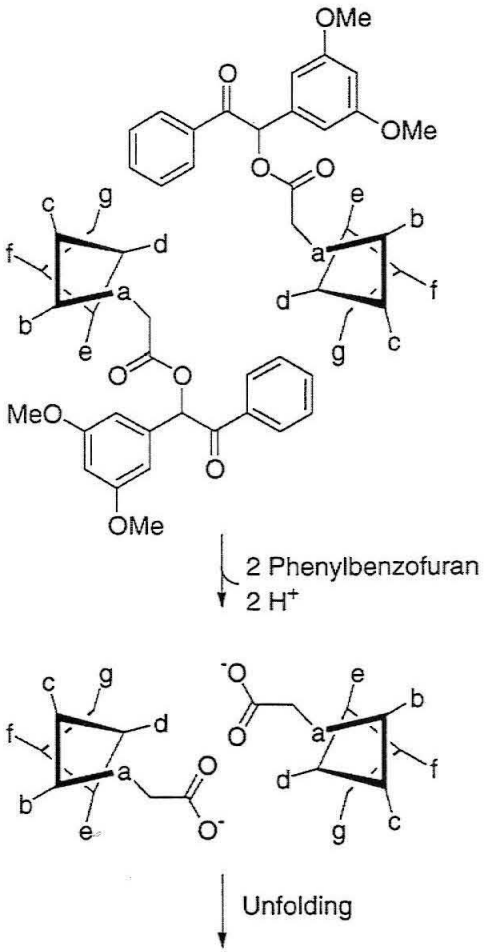

Figure 4. The photolysis scheme for GCN4-p1 (N16D(DMB)).

Synthesis of Caged Peptides

Synthesis of GCN4-p1 N16D(DMB) was hindered by aspartimide formation, a common side reaction that occurs under the basic conditions of Fmoc removal. The overall yield of the desired peptide (1 mg for a 0.1 mmol scale synthesis) was quite low, so the amide backbone was protected with an HMB group on Tyr17, which protects the site of cyclization. Unfortunately, the required protected amino acid for Tyr17, Fmoc-(Fmoc-HMB)Tyr-OH, is not commercially available, so the HMB group was added on the solid-phase according to the method of Ede *et al.* (24). Coupling of Fmoc-

Asp(DMB)-OH was performed using the symmetrical anhydride. In test reactions, coupling efficiencies were much higher when DCM was used as the coupling solvent, as opposed to DMF or NMP. In this manner, the yield of GCN4-p1 (N16D(DMB)) was increased to 16 mg from a 0.2 mmol scale synthesis (1.9%). The main side product was GCN4-p1 (N16D), most likely formed from partial loss of the DMB group under the cleavage conditions.

The specific Rink amide used here is critical for successful synthesis of peptides containing DMB protecting groups. Resins from other manufacturers produced peptides that were cleaved at the peptide backbone adjacent to the DMB, presumably due to a side reaction of the cage with resin-bound cations that can form during the cleavage reaction.

Steady-State Photolysis

The purified peptide GCN4-p1 (N16D(DMB)) had the correct mass as determined by MALDI-TOF MS. To verify that the proper peptide photoproducts were created, additional samples were irradiated prior to MS characterization. The only change upon irradiation was the loss of a fragment with a *m/z* of 254, which corresponds to the mass of the DMB protecting group, as expected.

CD spectroscopy revealed that the peptide GCN4-p1 (N16D(DMB)) was predominantly helical prior to photolysis. Upon photolysis GCN4-p1 (N16D(DMB)) unfolded, as expected for a peptide with an unfavorable buried charge interaction. The magnitude of $[\theta]_{222}$ after photolysis indicated that the GCN4-p1 (N16D) was largely in a random coil configuration, with some residual helical structure. Comparison of the change in $[\theta]_{222}$ with the values observed by DeGrado and coworkers indicated that

photolysis was 85% complete under the experimental conditions.

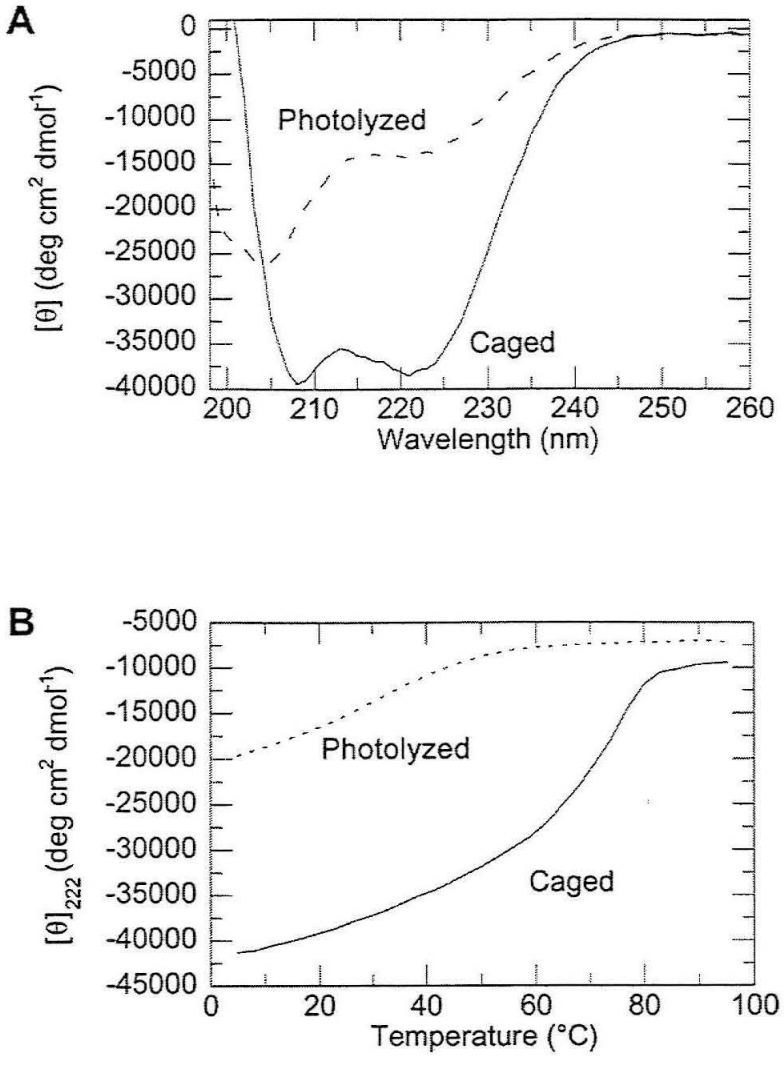

Figure 5. (A) CD spectrum of GCN4-p1 (N16D(DMB)). 50 μM peptide in 50 mM Na phosphate, 150 mM NaCl, pH 7.00. Samples were measured before (Caged) and after photolysis (Photolyzed) for 90 sec under standard conditions. (B) Thermal melts of GCN4-p1 (N16D(DMB)). 50 μM peptide in 50 mM Na phosphate, 150 mM NaCl, pH 7.00. Samples were measured before (Caged) and after photolysis (Photolyzed) for 90 sec under standard conditions.

Thermal melts of GCN4-p1 (N16D(DMB)) showed a cooperative melting transition at 75°C, suggesting that this peptide is more stable than GCN4-p1. This higher

melting temperature could be due to the large hydrophobic surface area of the cage, which may be partially buried in the folded state. In contrast, the photolyzed peptide GCN4-p1 (N16D) did not undergo a thermal melting transition within the temperature range of 5 - 95°C. As a result of the quite different melting behavior of GCN4-p1 (N16D(DMB)) and GCN4-p1 (N16D), protein unfolding upon photolysis may be monitored in the broad temperature range of 5 - 75°C.

Transient Kinetics of GCN4-p1 (N16D(DMB)) Unfolding

The GCN4-p1 (N16D(DMB)) peptide allows the photoinitiated study of rapid unfolding processes. Since unfolding reactions begin from a single conformation, as opposed to refolding reactions that begin from a random coil ensemble, studies of unfolding can reveal intermediates that would be obscured in folding processes.

Volume changes and enthalpies of unfolding for GCN4-p1 (N16D(DMB)) were monitored by photoacoustic calorimetry (PAC) and photothermal beam deflection (PBD). Both techniques involve photoexcitation of a molecular system of interest in which excess energy is dissipated by vibrational relaxation to the ground state. During this process, the excitation energy is converted to thermal motion of the surrounding solvent molecules. This photothermal heating of a solvent (such as water) causes a rapid volume expansion that changes the refractive index of the solution and develops an acoustic wave (25, 26). Additionally, volume changes in the molecular system of interest induced by a photoinitiated reaction also contribute to the refractive index/acoustic wave. In PAC, the volume expansion is monitored by detecting the accompanying acoustic wave, whereas in PBD, changes in the refractive index are followed optically by a probe beam. Because these techniques explore physically related phenomena, the mathematical evaluations of

the instrumental signals bare resemblance; however, only the PBD treatment will be given here.

The deflection signal arising from changes in the refractive index of the sample can be written as

$$S = AE_{hv}\Phi[(dn/dT)(1/\rho C_p)Q + \rho(dn/d\rho)\Delta V + B\Delta n_{abs}] \qquad (2)$$

where A represents the geometrical parameters of the instrument, E_{hv} is the photon energy absorbed, Φ is the quantum yield, ρ is density (g/mL), C_p is the heat capacity (cal/deg K), Q is the heat released to the solvent by the sample upon excitation, n is the solution refractive index and $B\Delta n_{abs}$ is the change in refractive index due to absorption changes in the sample (27). The experimentally determined values (dn/dT) provided by Abbate *et al.* (28) have been used here.

In principle, the amount of heat deposited to the solvent could be derived from the deflection angle of the probe beam created by the refractive index gradient within the solution. However, in practice the amount of deflection can be quantified by comparing the signal amplitude of the unknown sample to that of a reference compound (27). The reference typically absorbs the pulse energy that is deposited, in its entirety, to the solvent as heat without additional photochemistry. Thus the expression of the PBD signal for the reference compound has no volume change terms, a quantum yield of unity and a Q_{ref} term equal to E_{hv}, which is given as

$$R = AE_{hv}(dn/dT)(1/\rho C_p)E_{hv} \qquad (3)$$

By using the ratio of the sample signal to that of the reference, the normalized PBD signal provides an expression which eliminates the instrument response factor, A:

$$(S/R)*E_{hv} = \Phi Q + \Phi[\rho(dn/d\rho)\Delta V + B\Delta n_{abs}]/(dn/dT)(1/\rho C_p) \qquad (4)$$

Plotting $(S/R)E_{hv}$ versus $\rho C_p/(dn/dT)$ gives a slope proportional to the volume change and an intercept equal to the amount of heat released to the solvent. Since Q is the amount of heat released by the photoinitiated reaction, subtracting Q from E_{hv} (the amount of energy absorbed by the molecule) gives ΔH for the reaction. In our calculations, the $B\Delta n_{abs}$ term is negligible. The term, $\rho(dn/d\rho)$, is a unitless constant (equal to 0.326 ± 0.001; 0≤ T ≤35 ^{0}C) that is independent of the temperature range of this experiment and originates from a component of the refractive index change involving the volume expansion coefficient of the solvent, $\beta^{-1}(\delta lnf/\delta P)_T$. (27). Values for both the density and the heat capacity of water were obtained from (29).

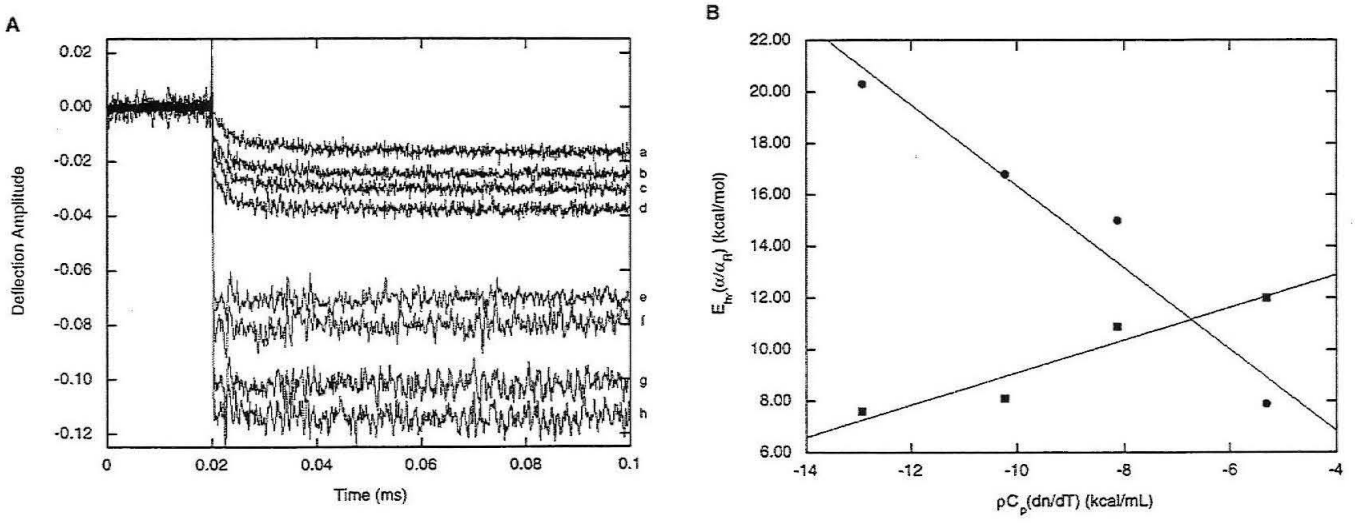

Figure 6. (A) Overlay of the photothermal beam deflection traces of GCN4-p1 (N16D(DMB)) subsequent to photolysis and the reference compound. All traces are normalized to the absorbance at the excitation wavelength (337 nm). Sample: (a) 13°C; (b) 20°C; (c) 26°C; (d) 35°C; Reference: (e) 13°C; (f) 20°C; (g) 26°C; (h) 35°C. (B) Plots of $(\alpha_I/\alpha_R)^* E_{hv}$ versus $\rho C_p/(dn/dT)$ for α_0 (circles) and α_1 (squares). Values for α_0 and α_1 were obtained from fitting the traces in Figure 7 to $F = \alpha 0 + \alpha_1 (1\text{-}exp[-k/\tau_1])$. The slopes of these plots are proportional to ΔV and the intercepts to the amount of heat released to the solvent.

For GCN4-p1 (N16D(DMB)), PBD revealed a fast volume contraction of –2.6 mL $mole^{-1}$, on a timescale faster than could be resolved by the setup. This fast phase was followed by a single phase of volume expansion of 1.5 mL $mole^{-1}$, occurring at a rate of 1.8×10^5 sec^{-1} (figure 4). These results are consistent with an initial electrostrictive contraction of the solvent upon generation of the free carboxylate at residue 16, followed by a slower volume expansion upon unfolding due to exposure of hydrophobic residues in the core of GCN4-p1. Additional kinetic phases, with rates of 1.4×10^6 sec^{-1} and 3.3×10^6 sec^{-1}, were detected by PAC (data not shown). Importantly, photochemical cleavage of a DMB model compound (14) was instantaneous, as detected by both PAC and PBD, and therefore does not contribute to the rates measured here.

In interpreting kinetics on the GCN4-p1, Sosnick and coworkers have suggested that the transition state contains little if any helical secondary structure (33). In this model, folding is initiated by the collision of two unstructured monomers. In contrast, Steinmetz and coworkers have proposed a model for GCN4 leucine zipper folding that is based on a helical trigger segment (34). In addition, this group went on to show that the C terminus (GCN4p16-31) forms an autonomous helical folding unit that is stabilized by an intrahelical salt bridge (35).

An N terminal crosslinked variant of the GCN4 coiled coil was made by Sosnick and coworkers (36). They used this monomeric version of GCN4 to draw the conclusions that folding occurs along a single pathway starting at the region closest to the crosslink, despite this region of the helices having the lowest helix propensity. In this work they present a folding model where folding occurs along multiple routes with nucleation sites located throughout the protein. In this model they offer that minimal

helix is present before productive collision of the two chains, but that approximately one-third to one-half of the helical structure is formed in the postcollisional transition state ensemble. It is likely that minimal residual structure may be present under some conditions; however, transient helix formation in the denaturing environment may be required for the productive folding of the dimer.

Matthews *et al.* have proposed the following model for the folding of GCN4-p1 that is shown in Figure 5 (37). In this model the ensemble of unfolded conformations is in rapid equilibrium with a subset of conformations, I, that contain short α-helical stretches primarily localized in the C terminal region of the molecule. The transition state is a result of a productive collision between two monomers with the correct nucleation sites. The native state is achieved by the rapid "zippering" of the remaining sequence. While this model implies three-state model, it is possible that it is still consistent with the commonly observed two-state kinetics. The rate for formation of the I state is expected to be on the 10 to 100 ns time scale (38, 39). This is substantially faster than the association/folding step that is rate limiting and faster than the previous methods that have been used to study the folding process.

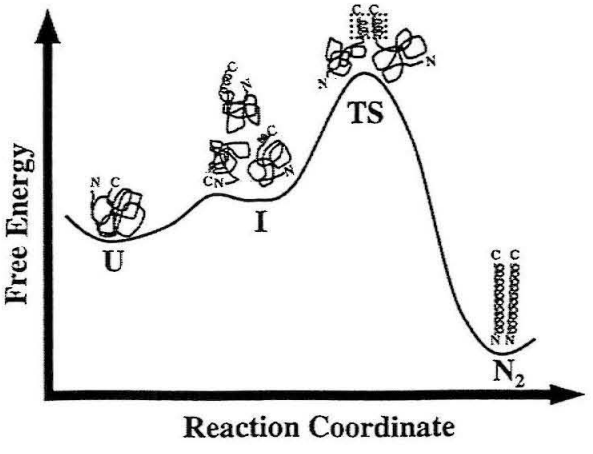

Figure 7. Matthews *et al.* transition State model for the folding of GCN4-p1.

Conclusions

In the study on GCN4-p1 presented here, the fact that photolysis of side chain cages can trigger conformational switching has been demonstrated. In particular, salt bridges are suitable targets for caging strategies, given the ease of protecting carboxylates by benzoinyl cages. However, some charge interactions are particularly sensitive to caging, making the identification of potential caging sites critical. The best targets are buried residues involved in charge interactions that are incapable of making local adjustments due to sterics. The low dielectric environment of buried sites also increases the stability impact of a caged residue, when compared to solvent-exposed residues.

The general strategy of caging a buried charge interaction has been successfully demonstrated using GCN4-p1 (N16D(DMB)), allowing rapid photochemical triggering of protein unfolding. Future work on triggering protein folding will focus on naturally occurring, buried salt bridges in synthetically accessible proteins. Some proteins that may be targeted include the c-Myc-Max leucine zipper heterodimer, which contains a buried Glu-His-Glu interaction; (30) the 434 repressor DNA-binding domain, which contains a buried Arg-Glu salt bridge; (31) and bacteriophage P22 Arc repressor, which contains an Arg-Glu-Arg triad with a completely buried Glu residue (32).

The initial PAC experiments demonstrated that these caging methods are capable of triggering rapid conformational changes in proteins, allowing the observation of unfolding events occurring in 300 ns. Since the photolysis event itself is complete within picoseconds (14) (a timescale on the order of several thousand single-bond vibrations), triggering with benzoinyl cages is capable of revealing the kinetics of even the most rapid protein conformational changes.

A particular advantage to the flash photolysis triggering scheme is the large change in stability upon photolysis. For the GCN4-p1 (N16D) model system described here, the conversion to the unfolded form was essentially complete, even under native solvent conditions in the absence of denaturant. The fact that unfolding kinetics can be measured without chemical denaturants, and with solvent conditions that are identical both before and after the triggering event, should greatly facilitate theoretical modeling of the unfolding process.

Finally, it is important to point out that the caging techniques described here are not limited to proteins that may be synthesized in their entirety by solid-phase synthesis. Recent advances in semisynthesis methods will allow the solid-phase synthesis of short, side chain caged peptides, that may then be coupled to a large protein fragment.

References

1. Balbach, J., Forge, V., van Nuland, N. A., Winder, S. L., Hore, P. J., Dobson, C. M. (1995) *Nat Struct Biol* **2,** 865-70.
2. Fersht, A. R. (1995) *Philos Trans R Soc Lond B Biol Sci* **348,** 11-5.
3. Wood, T. D., Chorush, R. A., Wampler, F. M., 3rd, Little, D. P., O'Connor, P. B., McLafferty, F. W. (1995) *Proc Natl Acad Sci U S A* **92,** 2451-4.
4. Deniz, A. A., Laurence, T. A., Beligere, G. S., Dahan, M., Martin, A. B., Chemla, D. S., Dawson, P. E., Schultz, P. G., Weiss, S. (2000) *Proc Natl Acad Sci U S A* **97,** 5179-84.
5. Rief, M., Gautel, M., Oesterhelt, F., Fernandez, J. M., Gaub, H. E. (1997) *Science* **276,** 1109-12.
6. Roder, H., Elove, G. A., Englander, S. W. (1988) *Nature* **335,** 700-4.
7. Stowell, M. H. B., Rock, R. S., Rees, D. C., Chan, S. I. (1996) *Tet. Lett.* **37,** 307-310.
8. Larsen, R. W., Osborne, J., Langley, T., Gennis, R. B. (1998) *Journal of the American Chemical Society* **120,** 8887-8888.
9. Lu, H. S. M., Volk, M., Kholodenko, Y., Goodling, E., Hochstrasser, R. M., DeGrado, W. F. (1997) *Journal of the American Chemical Society* **119,** 7173-7180.
10. Gurney, A. M. & Lester, H. A. (1987) *Physiol. Rev.* **67,** 583-617.
11. Adams, S. R. & Tsien, R. Y. (1993) *Ann. Rev. Of Physiol.* **55,** 755-784.
12. Sheehan, J. C. & Wilson, R. M. (1964) *J. Am. Chem. Soc.* **86,** 5277-5281.
13. Sheehan, J. C., Wilson, R. M. & Oxford, A. W. (1971) *J. Am. Chem. Soc.* **93,** 7222-7228.
14. Rock, R. S., Chan, S. I. (1998) *Journal of the American Chemical Society* **120,** 10766-10767.
15. O'Shea, E. K., Rutkowski, R., Kim, P. S. (1989) *Science* **243,** 538-42.
16. Rasmussen, R., Benvegnu, D., O'Shea, E. K., Kim, P. S., Alber, T. (1991) *Proc Natl Acad Sci U S A* **88,** 561-4.
17. Oas, T. G., McIntosh, L. P., O'Shea, E. K., Dahlquist, F. W., Kim, P. S. (1990) *Biochemistry* **29,** 2891-4.

18. O'Shea, E. K., Klemm, J. D., Kim, P. S., Alber, T. (1991) *Science* **254,** 539-44.

19. Harbury, P. B., Zhang, T., Kim, P. S., Alber, T. (1993) *Science* **262,** 1401-7.

20. Gonzalez, L., Jr., Woolfson, D. N., Alber, T. (1996) *Nat Struct Biol* **3,** 1011-8.

21. Gonzalez, L., Jr., Brown, R. A., Richardson, D., Alber, T. (1996) *Nat Struct Biol* **3,** 1002-9.

22. Gonzalez, L., Jr., Plecs, J. J., Alber, T. (1996) *Nat Struct Biol* **3,** 510-5.

23. Schneider, J. P., Lear, J. D., DeGrado, W. F. (1997) *Journal of the American Chemical Society* **119,** 5742-5743.

24. Ede, N. J., Ang, K. H., James, I. W., Bray, A. M. (1996) *Tetrahedron Letters* **37,** 9097-9100.

25. Braslavsky, S. E., Heibel, G. E. (1992) *Chemical Reviews* **92,** 1381-1410.

26. Yeh, S. R., Falvey, D. E. (1995) *Journal of Photochemistry and Photobiology a-Chemistry* **87,** 13-21.

27. Schulenberg, P. J., Gartner, W., Braslavsky, S. E. (1995) *Journal of Physical Chemistry* **99,** 9617-9624.

28. Abbate, G., Attanasio, A., Bernini, U., Ragozzino, E., Somma, F. (1976) *Journal of Physics D-Applied Physics* **9,** 1945-1951.

29. (1978) *CRC Handbook of Chemistry and Physics* (CRC Press).

30. Lavigne, P., Kondejewski, L. H., Houston, M. E., Jr., Sonnichsen, F. D., Lix, B., Skyes, B. D., Hodges, R. S., Kay, C. M. (1995) *J Mol Biol* **254,** 505-20.

31. Pervushin, K., Billeter, M., Siegal, G., Wuthrich, K. (1996) *J Mol Biol* **264,** 1002-12.

32. Waldburger, C. D., Schildbach, J. F., Sauer, R. T. (1995) *Nat Struct Biol* **2,** 122

33. Sosnick, T. R.; Jackson, S.; Wilk, R. R.; Englander, S. W.; DeGrado, W. F. *Proteins* **1996**, *24*, 427-32.

34. Kammerer, R. A.; Schulthess, T.; Landwehr, R.; Lustig, A.; Engel, J.; Aebi, U.; Steinmetz, M. O. *Proc Natl Acad Sci U S A* **1998**, *95*, 13419-24.

35. Kammerer, R. A.; Jaravine, V. A.; Frank, S.; Schulthess, T.; Landwehr, R.; Lustig, A.; Garcia-Echeverria, C.; Alexandrescu, A. T.; Engel, J.; Steinmetz, M. O. *J Biol Chem* **2001**, *276*, 13685-8.

36. Moran, L. B.; Schneider, J. P.; Kentsis, A.; Reddy, G. A.; Sosnick, T. R. *Proc Natl Acad Sci U S A* **1999**, *96*, 10699-704.

37. Zitzewitz, J. A.; Ibarra-Molero, B.; Fishel, D. R.; Terry, K. L.; Matthews, C. R. *J Mol Biol* **2000**, *296*, 1105-16.

38. Williams, S.; Causgrove, T. P.; Gilmanshin, R.; Fang, K. S.; Callender, R. H.; Woodruff, W. H.; Dyer, R. B. *Biochemistry* **1996**, *35*, 691-7.

39. Thompson, P. A.; Eaton, W. A.; Hofrichter, J. *Biochemistry* **1997**, *36*, 9200-10.

Chapter 8:

A Method for Photoinitating Protein Folding in a Nondenaturing Environment

Abstract

A general method for photoinitiating protein folding has been developed using the photolabile linker 3'-(carboxymethoxy)benzoin (CMB). We have applied this strategy to the 35 amino-acid headpiece subdomain of the actin bundling protein Villin, creating a denatured or non-native state of the peptide by cyclizing the N-terminus to a cysteine introduced 12 residues away using the CMB. Since destabilization of the native state is accomplished by the conformational constraint of a head-to-side chain cyclization, the refolding of the Villin headpiece can be initiated by rapid photolysis of the CMB linker and the folding process studied in real time in the absence of added denaturants. Upon irradiation (306-355 nm), the photoproduct benzofuran is observed along with a concomitant increase in the α-helical ellipticity. This work demonstrates a general methodology for studying early events in protein folding.

Introduction

The early kinetic events of protein folding are an important part of the folding pathway, yet our understanding towards the process is limited. Information from the study of these early events can allow us to distinguish between the various models that have been proposed to describe the folding of a protein in real time. Unlike "typical" chemical kinetics with well-defined initial and final states, the initial state of a denatured protein is relatively ill defined. This uncertainty introduces ambiguity in the interpretation of the experimental data on the early events in protein folding. Towards developing a unified theory of protein folding, it is necessary to begin the observation of the refolding process from a well-defined initial state, trigger folding as rapidly as

possible, and to follow the protein in real time as it samples its conformational space over its highly complex free-energy landscape.

Traditional stopped-flow methods have been employed to follow the kinetic course of protein folding reactions. However, such experiments are limited in time resolution and in that an external denaturant are used to achieve a non-native state. It is not known exactly how denaturants interact with a protein and how they affect the kinetic pathways. In addition, substantial refolding occurs during the dead time of mixing in the stopped-flow experiment. To circumvent the time domain limitation, several groups have recently developed strategies based on temperature,[1] pH[2] or pressure jumps,[3] flash photolysis of heme ligands,[4] photoreduction of metalloproteins,[5] and the photolysis of engineered disulfides[6] (for a recent review see ref. **#7, 8**). Although the above techniques have provided insight into protein folding, few studies have been done in the

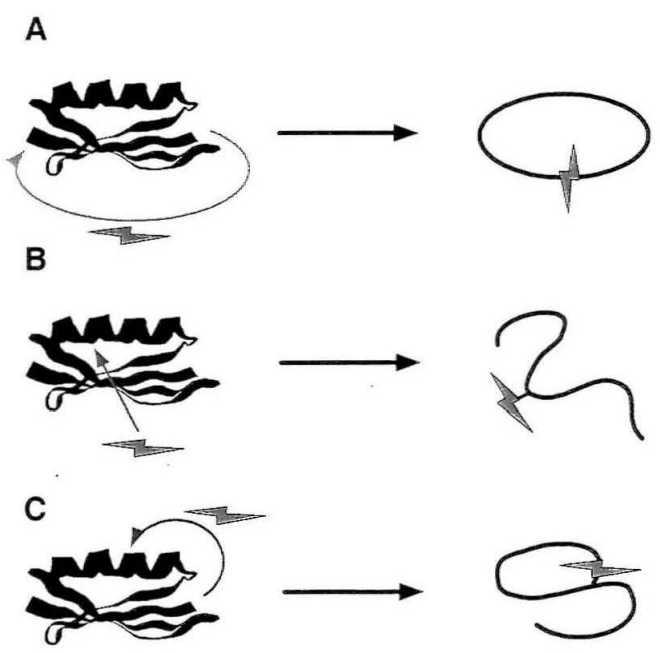

Figure 1. Three methods for denaturing a protein using photolabile protecting groups: (**A**) Head-to-tail cyclization; in this method the conformational constraint of having the N and C-terminus next to each other prohibits proper folding. (**B**) Side chain protection; the steric bulk of the cage prohibits proper core packing. (**C**) Head-to-side chain cyclization; the structural arrangement of the protein is dictated by the site of ligation. Once the linker is photocleaved the protein assumes a linear form that is free to form the native structure.

absence of denaturant. A general method to study the early events of folding in greater detail requires irreversibility, applicability to non-metalloproteins, fast triggering, and the elimination of external denaturants.

Our strategy for the initiation of protein folding is based on the picosecond flash photolysis of an organic photoprotecting group. Three general methods for denaturing a protein can be envisioned using such a photo-trigger (figure 1). The first uses the photolabile protecting group as a linker to cyclize the protein of interest from the N terminus to the C terminus. This approach will be applicable only in cases where bringing the N terminus and C terminus together sufficiently disrupts native structural elements. This disruption is more likely to occur when a considerable distance separates the N terminus and C terminus (ideally, they would lie on opposite sides of the protein). The second strategy involves placing a photoprotecting group on a side chain that resides in the core of the native structure. Thus, steric bulk of this group will prohibit proper hydrophobic packing and a unfolded state will result. It is likely that in many cases this strategy will result in a molten globule state as the hydrophobic collapse event is still likely to occur. The third general strategy involves head-to-side chain cyclization and likewise side chain-to-side chain cyclization. This method should make it possible to disrupt regions of a protein's fold and in some cases result in an almost completely unfolded state (no native contacts present). Each of these approaches for using photo-protecting groups to denature proteins has its own unique advantages and disadvantages. It is predicted that synthetically the side chain protecting technique will be the most chemically tractable yet the less useful for mapping the energy landscape (at least near the top of the folding funnel). The third method has more flexibility in terms of sites for

cyclization and therefore the number of possible starting conformations. This will be the method employed in this work.

Results and Discussion

A photolabile-protecting group that has been derivatized to act as a linker may be placed within a cyclic form of a protein of interest. If chosen correctly, the resulting loop conformation will prohibit proper folding of the protein. Thus, instead of manipulating the external conditions, such as temperature, pH, or denaturant concentration, the covalent structure of the protein is altered to yield a conformationally constrained unfolded state. During the triggering event the linker is irreversibly cleaved to yield the "linear" amino acid sequence that is free to fold into the native protein structure.

Photolabile Linker

In 1971 Sheehan *et al.* showed that esters of 3',5'-dimethoxybenzoin undergo efficient and clean photolysis under near-UV illumination,[7,8] and can thus serve as photolabile protecting groups, otherwise known as caging compounds (figure 2). The products of this photolysis are the phenylbenzofuran and the "free" form of the caged molecule, often a carboxylic acid. It has been shown that this compound can be used as an effective phototrigger for the spatially and temporally controlled release of biologically active compounds. This phototrigger is attractive when compared to the alternative o-nitrobenzyl derivatives due to its solubility, the rapid rate of

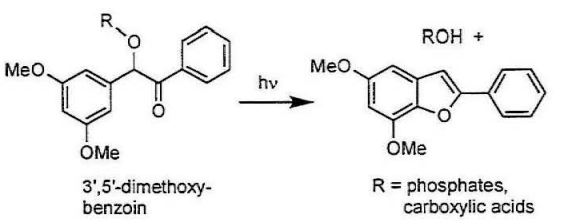

Figure 2. Derivatized Benzoin as a photolabile protecting group for phosphates or Carboxylic acids.

photorelease, and the formation of biologically compatible side products. Upon excitation of the derivatized benzoin, an intramolecular rearrangement occurs to yield the photoproduct benzofuran and the desired "free" molecule.

This protecting group has been converted into a linker by derivatization of the benzoin ring to give 3'-(carboxymethoxy)benzoin (CMB, Scheme 1, **1**).[9] Benzoinyl cages have the following properties which make them well suited for these studies: high quantum yields (0.6-0.7); inert photoproducts; good water solubility; and fast photolysis rates (predicted~10^{10} s^{-1}, observed >10^{9} s^{-1}).[10-13]

The strategy described here involves forming a small loop from the N-terminus of a protein to an internal amino-acid sidechain using CMB as a linker. To achieve selective linker attachment and subsequent cyclization of the peptide, the general synthetic strategy outlined in Scheme 1 was used. The first step in this method was to derivatize protected CMB (**1**) with a reactive chemical functionality to form a competent linker.

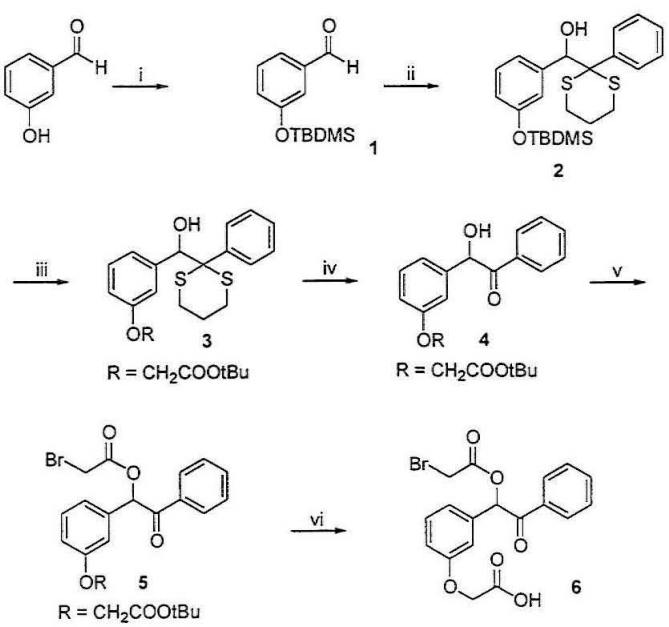

Scheme 1. Synthesis of BrAc-CMB.
Reagents: i: TBDMSCl, Et_3N. ii: a) Phenyl dithiane lithium anion; b) H_2O. iii: $BrCH_2COOtBu$, TBAF. iv: $Hg(ClO_4)_2$, H_2O. v: a) Ac_2O, DMAP. vi: TFA.

The dithiane protected, tert-butyl ester benzoin was synthesized according to the methods of Rock and Chan with some variation.[14] A linker may be derived from this compound by incorporation of a carboxylic acid moiety. Thus, in compound **4** a carboxy group has been added to the 3'-methoxy substituent, in a similar fashion as the water soluble BCMB described in chapter 4. This new group provides the second functional group for linkage through amide or ester bond formation. The benzoyl ring was left unsubstituted, as the results of Sheehan et al. showed that such substitution lowers the overall photolysis yield.

The synthesis of compound **6** proceeded as outlined in Scheme 1. The phenolic oxygen of 3-hydroxybenzaldehyde is first protected by base assisted halide displacement to produce **1**. This TBDMS ether eliminates dianion solubility problems. Addition of 2-phenyl-1,3-dithiane to **1**, via the lithium anion, was used to form the dithiane **2.** This process is effective at protecting the benzyl ketone during the following step. The phenolic hydroxyl was selectively alkylated by treatment with TBAF in the presence of tertbutyl bromoacetate, to yield the tertbutyl ester **3**. It was found that the overall yield was improved with the dithiane being hydrolyzed before the acylation step, hence the dithiane was removed with the addition of flouroboric acid and mercury(II)oxide to produce compound **4**. A Halide group provided the second site for linkage. The activated esterification of tert-butyl ester protected CMB with bromoacetic acid was mediated by the addition of DCC to provide **5**. This was followed by the cleavage of the tert-butyl group with 50% TFA yielding the desired bromoacetylated linker **6**. This derivatized benzoin serves as the sulfhydryl-selective cross-linking function for the preparation of the cyclic peptide.

Scheme 2. General cyclization strategy using BrAc-CMB.

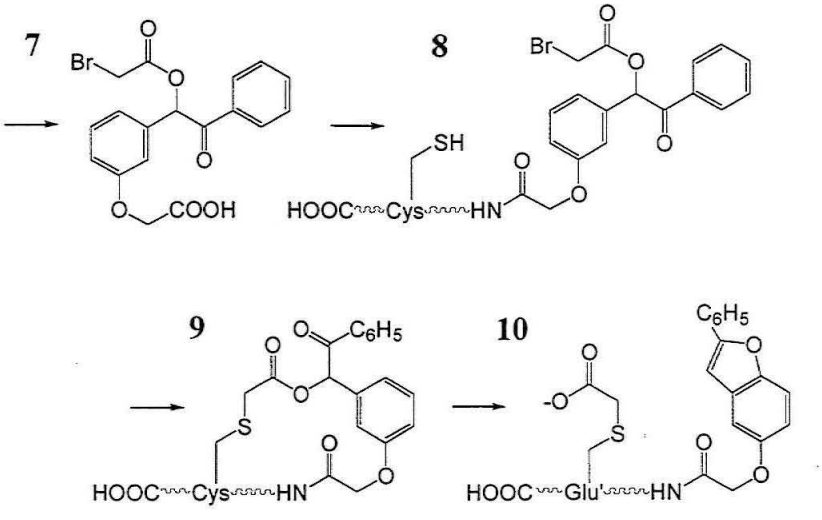

Peptide Cyclization

The general cyclization strategy for using compound **6** to cyclize a polypeptide from the N terminus to a cysteine side chain is depicted in scheme 3. In this procedure the fully side chain protected polypeptide is synthesized by standard solid-phase peptide synthesis, with the cysteine selectively protected by a weak acid-labile protecting group. Once the full-length peptide is synthesized and the terminal Fmoc group removed, the BrAc-CMB linker is attached to the N-terminus of the synthetic peptide through standard condensation coupling. The acid-labile Cys protecting group is selectively removed to produce the free thiol in **8**. Finally, cyclization through thioether formation is achieved using a non-nucleophilic amine base in an organic solvent. Upon completion, the resin was rinsed and neutralized. The peptide was cleaved from the solid support and purified by reverse-phase HPLC to yield the cyclized peptide **9**. This cyclized product is expected to eliminate the native tertairy fold of the protein. The use of a rapid light pulse of the correct frequency will cleave the photolinker and provides for

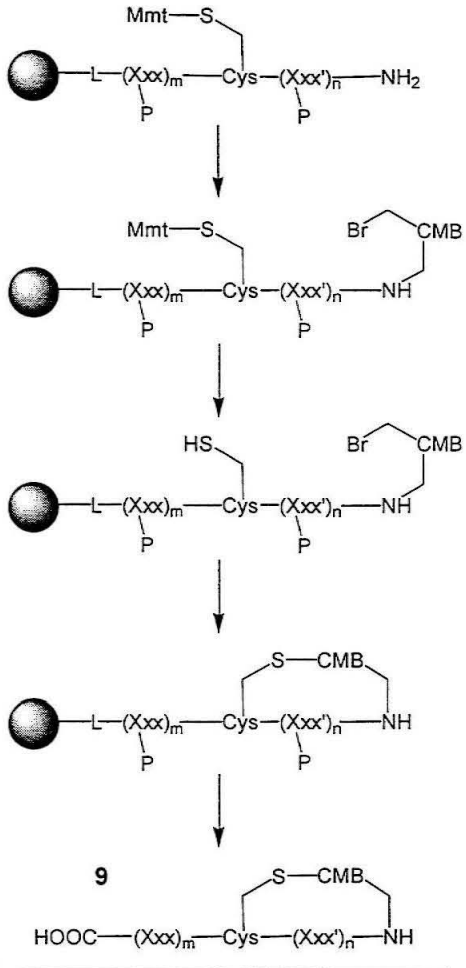

Scheme 3. Detailed on-resin synthetic scheme. Cys selective protection followed by site-specific cyclization.

a convenient means for rapid initiation of protein folding with spatial and temporal resolution to produce the modified protein **10**.

This form of the native protein has two noticeable differences: First, the photoproduct benzofuran is attached to the N-terminus. It is predicted that this modification will have little effect on the folding mechanism. The second difference is that the non-native carboxymethyl cysteine results at the cleavage site. This modified side chain is a thio-ether analog of glutamic acid. Thus, the most likely targets for cyclization will be surface glutamic acids or aspartic acids that do not form salt bridges. The carboxymethyl cysteine should have very little structural consequences for the final folded state. This may be checked by comparing the thermodynic stability of the mutation. A method to determine if this mutation affects the folding transition state would be to perform mutational Φ analysis on the protein using a different initiation method. However, it is predicted that the small difference of introducing a sulfur atom into glutamic acid will not significantly change the transition state.

At this time selective loop formation of the peptide must be made synthetically due to the wide variety of nucleophilic side chains present. However, with recent advances in protein synthesis and semi-synthesis, this technique can be applied to study virtually any protein. The synthesis of the peptide was performed using Fmoc-based chemistry, taking advantage of the flexibility it incurs on cysteine protection. To access the usefulness of this method, a small synthetically accessible protein is desired.

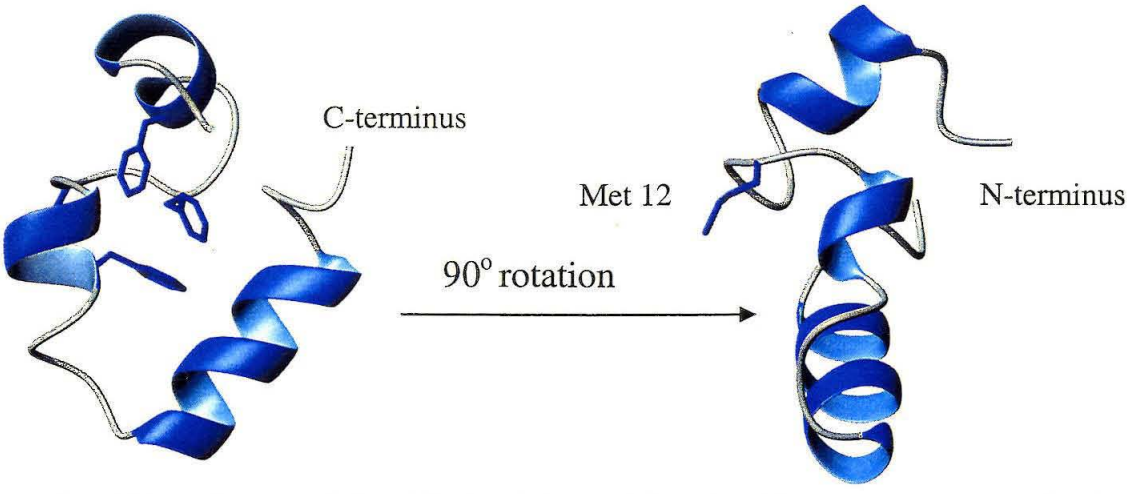

Figure 3. Ribbon diagram of the villin headpiece subdomain. Figures were generated using Molscript (pdb accession code 1vii).

Villin Headpiece Subdomain

To demonstrate this general approach, we have used the small α-helical villin headpiece subdomain (figure 3).[15] This autonomous monomeric folding unit consists of 35 residues, is highly thermostable (T_m ~70°C), and forms a compact primarily α-helical structure. This villin subdomain is expected to fold rapidly, and as such has been used as a model protein in a microsecond molecular dynamics simulation. [16,17] Residue Met 12 was chosen for mutation to Cys due to its close proximity in sequence to the N-terminus and its apparent high solvent exposure as shown by the NMR structure.[18] Accordingly, the peptide VHP-34 M12C was prepared with the *N*-terminal bromoacetylated CMB group attached. Cyclization and cleavage of the peptide and protecting groups, as described above, yielded the cyclic form of the peptide (cVHP-34 M12C-CMB, see materials and methods for sequence). Upon photolysis, the cyclized peptide was cleaved to yield the "linear" form containing a carboxymethylcysteine at residue 12 (**5**), a solvent-exposed position where a charged residue should be tolerated.

Steady State Photolysis

To evaluate the secondary structure of the cVHP, steady state photolysis was carried out and UV/Vis and CD spectra were recorded. Irradiation of the cVHP-34 revealed a spectra indicative of a clean conversion of the benzoin to benzofuran, an event that corresponds to the conversion of the cyclized peptide to the "linear" form. Two isosbestic points were present throughout the course of photolysis. This conclusion is corroborated by the molecular mass of the peptide before and after the photolysis, which were found to be 4191.9 and 4191.2 amu, respectively. The CD spectra (figure 4) before photolysis (B) and after (E) show the expected formation of α-helical secondary structure concomitant with the photolysis event. The change in helix content was approximately 50% for this 12 residue loop form of the villin headpiece.

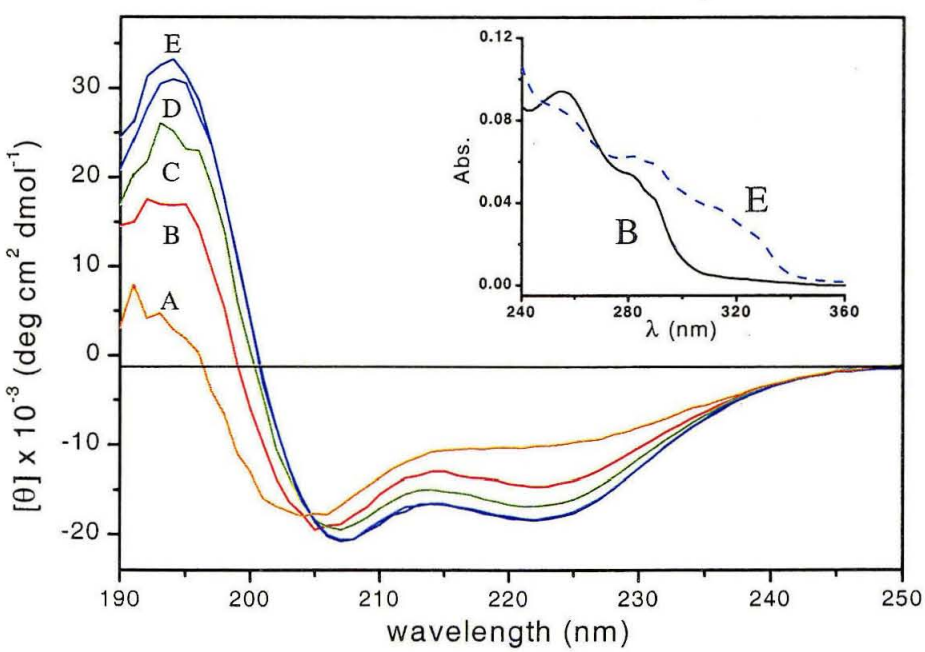

Figure 4. Steady-state photolysis of 28 μM cVHP M12C-CMB (**4**) in 10 mM $NaPO_4$ buffer, pH 7.4, irradiated from 300 to 400 nm using a filtered high-pressure mercury vapor arc lamp. Linear form at 95°C (above the melting temperature of VHP-35) (A); cyclized form, irradiation time (s): (B) 0, (C) 10, (D) 30, (E) 90. Inset UV spectra.

Modeling of the Cyclized Structure

Examination of our cVHP-34 M12C-CMB model reveals that it is possible to maintain a hydrophobic core in the cyclized form of this very stable small protein. The NMR structure was used to build a model of cVHP34 M12C-CMB. This model has retained the C-terminal α-helix and some of the Proline turn of the original NMR structure (figure 5). The native hydrophobic contacts are not present, but a looser hydrophobic clustering is evident. This model shows that it is possible to maintain a conformation that can allow for hydrophobic packing. It is likely that the cyclization eliminates the α-helix content contained in the first 12 residues, disrupts the rest of the middle helix, and only partially disrupts the other C-terminal α-helix primarily by taking away specific tertiary interactions.

Although cyclization did not eliminate all native structure in this very stable small protein, it is likely that it could in other proteins. With typical free energies of folding around that of a few hydrogen bonds, the cyclization of the protein will, in many cases, be enough to disrupt the balance of the global fold.

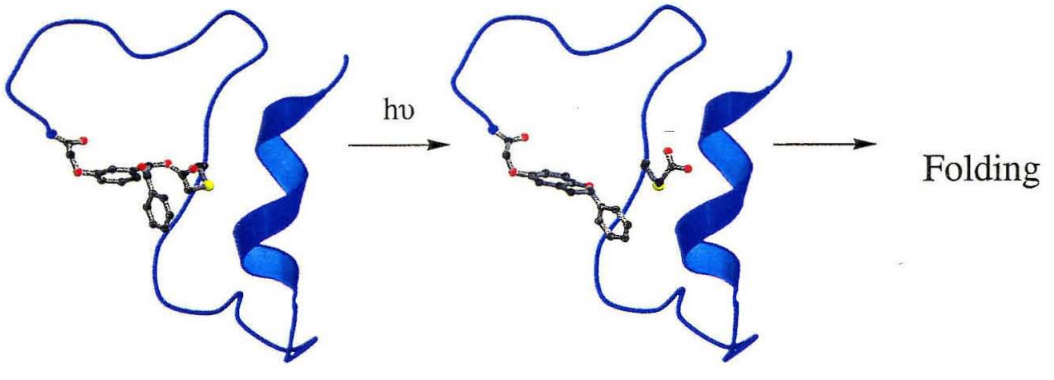

Figure 5. Computer generated model of cVHP-34 M12C-CMB. The structure was minimized and then heated to 1000 K to unfold the native structure. This was followed by a 300 K annealing phase to give the shown model.

Kinetics of Photolysis

To ascertain the time course of the structural response of the peptide following linker cleavage, we have utilized time-resolved photoacoustic calorimetry (PAC) and photothermal beam deflection (PBD), two methods that are sensitive to photochemically induced volume changes.[19,20] Deconvolution of the experimental PAC data revealed two kinetic phases with time constants of approximately 100 and 400 ns (raw data presented in materials and methods). PBD measurements revealed that the folding process was essentially complete within the dead time of our experimental setup (~10 μs). It is likely that fast helix formation was responsible for at least one of the phases in the observed PAC signal.

The observed rates of folding are in accord with existing theory and experiment. Based on a length dependent diffusion calculation with an alpha-helical correction, this peptide is predicted to fold between approximately 15-100 μs.[21] The two nanosecond phases observed by PAC are of the same magnitude as experimental and theoretical rates based on helix-coil transitions and other fast folding experiments. Although the helix-coil relaxation rates yield important information, it is necessary to follow the coil-helix transition to obtain specific information about nucleation and chain propagation rates.

A molecular dynamics simulation was performed on the villin headpiece.[16,17] In this work Duan and Kollman used an all atom representation of the villin headpiece with 3000 water molecules to perform a 1 us (0.5 billion integration) folding trajectory. Their starting structure was generated using the NMR coordinates in a 1 ns molecular dynamic simulation carried out at 1000 K to produce an unfolded model. The resulting unfolded state contained very few native contacts (<3%) and no helical content. However, the

turn formed by Asn20-Leu21-Pro22 and Leu23 was partially retained. The trajectory began with an initial burst phase (60 ns) in which the amount of helical content increased to 60% of that in the native state and the native contacts increased to ~45%. They report that this initial phase is most likely driven by burial of exposed hydrophobic surface. Within 20 ns their in-silico structure went from a 10.7 Å mainchain rms deviation to below 6 Å. The structure that resulted at this stage consists of three short helices and these are held together by hydrophobic clusters. However, these hydrophobic clusters are different than those found in the native structure and result in a loosely packed core. This state labeled as a possible intermediate lasted until about 400 ns and then a slow expansion was observed to give structures with mainchain rms deviations of 15 Å. It is uncertain whether this "adjustment" phase is a real representation of a folding process or an artifact of the calculation.

In a following paper by Kollman *et al.* they used a combined molecular mechanical/continuum model to estimate the free energies of the unfolded, folded and intermediate states of the villin headpiece.[22] Taking structural ensembles from their 1-μs molecular dynamics folding simulation for the unfolded state and an intermediate (the lowest energy species found during the simulated trajectory) along with a 100-ns control simulation on the native structure, they calculated the native ensemble to be ~26 kcal/mol more stable than the folding intermediate and ~39 kcal/mol more stable than the random coil ensemble. With an experimental estimate free energy of denaturation of 3 kcal/mol, they approximate the non-native degeneracy to lie between 10^{16} and 10^{25}. They propose a model for the folding kinetics based on their calculations that involves the unfolded state collapsing down to a compact stable intermediate around 200 ns and then a

transition state that lies around 700 ns followed by a first-order exponential decay to the native state. If this is the case, then they predict a half time for folding of 1.05 μs which gives a transition from the unfolded state to 90% folded in approximately 4.2 μs. In lines with their earlier work, if the protein does not undergo smooth first-order decay but instead continues to fall into metastable intermediates until it reached the native structure, the predicted range of folding times is 10-100 μs. Based on a conformational random search of the folding space, Kuntz *et al.* predict that the folding will be a millisecond time scale event.[23] However, they go on to recognize that the slope of the folding funnel should increase the rate 1-2 orders of magnitude above random exploration rates.

The experimental kinetics from this work may indicate that the first of these three scenarios is the correct one. The ~100 ns phase that we observed could correspond to the 200 ns compact intermediate collapse, and our ~400 ns phase could be the protein traveling over the predicted 700 ns transition barrier. The small discrepancies in the actual times are within the experimental error of the PBD measurement and the described calculations. However, there are other folding mechanisms that could explain the observed kinetics and several assumptions have gone into the calculated numbers, which may not be completely correct. In addition, it is not clear how the cyclized unfolding state affects the overall folding mechanism and kinetics. It is possible that the unfolded state is already close to the compact intermediate state which would result in overall faster rates to the fully folded state in mechanisms where the initial folding events are collapse to a compact core. In order to make the kind of comparisons that can validate computation predictions, it will be necessary to get molecular detail of the folding process.

The most recent work by Kollman and coworkers on the VHP begins with the rosetta algorithm (homology modeling) and ends with the all atom molecular dynamics simulation.[24] This method was able to take one of four starting structures (no bias) to a structure with 1.4 Å backbone rmsd from the experimental structure. It seems likely that as computers become more powerful and molecular dynamic methods are refined, structural prediction will become more powerful. The prospect of predicting a structure with correct side chain conformation and larger multidomain structures appears to be a long way off. To accomplish this goal we will need a more detailed picture of folding mechanism; kinetic experiments will continue to play an important role in this task. Often kinetics, and not thermodynamics, determine a protein's physiological structure.

Conclusions

The head-to-side chain cyclization strategy outlined here has several advantages for the rapid triggering of protein folding reactions. The synthetic scheme allows the somewhat sensitive BrAc-CMB group to be introduced at the end of the solid-phase synthesis process. With this technique loops of varying size may be formed, including small, synthetically accessible loops. Finally, the irreversible triggering event allows us to monitor the entire refolding process without kinetic competition from the reverse triggering reaction that was observed in earlier studies.[1-5] We are particularly interested in determining the effects of the initial unfolded state on the observed kinetic pathways. Our cyclization approach enables us to confine the protein to a subset of phase space, thus making it possible to map out sections of the folding landscape. In contrast to traditional folding experiments that start from an ensemble of unfolded states around the

top of the funnel, this technique has the potential to discern between folding occurring in series or parallel pathway processes (as discussed in chapter 6). If cyclization at different locations leads to different folding mechanisms, then this would support the idea that the folding landscape has parallel pathways on the energy landscape that are being sampled. Likewise, if the rates and mechanisms remain unchanged, this would indicate a convergent series process.

Although cyclization did not eliminate all native structure in this very stable small protein, it is likely that it could in other proteins. With typical free energies of folding around that of a few hydrogen bonds, the cyclization of the protein will, in many cases, be enough to disrupt the balance of the global fold.

The goal of this work is to determine the sequence of intermediates and their rates of interconversion and to characterize their structures and energetics with as much detail as possible to provide the essential basis for calculations and simulations. While the work outlined herein has the ability to answer many general questions regarding protein folding, it will be necessary to study several different protein systems. Solving this complicated problem will require the study of proteins with different folds, number of domains, and oligomerization states. Most likely, proteins with structural differences will have differences in folding mechanisms. Application of the techniques detailed in this chapter and chapter 7 to larger proteins is a realistic goal with recent advances in semisynthesis and chemical synthesis of proteins. This technique is not limited to aqueous media; therefore, the effect of viscosity and the effects of added denaturants on folding can be studied in alternative solvent systems. This method allows for the study of protein folding under more physiologically relevant conditions.

In summary, we have demonstrated an irreversible rapid triggering method to study protein folding that utilizes a conformational constraint to achieve an unfolded state so that the use of denaturant is unnecessary.

Materials and Methods

Note: VHP-34 M12C prepared with the *N*-terminal bromoacetylated CMB group attached = (BrAc-CMB)-LSDEDFKAVFGCTRSAFANLPLWKQQLKKEKGL-NH_2. To minimize the differences between the VHP-35 and the relinearized peptide product, the N-terminal Phe in the VHP-35 was not included as part of the cVHP-34 M12C-CMB. This truncation was justified on the grounds that the photolysed benzofuran with its aromatic rings would roughly substitute for the terminal Phe in the native protein.

Synthesis of protected CMB

3-(tert-Butyldimethylsilyloxy)benzaldehyde (1)

To a solution of 3-hydroxybenzaldehyde (12.21 g, 100 mmol) in 600 mL THF was added *tert*-butyldimethylsilyl chloride (TBDMSCl, 18.84 g, 125 mmol). The solution was cooled to 0°C and triethylamine (12.65 g, 17.4 mL, 125 mmol) was added dropwise. The reaction mixture was brought to room temperature and stirred 5 hours. The mixture was filtered and the THF removed under reduced pressure. The oil was repeatedly dissolved in 200 mL portions of THF and evaporated, until no more triethylamine hydrochloride precipitated. The oil was then dissolved in 150 mL diethyl ether, filtered through a plug of neutral alumina and activated charcoal to remove the salt and the yellow color, and evaporated. The colorless, mobile oil was dried *in vacuo*

overnight. Yield: 21.43 g (91%). IR: 1703, 1583, 1482, 1278, 1145, 840 cm^{-1}. ^1H NMR ($CDCl_3$, TMS) δ 9.927 (s, 1 H), 7.447 (d, J = 7.50 Hz, 1 H), 7.379-7.335 (m, 2 H), 7.096-7.074 (m, 1 H), 0.994 (s, 9 H), 0.215 (s, 6 H). ^{13}C NMR ($CDCl_3$, TMS) δ 191.60, 156.34, 138.03, 130.03, 126.34, 123.46, 119.70, 25.59, 18.12, -4.52. Anal. Calcd for $C_{13}H_{20}O_2Si$: C, 66.05; H, 8.53. Found: C, 66.13; H, 8.53.

*(±)-1-Hydroxy-1-(3-*tert*-butyldimethylsilyloxyphenyl)-2-phenyl-2-(1,3-dithian-2-yl)-ethane (2)*

A solution of 2-phenyl-1,3-dithiane (15.71 g, 80 mmol) in 125 mL THF was prepared. The solution was treated at 0°C under a nitrogen atmosphere with 40 mL of *n*-butyllithium (2.0 M in cyclohexane, 80 mmol). After 30 min, **1** (18.91 g, 80 mmol) was added. The solution was stirred for 1 hr. at 0°C, then poured into 100 mL of 1 N HCl and extracted with methylene chloride (4 x 50 mL). The organic phase was washed with brine, dried with $MgSO_4$, filtered through a plug of activated charcoal and silica gel, and evaporated under reduced pressure. The resulting oil was crystallized from ethanol / water to form a white powder. Yield: 28.98 g (84%). mp 75-76°C. IR: 3449 (br), 1601, 1484, 1275, 1152, 834 cm^{-1}. ^1H NMR ($CDCl_3$, TMS) δ 7.70 (d, J = 7.50 Hz, 2 H), 7.308-7.235 (m, 3 H), 6.937 (t, J = 7.79 Hz, 1 H), 6.682-6.660 (m, 1 H), 6.427-6.404 (m, 2 H), 4.926 (d, J =3.73 Hz, 1 H), 2.936 (d, J = 3.76 Hz, 1 H), 2.739-2.610 (m, 4 H), 1.942-1.879 (m, 2 H), 0.935 (s, 9 H), 0.111 (s, 6 H). ^{13}C NMR ($CDCl_3$, TMS) δ 154.43, 138.89, 137.47, 130.42, 128.00, 127.69, 127.36, 121.23, 119.89, 119.54, 80.74, 66.36,

27.22, 26.93, 25.65, 24.69, 18.03, -4.40. Anal. Calcd. $C_{23}H_{32}O_2S_2Si$: C, 63.84; H, 7.45. Found: C, 63.83; H, 7.26.

{3-[Hydroxy-(2-phenyl-[1,3]dithian-2-yl)-methyl]-phenoxy}-acetic acid tert-butyl ester (3)

A solution of **2** (19.467 g, 45 mmol) and *tert*-butyl bromoacetate (10.971 g, 56.25 mmol) was prepared in 150 mL dry THF. The solution was cooled to 0°C, and tetrabutylammonium fluoride (1 M in THF, 47.25 mL, 47.25 mmol) was added dropwise under nitrogen. After stirring for 12 h, the solution was poured into 300 mL diethyl ether and extracted with a total of 1.5 L water. The organic layer was dried with $MgSO_4$ and evaporated. The residue was dried overnight under vacuum to yield 20.698 g (100%) of **2** as an oil that slowly crystallizes upon standing. ^{1}H-NMR ($CDCl_3$, TMS) δ 7.688 (m, 2 H), 7.292 (m, 3 H), 7.050 (t, J = 7.9 Hz, 1 H), 6.794 (m, 1 H), 6.549 (d, J = 7.6 Hz, 1 H), 6.307 (s, 1 H), 4.962 (s, 1 H), 4.371 (s, 1 H), 3.032 (s, 1 H), 2.678 (m, 4 H), 1.927 (m, 2 H), 1.498 (s, 9 H).

3'-(carboxymethoxy)benzoin-otBu (4)

A solution of (±)-1-Hydroxy-1-[3'-((carboxymethoxy)tert-butyl)benzoin (5.0 g, 14.2 mmol) in 5 ml of THF is added to a solution of mercury(II)oxide (5.04 g, 23.3 mmol) and fluoroboric acid (12.26 ml, 35% aqueous soln.) in 15 ml of THF. After 5 minutes of stirring at room temperature the solution is filtered and concentrated to 5 ml. The crude product was brought up in ether and washed

with 10% NaOH, 10% KI, and H_2O. Water was removed using a brine wash and treatment with $MgSO_4$. An off white solid (3.48 g, 72%) was obtained after solvent removal. (^{1}H NMR ($CDCl_3$, 300 MHz) δ 7.896 (d, *J* = 6.9 Hz, 2 H), δ 7.525 (t, *J* = 7.5 Hz, 1 H), δ 7.394 (t, *J* = 7.20 Hz, 2 H), δ 7.239 (s, 2 H), δ 6.976 (d, *J* = 7.8 Hz, 1 H), δ 6.873 (t, 1 H), δ 6.811 (d, *J* = 8.1, 1 H), δ 5.903 (s, 1 H), δ 4.462 (s, 2 H), δ 1.456 (s, 9 H).

Synthesis of BrAc-CMB

[(±)-O-bromoacetyl-3'-(carboxymethoxy)benzoin] (5 and 6)

A solution of 3'-(carboxymethoxy)benzoin-OtBu (685 mg, 2 mmol) and bromoacetic acid (694 mg, 5 mmol) was prepared in 10 mL DCM. This solution was treated with DCC (866 mg, 4.2 mmol). After 12 h, the resulting suspension was filtered, and the filtrate was poured into diethyl ether. The organic phase was washed with 5% sodium bicarbonate and water, dried with $MgSO_4$, and evaporated. The residue was treated with 1:1 TFA / DCM for 45 min, then evaporated. The crude BrAc-CMB was purified by flash chromatography (silica gel, 1:1 hexanes / ethyl acetate) to yield 629 mg (70%) as an oil. R_f = 0.25 (1/1 hexane/EtOAc); ^{1}H NMR ($CDCl_3$, 300 MHz) δ 7.906 (d, *J* = 7.2 Hz, 2 H), δ 7.508 (t, *J* = 7.5 Hz, 1 H), δ 7.383 (t, *J* = 7.20 Hz, 1 H), δ 7.286 (t, 1 H), δ 7.103 (d, *J* = 5.70 Hz, 1 H), δ 7.056 (t, 1 H), δ 6.887 (d, *J* = 8.4 Hz, 1 H), δ 6.865 (s, 1 H), δ 4.672 (s, 2 H), δ 3.99 (d, *J* = 1.8 Hz,2 H); HRMS (FAB) *m/z* (MNa^+) cacld. 428.9950, obsd. 428.9957.

Peptide Synthesis and Cyclization

All peptides were synthesized using Fmoc chemistry on a Perceptive Biosystems model 9050 peptide synthesizer. Standard side chain protecting groups were used except for the mild acid labile Cys(Mmt). All couplings were performed using a four-fold excess of a 0.3 M Fmoc-amino acid solution, preactivated with 1:1:1.5 HBTU / HOBt / DIEA. Fmoc groups were cleaved with 20% (v/v) piperidine in DMF. VHP-34 was prepared on a 0.2 mmol scale, using Novasyn TGR© Rink amide resin (Novabiochem). Once the synthesis was complete, the resin was rinsed with DCM and dried. A resin sample was cleaved using 95% TFA / 2.5% TIS / 2.5% water / 2.5% EDT, and the crude peptide isolated and characterized by MALDI-TOF MS ($[M+H]^+$ exp. 3883.51, found 3883.42). The peptide on resin (0.025 mmol) was capped with BrAc-CMB-OH (200 mg, 0.5 mmol) using 75 mL DIPCDI in 3 mL DMF until a ninhydrin test on a small aliquot indicated completion of the amide bond formation, 12 hrs. The resin was then rinsed with 3 x 5 mL DMF followed by 3 x 5 mL DCM. The cysteine Mmt protecting group was then selectively removed with 5 x 3 mL treatments (10 min ea.) of the resin with 2% TFA / 2% TIS (v/v) in DCM. Deprotection was determined to be complete when the solution remained colorless after the addition of the deprotection mixture. The peptide was rinsed extensively with DCM, then cyclized for 24 hrs, by treating the resin with 5% (v/v) DIEA in NMP. After cyclization, the resin sample was rinsed with DCM, dried, then cleaved using 95% TFA / 2.5% TIS / 2.5% water / 2.5% EDT. The peptide products were collected by four cycles of precipitation into MTBE followed by centrifugation. MALDI-TOF MS, $[M+H]^+$ exp. 4191.8 found 4191.94 (monoisotopic). The crude peptide was dissolved in 50 mM Na phosphate buffer, pH 7.0, and any residual ether was removed

under a stream of nitrogen prior to purification by RP-HPLC. All RP-HPLC was performed on a 10 mm x 250 mm C4 column (Phenomenex), using a gradient of 0.1% (w/v) TFA in water (solvent A), and 0.1% TFA in acetonitrile (solvent B).

Steady State Photolysis

Samples where placed in a quartz cuvette irradiated with an Oriel 66011 Hg vapor arc lamp operating at 450 W and filtered through a 355 nm UG11 band pass filter. A sample of cVHP-34 M12C-CMB was dissolved in 10 mM sodium phosphate buffer, pH 7.0. The optical absorbance was monitored with an HP 8452 diode array spectrophotometer. The photolysis was judged to be complete when no further spectral changes occurred. HPLC analysis was performed using a phenomenex analytical C18 reverse phase column. MALDI-TOF MS, $[M+H]^+$ exp. 4191.8, found 4191.25 (average) (figure 6).

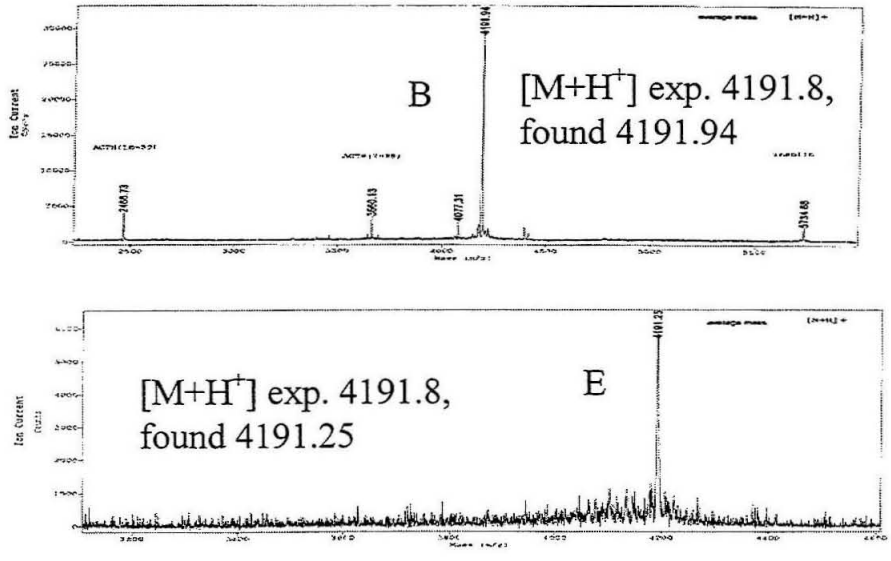

Figure 6. MALDI-TOF MS corresponding to the sample shown in figure 4. Addition peaks observed in sample B are standards.

Steady-State Circular Dichroism Studies

Samples for CD Spectroscopy were brought up in 10 mM sodium phosphate buffer, pH 7.4. Spectra were recorded on an Aviv 62A DS spectrometer in a 1mm cell at 25°C. The results are expressed as mean residue molar ellipticities [θ].

Photoacoustic Calorimetry and Photothermal Beam Deflection

Curve fitting and experimental setup for beam photothermal deflection (PBD) were as previously described.[19] This technique involves photoexcitation of a molecular system of interest in which excess energy is dissipated by vibrational relaxation to the ground state and results in thermal motion of the solvent. This causes a rapid volume expansion that changes the refractive index of the solvent. Additionally, volume changes in the molecular system of interest also contribute to the refractive index change so that the change in volume can be measured for a given reaction. In PBD, the changes in the refractive index are monitored optically by a probe beam following an initiation event. This technique has

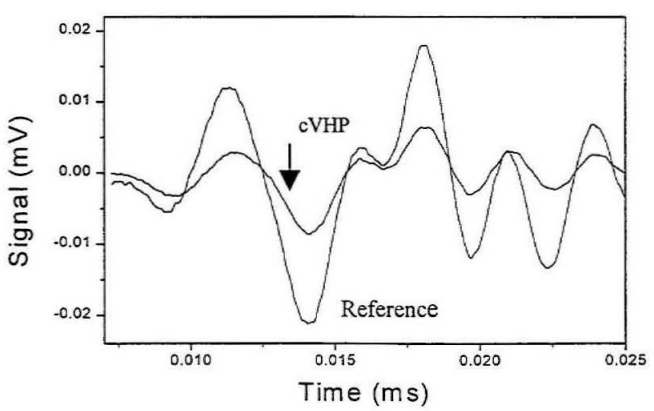

Figure 7. Graphical Representation of PAC signal. A.) Reference compound B.) Photolysis of cVHP-34 M12C-CMB.

the unique advantage that it can be used to collect both kinetic and thermodynamic information in the same experiment.

References

1)Ballew, R. M.; Sabelko, J.; Gruebele, M. *Proc Natl Acad Sci U S A* **1996**, *93*, 5759-64.

2)Abbruzzetti, S.; Crema, E.; Masino, L.; Vecli, A.; Viappiani, C.; Small, J. R.; Libertini, L. J.; Small, E. W. *Biophys J* **2000**, *78*, 405-15.

3)Jacob, M.; Holtermann, G.; Perl, D.; Reinstein, J.; Schindler, T.; Geeves, M. A.; Schmid, F. X. *Biochemistry* **1999**, *38*, 2882-91.

4)Jones, C. M.; Henry, E. R.; Hu, Y.; Chan, C. K.; Luck, S. D.; Bhuyan, A.; Roder, H.; Hofrichter, J.; Eaton, W. A. *Proc Natl Acad Sci U S A* **1993**, *90*, 11860-4.

5)Pascher, T.; Chesick, J. P.; Winkler, J. R.; Gray, H. B. *Science* **1996**, *271*, 1558-60.

6)Lu, H. S. M.; Volk, M.; Kholodenko, Y.; Goodling, E.; Hochstrasser, R. M.; DeGrado, W. F. *Journal of the American Chemical Society* **1997**, *119*, 7173-7180.

7)Sheehan, J. C.; Wilson, R. M.; Oxford, A. W. *J. Am. Chem. Soc.* **1971**, *93*, 7222-7228.

8)Sheehan, J. C.; Wilson, R. M. *J. Am. Chem. Soc.* **1964**, *86*, 5277-5281.

9)Rock, R. S.; Chan, S. I. *J. Org. Chem.* **1996**, *61*, 1526-1529.

10)Rock, R. S.; Chan, S. I. *J. Am. Chem. Soc.* **1998**, *120*, 10766.

11)Shi, Y.; Corrie, J. E. T.; Wan, P. *J. Org. Chem.* **1997**, *62*, 8278-8279.

12)Hansen, K. C.; Schultz, B. E.; Wang, G.; Chan, S. I. *Biochim. Biophys. Acta* **2000**, *1456*, 121-37.

13)Conrad, P. G.; Givens, R. S.; Hellrung, B.; Rajesh, C. S.; Ramseier, M.; Wirz, J. *J. Am. Chem. Soc.* **2000**, *122*, 9346.

14)Rock, R. S. Chan., S. I. *J. Org. Chem.* **1996**, *61*, 1526-1529.

15)McKnight, C. J.; Doering, D. S.; Matsudaira, P. T.; Kim, P. S. *J Mol Biol* **1996**, *260*, 126-34.

16)Duan, Y.; Kollman, P. A. *Science* **1998**, *282*, 740-4.

17)Duan, Y.; Wang, L.; Kollman, P. A. *Proc Natl Acad Sci U S A* **1998**, *95*, 9897-902.

18)McKnight, C. J.; Matsudaira, P. T.; Kim, P. S. *Nat Struct Biol* **1997**, *4*, 180-4.

19)Larsen, R. W.; Langley, T. *J. Am. Chem. Soc.* **1999**, *121*, 4495-9.

20)Larsen, R. W.; Osborne, J.; Langley, T.; Gennis, R. B. *Journal of the American Chemical Society* **1998**, *120*, 8887-8888.

21)Debe, D. A.; Goddard, W. A., 3rd *J Mol Biol* **1999**, *294*, 619-25.

22)Lee, M. R.; Duan, Y.; Kollman, P. A. *Proteins* **2000**, *39*, 309-16.

23)Sullivan, D. C.; Kuntz, I. D. *Proteins* **2001**, *42*, 495-511.

24)Lee, M. R.; Baker, D.; Kollman, P. A. *J Am Chem Soc* **2001**, *123*, 1040-1046.